UNIVERSIDADE FEDERAL DE VIÇOSA

Assessment of rehabilitation process in post-dam-collapse and post-mining sites: the role of technogenic soils and pedogenetic evidence

Rugana Imbaná
Doctor Scientiae

VIÇOSA - MINAS GERAIS
2025

RUGANA IMBANÁ

Assessment of rehabilitation process in post-dam-collapse and post-mining sites: the role of technogenic soils and pedogenetic evidence

Thesis submitted to the Soil Science and Plant Nutrition Graduate Program of the Universidade Federal de Viçosa in partial fulfillment of the requirements for the degree of *Doctor Scientiae*.

Adviser: Igor Rodrigues de Assis

Co-advisers: Elpidio I. F. Filho
Lukasz Uzarowicz

VIÇOSA - MINAS GERAIS
2025

Ficha catalográfica elaborada pela Biblioteca Central da Universidade Federal de Viçosa - Campus Viçosa

T

I32a
2025

Imbaná, Rugana, 1994-

Assessment of rehabilitation process in post-dam-collapse and post-mining sites: the role of technogenic soils and pedogenetic evidence / Rugana Imbaná. – Viçosa, MG, 2025.

1 tese eletrônica (125 f.): il. (algumas color.).

Texto em inglês.

Inclui anexos.

Orientador: Igor Rodrigues de Assis.

Tese (doutorado) - Universidade Federal de Viçosa, Departamento de Solos, 2025.

Inclui bibliografia.

DOI: https://doi.org/10.47328/ufvbbt.2025.496

Modo de acesso: World Wide Web.

1. Solos - Descontaminação. 2. Restauração ecológica. 3. Ecossistemas - Efeito da mineração. 4. Resíduos industriais - Aspectos ambientais. I. Assis, Igor Rodrigues de, 1980-. II. Universidade Federal de Viçosa. Departamento de Solos. Programa de Pós-Graduação em Solos e Nutrição de Plantas. III. Título.

CDD 22. ed. 631.4

Bibliotecário(a) responsável: Euzébio Luiz Pinto CRB-6/3317

RUGANA IMBANÁ

Assessment of rehabilitation process in post-dam-collapse and post-mining sites: the role of technogenic soils and pedogenetic evidence

Thesis submitted to the Soil Science and Plant Nutrition Graduate Program of the Universidade Federal de Viçosa in partial fulfillment of the requirements for the degree of *Doctor Scientiae*.

APPROVED: July 3, 2025.

Assent:

Rugana Imbaná
Author

Igor Rodrigues de Assis
Adviser

To my family — especially my mother, Sábado Antônio da Silva (Sâhbá); my mother's siblings, Maria da Costa (Nni Nduka Tchali Mang); my father, Tchetena Imbaná (Klabus); my sisters, Sábado Imbaná (Sâhdo) and Celeste Imbaná (Silé); my brothers, Joaquim Imbaná (Mano Djokas) and Mário Imbaná (Rock); and all my relatives in Guinea-Bissau — my unwavering foundation. I offer you my eternal gratitude.

ACKNOWLEDGMENTS

This doctoral journey has been one of the most transformative experiences of my life, and it would not have been possible without the Nghâla grace, as well as the support, generosity, and inspiration of many.

I wish to express my deepest gratitude to the Graduate Program in Soils and Plant Nutrition at the Federal University of Viçosa (UFV) for the structured academic and institutional support that sustained me throughout this journey. I am equally thankful to VALE S.A.. This work has been sponsored by the following Brazilian research agencies: Coordination for the Improvement of Higher Education Personnel (CAPES; Financing code 001), Minas Gerais State Foundation for Research Aid (FAPEMIG) and National Council of Scientific and Technological Development (CNPq).

I owe my profound appreciation to Professor Igor Rodrigues de Assis, my adviser. His enduring support, belief in my potential, and insightful guidance have not only shaped the direction of this research but also my growth as a soil scientist, one who is passionate about ecological restoration. I enthusiastically look forward to continuing our collaboration and friendship, both of which have been constant sources of motivation and inspiration.

I am also deeply indebted to Professor Dr. Hab. Lukasz Uzarowicz, who welcomed me into his group at the Warsaw University of Life Sciences (SGGW) with remarkable warmth and rigor. His mentorship, generosity, and scientific brilliance were fundamental to my academic and personal development. The opportunities he provided me—from field trips, meetings, and conferences across Europe to engaging scientific discussions—were transformative. The investigation in Poland, as presented in this doctoral thesis, was financially supported by the Polish Ministry of Science and Higher Education (grant no. N305 3251 33). The publication was (co)financed by the Science Development Fund of the Warsaw University of Life Sciences – SGGW.

I also gratefully acknowledge Grzegorz Widlicki (University of Warsaw, Faculty of Geology, Poland) for his support during the preparation of thin sections. I extend special thanks to Prof. Jerzy Jonczak (Head of the Department) for the opportunity to work in the Department of Soil Science at SGGW. Additionally, I would like to express my appreciation to Dr. Piotr Jankowski, Dr. Wojciech Kwasowski, Dr. Artur Pedziwiatr, and Mr. Damian Murach for their invaluable assistance during fieldwork and laboratory activities. To all those I met at SGGW and along the way across Europe (e.g., Prof. Geoffroy Séré at Université de Lorraine), thank you for the knowledge you shared and the memories we created. And yes—thank you for the “jedzenie, piwo i dobre towarzystwo.”

I am grateful to Prof. Elpídio Inácio Fernandes-Filho and my colleagues and friends at the Pedometric and Geoprocessing Research Laboratory (LabGeo-UFV) and at the Environmental Rehabilitation Laboratory (GERAD-UFV) for the meaningful exchanges, shared curiosity, and genuine friendship. To my peers at UFV, SGGW, and Université de Lorraine, thank you for the partnership and kindness that made my time abroad truly special.

To my family — especially my mother, Sábado Antônio da Silva (Sâhbá); my mother's siblings, Maria da Costa (Nni Nduka Tchali Mang); my father, Tchetena Imbaná (Klabus); my sisters, Sábado Imbaná (Sâhdo) and Celeste Imbaná (Silé); my brothers, Joaquim Imbaná (Mano Djokas) and Mário Imbaná (Rock); and all my relatives in Guinea-Bissau — my unwavering foundation. I offer you my eternal gratitude. Your support, in its many forms, has carried me to this moment. Your belief in my path gave me the strength I needed when I needed it most. You have not only helped shape the scientist I am becoming but have also profoundly influenced the person I strive to be.

Finally, thank you to everyone across the globe who accompanied me in any way during this journey—through words, deeds, presence, or encouragement. This achievement is also yours.

ABSTRACT

IMBANÁ, Rugana, D.Sc., Universidade Federal de Viçosa, July, 2025. **Assessment of rehabilitation process in post-dam-collapse and post-mining sites: the role of technogenic soils and pedogenetic evidence**. Adviser: Igor Rodrigues de Assis. Co-advisers: Elpidio Inacio Fernandes Filho and Lukasz Uzarowicz.

In an era marked by global environmental disturbance and profound socio-ecological transformation, the United Nations' 17 Sustainable Development Goals (SDGs) present an unprecedented vision for a just and sustainable future. However, amidst overlapping crises—climate change, resource scarcity, and biodiversity loss—questions of priority, trade-offs, and feasibility remain unresolved, particularly within the contested framework of the Anthropocene. This doctoral thesis explores one such paradox: the urgent need to restore ecosystems degraded by mining and industrialization, even as these activities remain essential to the energy transition itself. Focusing on Technosols—engineered or derived from anthropogenic materials—this research examines their ecological functionality and potential as tools for sustainability in post-dam-collapse and post-mining contexts. Drawing on fieldwork across Brazil and Poland, the thesis comprises three integrative studies that assess Technosols from physical, chemical, biological, and micromorphological perspectives. The first study, based in Brumadinho (Brazil), evaluates a constructed Technosol at the “Marco Zero” area, where lateritic waste and topsoil were combined to jumpstart ecological restoration following the 2019 B1 dam collapse. Over a 2.5-year period, modest but significant gains in microbial activity and nutrient cycling suggest that Technosols can facilitate ecological recovery when coupled with sustained management and monitoring. The second study investigates Technosol performance in the hydrologically dynamic Pantanal biome. Using a customized Rehabilitation Quality Index (RQI), seasonal analyses showed improved ecosystem similarity to reference areas during the rainy season and significant vulnerabilities during the dry period, highlighting the importance of climate-responsive post-mining restoration design in the highlands of the Pantanal tropical wetland systems. The third study shifts to a temperate European context, where Spolic Technosols derived from sulfide-rich mining waste in southern Poland were analyzed micromorphologically. Despite their recent formation (dating back up to 200 years), these technogenic soils exhibit pedogenic features such as clay illuviation and iron oxide coatings, providing evidence of slow but ongoing soil-forming processes and hinting at the long-term viability of Technosols, even in acidic, metal-rich substrates. Together, these three studies contribute to a nuanced understanding of Technosols not as inert substrates but as dynamic systems capable of evolving ecological functionality. By bridging macro- and microscale indicators, this doctoral thesis advances theoretical frameworks in soil science and restoration ecology while offering actionable insights for post-industrial land management. It argues for restoration approaches that are locally grounded, climate-adapted, and socially informed—essential considerations in a world where the boundaries between natural and anthropogenic systems are increasingly blurred. In summary, this doctoral research explains how engineered and derived soils from anthropogenic materials, when carefully designed and monitored, can transform degraded environments into thriving, functional ecosystems. In doing so, it reframes waste not as an endpoint, but as a beginning—an opportunity for ecosystem rehabilitation and resilience in the Anthropocene.

Keywords: Technosols; Ecological restoration; Anthropocene

RESUMO

IMBANÁ, Rugana, D.Sc., Universidade Federal de Viçosa, julho de 2025. **Avaliação do processo de reabilitação em sítios pós-rompimento de barragem e pós-mineração: o papel dos solos tecnogênicos e evidências pedogenéticas**. Orientador: Igor Rodrigues de Assis. Coorientadores: Elpidio Inacio Fernandes Filho e Lukasz Uzarowicz.

Em uma era marcada por perturbações ambientais globais e transformações socioecológicas profundas, os 17 Objetivos de Desenvolvimento Sustentável (ODS) das Nações Unidas propõem uma visão sem precedentes de um futuro justo e sustentável. No entanto, em meio a crises sobrepostas—mudanças climáticas, escassez de recursos e perda de biodiversidade—questões fundamentais sobre prioridades, compromissos e viabilidade permanecem sem resposta, especialmente dentro do controverso marco do Antropoceno. Esta tese de doutorado investiga um dos principais paradoxos desse cenário: a necessidade urgente de restaurar ecossistemas degradados pela mineração e industrialização, mesmo quando essas atividades seguem sendo centrais para a transição energética. Com foco nos Tecnossolos—solos construídos ou originados a partir de materiais antrópicos—esta pesquisa avalia sua funcionalidade ecológica e potencial como ferramentas para a sustentabilidade em contextos de pós-desastre e pós-mineração. A partir de trabalho de campo realizado no Brasil e na Polônia, a tese é composta por três estudos integrados que analisam os Tecnossolos sob perspectivas físicas, químicas, biológicas e micromorfológicas. O primeiro estudo, realizado em Brumadinho (MG), avalia um Tecnossolo construído no “Marco Zero”, onde resíduos lateríticos foram combinados com solo estocado para iniciar a restauração ecológica após o rompimento da barragem B1 em 2019. Ao longo de 2,5 anos de monitoramento, foram observados avanços modestos, porém significativos, na atividade microbiana e nos ciclos de nutrientes, sugerindo que Tecnossolos podem catalisar processos de restauração, desde que acompanhados por manejo contínuo e monitoramento de longo prazo. O segundo estudo examina o desempenho de Tecnossolos no bioma Pantanal, uma das maiores áreas úmidas do planeta. Utilizando um Índice de Qualidade da Reabilitação (IQR) adaptado à variabilidade sazonal, a análise revelou maior similaridade ecológica durante o período chuvoso e vulnerabilidades associadas à retenção hídrica e resiliência vegetal na estação seca. Esses resultados destacam a necessidade de estratégias de restauração sensíveis ao clima e às heterogeneidades ecológicas de ambientes tropicais. O terceiro estudo oferece uma perspectiva complementar ao analisar Tecnossolos spólicos desenvolvidos a partir de resíduos sulfetados no sul da Polônia. Apesar de sua origem recente (200 anos), análises micromorfológicas revelaram processos pedogenéticos em curso, como iluviação de argila, bioturbação e precipitação de óxidos de ferro, indicando que esses solos artificiais podem evoluir funcionalmente mesmo em climas temperados e substratos ácidos. Conjuntamente, os três estudos oferecem uma visão integrada e multiescalar dos Tecnossolos em paisagens degradadas. Ao conectar dados de campo com observações microscópicas e integrar indicadores ecológicos, químicos e morfológicos, esta tese avança tanto o conhecimento teórico quanto as práticas aplicadas em restauração ecológica. Destaca-se a importância de adaptar as técnicas de restauração aos contextos ambientais e socioculturais específicos, contribuindo também para o debate mais amplo sobre sustentabilidade no Antropoceno. Em síntese, esta pesquisa demonstra que Tecnossolos, quando adequadamente projetados e monitorados, podem transformar passivos ambientais em sistemas vivos e funcionais. Ao reconceituar resíduos como recursos, oferece caminhos concretos para regenerar paisagens degradadas e promover resiliência socioecológica em um mundo em mudança.

Palavras-chave: Tecnossolos; Restauração Ecológica; Antropoceno

SUMÁRIO

1. General Introduction

Imagine a world where 193 nations unite under a shared vision: the United Nations' 17 Sustainable Development Goals (SDGs), conceived to guide us toward a just, equitable, and environmentally sustainable future by the year 2030 (Fertő and Harangozó, 2025; Pattberg and Bäckstrand, 2023; Sugiawan et al., 2023). Despite this unprecedented global accord, fundamental questions remain unanswered: Which of these goals should be prioritized on a worldwide scale, and how should individual nations determine their specific priorities (Ma et al., 2025; Qi et al., 2024)? These questions are further complicated in the context of the Anthropocene, a proposed geological epoch characterized by humanity's profound and accelerating impact on Earth's systems. In this context, the pursuit of sustainability is fraught with paradoxes.

One of these paradoxes is the reliance of renewable energy technologies on extensive mineral extraction. While intended to mitigate climate change, the extraction of metallic, rare earth, and other strategic minerals often results in substantial ecological destruction (Roland et al., 2024; Witze, 2024a). Consequently, the global sustainability agenda encounters inherent contradictions that pose challenges to simplistic solutions. In light of these complexities, in-depth studies are necessary to explore some of the most pressing ecological and ethical dilemmas of our time.

Humanity now stands at a critical juncture, facing an existential crisis driven by centuries of cumulative environmental degradation. Over the past 100,000 years, humanity has accumulated immense power through the mastery of fire, agriculture, metallurgy, and industrialization. These advancements have catalyzed remarkable progress in human development. However, they have also contributed to the destabilization of planetary boundaries (Ascenzi et al., 2025; Rowland et al., 2025; Willcock et al., 2023). The Industrial Revolution, which began in the 18th century, catalyzed a pivotal shift in humanity's capacity to alter natural systems (Hulme, 1927). This transformative time, widely acknowledged as second only to the Neolithic Revolution in shaping human civilization, ushered in unprecedented material prosperity while concurrently intensifying human interactions with Earth's systems through the processes of manufacturing, urbanization, and mining (Anwar et al., 2025; Hossin et al., 2025; Jin et al., 2025; Kallio et al., 2025; McDowell et al., 2025).

Today, the evidence of anthropogenic influence on Earth's landscapes, atmosphere, and biogeochemical cycles is undeniable. From the rise in greenhouse gas concentrations to extensive land-use changes and biodiversity loss, the ecological footprint of humanity has reached a global scale. This ongoing process of anthropization—human-driven transformation of ecosystems—is a central justification for the concept of the Anthropocene (Subramanian, 2019; Witze, 2023, 2024a, 2024b). Within this context, an increasing number of scientists and practitioners are focusing on SUITMAs—Soils of Urban, Industrial, Traffic, and Mining Areas—as both indicators and tools for measuring human influence on the critical zone (Morel et al., 2015; Pindral et al., 2022).

SUITMAs, particularly Technosols—a class of soils that have been either created or significantly altered by human activities—have emerged as a promising solution to the environmental challenges associated with anthropogenic activities, including industrialization, mining, and urbanization. Notably, the rehabilitation of degraded lands through the construction of Technosols from anthropogenic waste materials presents a potentially sustainable avenue for restoring ecosystem services, augmenting soil functionality, and bolstering climate resilience (Gazitúa et al., 2021; Ruiz et al., 2023; Stępniewska et al., 2020; Uzarowicz et al., 2020). Nevertheless, the efficacy of such interventions remains uncertain and context-specific, influenced by a complex interplay of environmental factors, design approaches, and socio-political considerations (Imbaná et al., 2024; Kanianska et al., 2022; Khelifi et al., 2025; Ruiz et al., 2020; Uzarowicz and Skiba, 2011). Through interdisciplinary inquiry and drawing upon diverse field experiences across Brazil and Poland, the thesis seeks to gain insights into technogenic soils within these complex issues.

The primary objective of this doctoral thesis is to explore the dual tension inherent in the mining industry. While it holds significant socioeconomic importance, it often overshadows concerns regarding environmental degradation. Conversely, there is an urgent need to restore ecosystems that extractive industries have compromised. This research addresses these challenges through an in-depth analysis of Technosols derived from industrial and mining waste in Brazil and Poland. A particular emphasis is placed on their physical, chemical, biological, and micromorphological characteristics. The thesis comprises three interrelated studies that provide a comprehensive multiscale assessment of Technosol behavior and performance across diverse post-disaster and post-mining rehabilitation scenarios.

The first study focuses on short- and medium-term Technosol improvement at the "Marco Zero" site in Brumadinho, Brazil, a location associated with the catastrophic failure of the B1 tailings dam in 2019. Here, a mixture of lateritic mining waste and stockpiled topsoil was used to construct an engineered Technosol aimed at starting ecological restoration. Over a 2.5-year monitoring period, we observed modest but measurable changes in microbial activity, enzymatic function, pH, and nutrient cycling. These findings suggest that while Technosols can play a role in initiating restoration, their effectiveness hinges on sustained management and long-term ecological monitoring.

The second study shifts the focus to the Pantanal biome, one of the world's largest and most hydrologically dynamic wetlands. In this tropical savanna-forest mosaic, we assessed post-mining rehabilitation efforts using a Rehabilitation Quality Index (RQI) personalized to capture seasonal variability. Our analysis revealed significant differences between wet and dry seasons, with the rainy period promoting greater ecological similarity to reference ecosystems, while the dry season exposed vulnerabilities in water retention and vegetative resilience. The study emphasizes the necessity for climate-responsive restoration strategies that account for the temporal and spatial heterogeneity inherent to tropical ecosystems.

The third and final study presents a complementary perspective by examining the micromorphological characteristics of Spolic Technosols developed from sulfide-rich mine waste in southern Poland. Despite their relatively recent origin in a temperate climate context (dating back up to 200 years), thin-section analysis revealed key pedogenic features, such as iron oxide coatings, clay illuviation, and signs of bioturbation. These micro-level indicators provide compelling evidence that even freshly established Technosols can undergo natural soil-forming processes, even though at a slow pace. This observation is critical for understanding the long-term viability and functional maturation of Technosols in cold-temperate settings with acidic mine substrates.

Together, these three studies deliver an integrated and holistic understanding of Technosols in post-mining and post-disaster landscapes. By linking macroscopic field data with microscopic observations and integrating ecological, chemical, and morphological indicators, this thesis seeks to advance both theoretical knowledge and practical approaches to ecological restoration. It highlights the importance of tailoring restoration techniques to specific environmental and cultural contexts, while also contributing to broader discussions about sustainability in the Anthropocene.

References

Anwar, A., Mezbah Uddin, A.H.M., Hasan, M.S., Parvez, M.S., Sipos, B., Bibi, D., Sajtos, Z., Tótmérész, B., Magura, T., Simon, E., 2025. Assessment of anthropogenic activities impact based on metals in soil and tree leaves along roadside in Bangladesh. Sci Rep 15, 1–14. https://doi.org/10.1038/S41598-025-91683-9

Ascenzi, I., Hilbers, J.P., van Katwijk, M.M., Huijbregts, M.A.J., Hanssen, S. V., 2025. Increased but not pristine soil organic carbon stocks in restored ecosystems. Nat Commun 16, 637. https://doi.org/10.1038/s41467-025-55980-1

Fertő, I., Harangozó, G., 2025. Trade-offs and synergies when balancing economic growth and globalization for sustainable development goals achievement. Sci Rep 15, 1–10. https://doi.org/10.1038/s41598-025-93360-3

Gazitúa, M.C., Morgante, V., Poupin, M.J., Ledger, T., Rodríguez-Valdecantos, G., Herrera, C., del Carmen González-Chávez, M., Ginocchio, R., González, B., 2021. The microbial community from the early-plant colonizer (Baccharis linearis) is required for plant establishment on copper mine tailings. Sci Rep 11, 1–16. https://doi.org/10.1038/s41598-021-89769-1

Hossin, M.A., Yin, S., Dan, R., Chen, L., 2025. Integrating artificial intelligence in unmanned vehicles: navigating uncertainties, risks, and the path forward for the fourth industrial revolution. Humanit Soc Sci Commun 12, 1–15. https://doi.org/10.1057/s41599-025-04554-z

Hulme, E.W., 1927. The Industrial Revolution. Nature 119, 892. https://doi.org/10.1038/119892c0

Imbaná, R., Valente, F.D.A., Siqueira, R.G., Moquedace, C.M., Assis, I.R., 2024. Assessing the quality of constructed technosols enabled holistic monitoring of ecological restoration. J Environ Manage 353. https://doi.org/10.1016/j.jenvman.2024.120237

Jin, J., Liao, Z., Liu, T., Wang, M., Zhang, J., Zhang, X., Fan, Y., 2025. Anthropogenic activities accelerate LULC conversion and only a sustainable development scenario is optimal for agro-pastoral ecotone development. Sci Rep 15, 1–16. https://doi.org/10.1038/s41598-025-98263-x

Kallio, N., Andersen, J.H., Carstensen, J., Gissi, E., Halpern, B.S., Hammar, L., Murray, C., Stelzenmüller, V., Stock, A., Korpinen, S., 2025. Challenges in expert ratings of marine habitat and species sensitivity to anthropogenic pressures. Sci Rep 15, 1–11. https://doi.org/10.1038/s41598-025-96913-8

Kanianska, R., Varga, J., Benková, N., Kizeková, M., Jančová, Ľ., 2022. Floodplain soils contamination assessment using the sequential extraction method of heavy metals from past mining activities. Sci Rep 12, 1–15. https://doi.org/10.1038/s41598-022-06929-7

Khelifi, F., Zhao, X., Dino, G.A., Padoan, E., 2025. Quality assessment of new constructed technosols: Key findings on their biogeochemical and environmental characteristics. J Hazard Mater 489, 137571. https://doi.org/10.1016/j.jhazmat.2025.137571

Ma, F., Wang, H., Tzachor, A., Hidalgo, C.A., Schandl, H., Zhang, Y., Zhang, J., Chen, W.Q., Zhao, Y., Zhu, Y.G., Fu, B., 2025. The disparities and development trajectories of nations in achieving the sustainable development goals. Nat Commun 16, 1107. https://doi.org/10.1038/s41467-025-56076-6

McDowell, R.W., Luo, D., Pletnyakov, P., Upsdell, M., Dodds, W.K., 2025. Anthropogenic nutrient inputs cause excessive algal growth for nearly half the world's population. Nature Communications 16, 1–15. https://doi.org/10.1038/s41467-025-57054-8

Morel, J.L., Chenu, C., Lorenz, K., 2015. Ecosystem services provided by soils of urban, industrial, traffic, mining, and military areas (SUITMAs). J Soils Sediments 15, 1659–1666. https://doi.org/10.1007/s11368-014-0926-0

Pattberg, P., Bäckstrand, K., 2023. Enhancing the achievement of the SDGs: Lessons learned at the half-way point of the 2030 agenda. Int. Environ. Agreements Politics Law Econ. 23, 107–114. https://doi.org/10.1007/s10784-023-09615-9

Pindral, S., Kot, R., Hulisz, P., 2022. The influence of city development on urban pedodiversity. Sci Rep 12, 1–13. https://doi.org/10.1038/S41598-022-09903-5

Qi, Y., Shi, X., Chen, Y., Shen, Y., 2024. Country-level evenness measure in assessing progress towards Sustainable Development Goals (SDGs). Humanit Soc Sci Commun 11, 1–13. https://doi.org/10.1057/S41599-024-03572-7

Roland, T.P., Swindles, G.T., Ruffell, A., 2024. The 'Anthropocene' is here to stay — and it's better not as a geological epoch. Nature 627, 735. https://doi.org/10.1038/d41586-024-00914-y

Rowland, J.A., Nicholson, E., Ferrer-Paris, J.R., Keith, D.A., Murray, N.J., Sato, C.F., Tóth, A.B., Tolsma, A., Venn, S., Asmüssen, M. V., Pliscoff, P., Zambrana-Torrelio, C., Lester, R.E., Regan, T.J., 2025. Assessing risk of ecosystem collapse in a changing climate. Nature Climate Change 2025 1–13. https://doi.org/10.1038/s41558-025-02324-y

Ruiz, F., Cherubin, M.R., Ferreira, T.O., 2020. Soil quality assessment of constructed Technosols: Towards the validation of a promising strategy for land reclamation, waste management and the recovery of soil functions. J Environ Manage 276. https://doi.org/10.1016/j.jenvman.2020.111344

Ruiz, F., Safanelli, J.L., Perlatti, F., Cherubin, M.R., Demattê, J.A.M., Cerri, C.E.P., Otero, X.L., Rumpel, C., Ferreira, T.O., 2023. Constructing soils for climate-smart mining. Communications Earth & Environment 2023 4:1 4, 1–6. https://doi.org/10.1038/s43247-023-00862-x

Stępniewska, H., Uzarowicz, Ł., Błońska, E., Kwasowski, W., Słodczyk, Z., Gałka, D., Hebda, A., 2020. Fungal abundance and diversity as influenced by properties of Technosols developed from mine wastes containing iron sulphides: A case study from abandoned iron sulphide and uranium mine in Rudki, south-central Poland. Applied Soil Ecology 145. https://doi.org/10.1016/j.apsoil.2019.08.011

Subramanian, M., 2019. Anthropocene now: influential panel votes to recognize Earth's new epoch. Nature. https://doi.org/10.1038/d41586-019-01641-5

Sugiawan, Y., Kurniawan, R., Managi, S., 2023. Assessing the United Nations sustainable development goals from the inclusive wealth perspective. Sci Rep 13, 1–13. https://doi.org/10.1038/s41598-023-28540-0

Uzarowicz, L., Skiba, S., 2011. Technogenic soils developed on mine spoils containing iron sulphides: Mineral transformations as an indicator of pedogenesis. Geoderma 163, 95–108. https://doi.org/10.1016/j.geoderma.2011.04.008

Uzarowicz, Ł., Wolińska, A., Błońska, E., Szafranek-Nakonieczna, A., Kuźniar, A., Słodczyk, Z., Kwasowski, W., 2020. Technogenic soils (Technosols) developed from mine spoils containing Fe sulphides: Microbiological activity as an indicator of soil development following land reclamation. Applied Soil Ecology 156, 103699. https://doi.org/10.1016/j.apsoil.2020.103699

Willcock, S., Cooper, G.S., Addy, J., Dearing, J.A., 2023. Earlier collapse of Anthropocene ecosystems driven by multiple faster and noisier drivers. Nature Sustainability 2023 6:11 6, 1331–1342. https://doi.org/10.1038/s41893-023-01157-x

Witze, A., 2024a. Geologists reject the Anthropocene as Earth's new epoch - after 15 years of debate. Nature 627, 249–250. https://doi.org/10.1038/d41586-024-00675-8

Witze, A., 2024b. It's final: the Anthropocene is not an epoch, despite protest over vote. Nature. https://doi.org/10.1038/d41586-024-00868-1

Witze, A., 2023. This quiet lake could mark the start of a new Anthropocene epoch. Nature 619, 441–442. https://doi.org/10.1038/d41586-023-02234-z

Chapter 1: The role of engineered soils in ecosystem rehabilitation after mining tailings dam failures in southeastern Brazil: The case of Brumadinho

Rugana Imbaná[1]*, Fernanda Daniele de Almeida Valente[1], Sandro Lucio Silva Moreira[1], Daniel Nunes da Silva Júnior[1], Cynthia Canêdo da Silva[2], Diego Aniceto dos Santos Oliveira[3], Elpídio Inácio Fernandes-Filho[1], Igor Rodrigues de Assis[1]

[1] Department of Soil Science, Universidade Federal de Viçosa, R. Purdue S/N, Campus Universitário, Viçosa, Minas Gerais, 36570-900, Brazil.
[2] Department of Microbiology, Universidade Federal de Viçosa, R. Purdue S/N, Campus Universitário, Viçosa, Minas Gerais, 36570-900, Brazil
[3] Vale S.A, Praia de Botafogo, 186 - Botafogo, Rio de Janeiro – RJ, 22250-145, Brazil

E-mail addresses: rugana.imbana@ufv.br*, fernanda.daniele@ufv.br, sandro.moreira@ufv.br, elpidio@ufv.br, ccanedo@ufv.br, diego.aniceto@vale.com, elpidio@ufv.br, igor.assis@ufv.br

Abstract: Technosols constructed with lateritic waste and topsoil have been applied in the ecological rehabilitation of areas impacted by the 2019 Brumadinho (MG, Brazil) tailings dam collapse. This study assessed the soil physical, chemical, and microbiological attributes in a 5-hectare rehabilitating area ("Marco Zero") over a 2.5-year period. Soils were sampled in three landscape positions (upper, middle, lower) and two reference forests across four periods. Analyses included pH, base saturation (PBS), soil organic carbon (SOC), and enzymatic activities (arylsulfatase and urease). Despite rehabilitation efforts, linear regression analyses revealed no significant temporal trends. Principal Component Analysis (PCA) identified arylsulfatase, urease, SOC, PBS, and pH as key indicators of variability. Reference areas showed higher enzymatic activities and SOC, while rehabilitating soils exhibited elevated PBS and pH, likely due to the initial amendments. Boxplots indicated spatial heterogeneity and incomplete convergence between Technosols and reference soils, particularly in microbial indicators. These findings highlight the slow and non-linear trajectory of Technosol development in early restoration stages. Our results highlight the importance of long-term monitoring of both chemical and biological soil properties to gain a deeper understanding of ecosystem functionality and recovery trajectories in post-disaster contexts.

Keywords: Dam failure, enzymatic activity, soil function, ecosystem rehabilitation monitoring.

1. Introduction

The Iron Quadrangle (IQ) in southeastern Brazil is globally recognized for its geological complexity, mineral wealth, and ecological significance. Characterized by mountainous landscapes composed of iron-rich banded iron formations (Bekker et al., 2010; Klein, 2005), this region preserves over 3 billion years of Earth's history, spanning the Archean to Proterozoic eons (Alkmim and Marshak, 1998; Dornellas et al., 2024). Furthermore, it serves as a critical ecoregion within the Atlantic Forest biome, harboring a high degree of biodiversity, a significant level of plant endemism, and distinctive vegetation such as *campo rupestre* grasslands (Fernandes-Filho et al., 2022). Nevertheless, the intensification of mining activities over the past century has exacerbated ecological degradation and environmental risks (Salles et al., 2019), underscoring the persistent conflict between mineral exploitation and biodiversity conservation (Cavalcanti et al., 2023).

Brazil ranks among the world's top iron ore exporters, with the IQ, Carajás, and the Southern Espinhaço Range driving this dominance (Saes and Bisht, 2020). In 2021 alone, iron ore accounted for 74% of the nation's mineral exports, up from 66% in 2020 (Dornellas et al., 2024), primarily propelled by the expansion of Vale S.A. since 1942. Yet, the rapid economic benefits of mining have come at a high environmental and social cost, including deforestation, water pollution, and catastrophic dam failures. Between 2015 and 2019, the IQ region experienced two of the most severe environmental disasters in Brazil's history. The 2015 Fundão dam collapse in Mariana released around 50 million m^3 of tailings across 600 km of the Doce River basin (Carmo et al., 2017; Queiroz et al., 2022). In 2019, the failure of dam B1 at the Córrego do Feijão mine in Brumadinho discharged ~12 million m^3 of tailings into the Paraopeba River system (Porsani et al., 2019; Thompson et al., 2020), resulting in 272 fatalities, the destruction of 70.56 ha of Permanent Preservation Areas, and the loss of 133.27 ha of native Atlantic Forest vegetation (Vergilio et al., 2020).

The Brumadinho disaster profoundly altered soil properties and quality in the affected landscapes (Buch et al., 2024), undermining the viability of natural regeneration. The possible presence of potentially toxic elements (PTEs) in these disturbed soils further compromises key ecological processes vital for local biodiversity (Guo et al., 2022). Additionally, the mandatory removal of tailings by court order has stripped many sites of topsoil and native seed banks, compounding restoration challenges and rendering conventional afforestation insufficient.

Innovative approaches have emerged to address the complex demands of ecological restoration. One promising strategy involves the development and application of Technosols—engineered soils created from mineral and organic materials sourced from industrial residues, urban waste, or local by-products. These soils are not inert substrates but are designed to recover or enhance critical ecosystem functions, including soil structure, nutrient cycling, and biological activity (Barredo et al., 2020; Fabbri et al., 2021; Grard et al., 2025; Séré et al., 2008). Technosols have recently demonstrated success in multiple applications, from carbon sequestration (Ruiz et al., 2023), and urban greening to the rehabilitation of mined and dam-affected sites, as well as post-industrial landscapes (Fourvel et al., 2019; Imbaná et al., 2024; Ivashchenko et al., 2021; Watteau et al., 2019). When tailored to site-specific conditions, these soils can facilitate the establishment of vegetation, stabilize substrates, and promote microbial activity crucial for ecological succession (Khelifi et al., 2025; Silva et al., 2024).

However, the long-term sustainability of Technosol-based restoration requires systematic evaluation. Functional monitoring is as important as initial soil construction and must consider local climate, topography, substrate composition, and management practices. While chemical amendments, such as liming and fertilization, may yield rapid improvements in soil pH or base saturation, they may not necessarily reflect the broader health of the ecosystem. In contrast, biological indicators—such as enzymatic activity and organic matter dynamics—offer sensitive and integrative measures of ecological recovery (Bieluczyk et al., 2025; Ferreira et al., 2025).

In this context, a Technosol was constructed in the "Marco Zero" (Mz) area in Brumadinho-MG to enable vegetation regrowth and resume critical ecosystem processes lost after the dam B1 collapsed. The designation 'Mz' stems from the fact that this area served as the first ecological restoration test site following the failure of the mining tailings dam. Despite the urgency of these efforts, empirical evidence on the performance of such interventions remains limited. Given the complexity of pedogenesis in anthropogenically altered substrates, continuous monitoring is essential for identifying trends and informing adaptive management. Furthermore, comparing Technosol's performance with that of nearby reference ecosystems provides a valuable benchmark for setting realistic restoration goals under local environmental conditions.

This study aimed to assess the ecological functionality of Technosols constructed in the Mz area over a 2.5-year monitoring period. We hypothesize that integrated analysis of physical, chemical and microbiological indicators of this technogenic soil across space and time can provide reliable insights into ecosystem health and help ensure the long-term sustainability of restoration in post-disaster landscapes.

2. Material and Methods

2.1. Study site description

The study area is a reclaimed site affected by the collapse of an iron tailings dam in Southeastern Brazil, known as "Marco Zero" (MZ), at the confluence of the Ferro-Carvão stream and the Paraopeba River in Brumadinho (Figure 1). This 5-hectare area has undergone approximately five years of rehabilitation, involving the removal of tailings, reshaping of the landscape with sterile mining material, application of topsoil, and the use of Green Wall technology. The sterile mining material was then topped with stockpiled topsoil and stabilized using a bio-blanket (Imbaná et al., 2024). Before reforestation, liming and fertilization were performed to enhance soil conditions. To increase biodiversity, cover crops and fast-growing native species such as *Cecropia* spp. (guava trees), *Tabebuia* sp. (trumpet trees), *Anadenanthera colubrina* (angico), and others were planted. Brumadinho has a tropical climate with dry winters and hot summers (*Cwa*). The region experiences an average annual temperature of 21.3°C and receives 1,325 mm of precipitation annually, mainly concentrated between November and April (Alvares et al., 2013). The region's geology is dominated by itabirite formations, with the main soil types being Latosols and Cambisols. (Embrapa, 2018). The local vegetation consists of a secondary, semi-deciduous, seasonal forest in a moderate stage of regeneration. (IBGE, 2012).

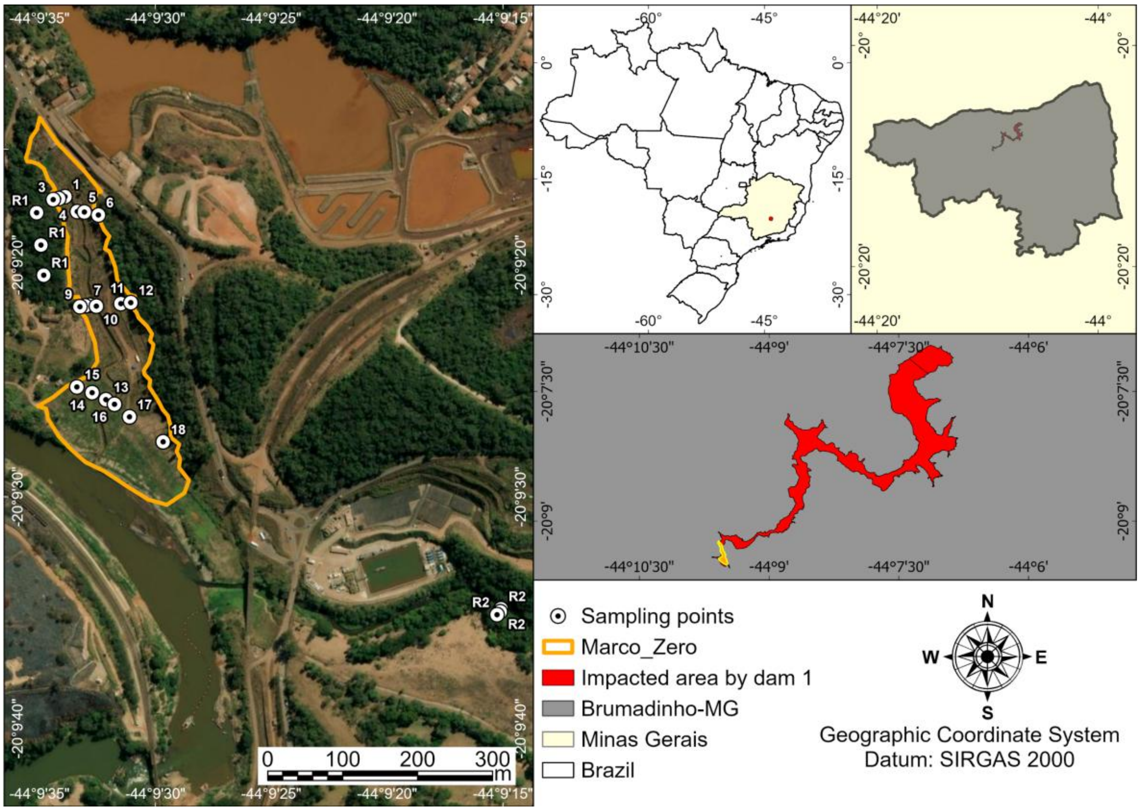

Figure 1 – Geographical locations of the study area and designated soil sampling points.

2.2. Fieldwork

During the fieldwork, the MZ area was divided into three sections: upper third (Mz_U), middle third (Mz_M), and lower third (Mz_L) near the Paraopeba River. Mz_U included sampling points 1-6, Mz_M 7-12, and Mz_L 13-18 (Figure 1). We also established two reference transects: one in a forested area along the left bank of the Ferro-Carvão stream (R1 in Figure 1), and another in the riparian forest along the Casa Branca stream (R2 in Figure 1). We collected six soil samples from 0–20 cm depth in each section (Mz_U, Mz_M, Mz_L) and three from each reference area (R1 and R2). Sampling occurred at intervals of six months (July 2020), one and a half years (August 2021), two years (March 2022), and two and a half years (September 2022) after the initiation of the rehabilitation process in January 2020. The samples were air-dried, ground, and passed through a 2-mm *mesh sieve*.

2.3. Soil properties

The bulk density (Bd, g cm^{-3}) was determined on-site using the excavation method (Al-shammary et al., 2018). The pH was measured in a soil-to-water ratio of 1:2.5. For the extraction of exchangeable Ca^{2+} and Mg^{2+} ions, a 1 M KCl solution was used. The Ca^{2+} and Mg^{2+} concentrations were analyzed using atomic absorption spectroscopy (AAS) (Embrapa, 2017). The available K, B, Cu, Zn, Fe, and Mn were extracted using a Mehlich-1 extraction solution (HCl 0.05 M and H_2SO_4 0.025 M) and then determined using AAS. The remaining P (Prem) was obtained via photocolorimetry after shaking the soil sample with a $CaCl_2$ 0.01 M solution containing 60 mg L^{-1} of P for one h (at a 1:10 soil-solution ratio). The Prem in solution indicates the soil's P adsorption capacity.

We measured soil organic carbon (SOC, dag kg^{-1}) using a CHNS elemental analyzer with a dry combustion method (Carmo and Silva, 2012). Colorimetric analysis at pH 6.5 and 11, conducted at 37°C for one hour, was used to evaluate, respectively, the enzymatic activities of acid and alkaline phosphatases (Eivazi and Tabatabai, 1977). The quantification of β-glycosidase was performed by colorimetry at pH 6 and 37°C for one hour (Eivazi and Tabatabai, 1988). The arylsulfatase enzyme was also determined by colorimetry at pH 5.8, 37°C, for one hour (Tabatabai and Bremner, 1970). The urease enzyme was assayed by colorimetry at pH 6.7, 37°C for two hours (Kandeler and Gerber, 1988).

2.4. Statistical analysis

Statistical analyses were performed in R (R Core Team, 2024). Soil attributes for the Minimum Data Set (MDS) were selected based on expert judgment and Principal Component Analysis (PCA) using the 'FactoMineR' (Lê et al., 2008) and 'Factoextra' (Kassambara and Mundt, 2020) packages. Temporal similarity between Marco Zero sections (Mz_U, Mz_M, Mz_L) and reference areas (R1, R2) was evaluated through simple linear regression models using 'ggpmisc' (Aphalo and Slowikowski, 2023), with data manipulation via 'tidyverse' (Wickham et al., 2019) and figure text customization using 'ggtext' (Wilke and Wiernik, 2022). Residual normality and variance homogeneity were assessed by Shapiro-Wilk and Bartlett's tests, respectively, using 'agricolae' (Mendiburu, 2019). When assumptions were violated, the Kruskal-Wallis test followed by Dunn's post hoc test was applied. Statistical significance was set at $p < 0.05$.

3. Results

To assess the temporal dynamics of ecosystem rehabilitation following the Córrego do Feijão dam failure and Technosol construction, simple linear regression analyses were applied to eighteen soil attributes across four monitoring periods over 2.5 years at the "Marco Zero" (Mz) area (Figure S1). No statistically significant temporal trends were observed for any of the variables. To reduce data dimensionality and identify key variables explaining most of the variance in soil properties across space and time, Principal Component Analysis (PCA) was conducted using the complete soil dataset. A minimum dataset was produced (Figures 2, 3, and 4), including arylsulfatase activity (Aryls), percentage of base saturation (PBS), soil solution pH, soil organic carbon (SOC), and urease activity (Ur). The PCA revealed that the first principal component (PC1) explained 52.06% of the variance, while the second component (PC2) accounted for an additional 24.43%, totaling 76.49% of the overall variation in the data (Figure 2).

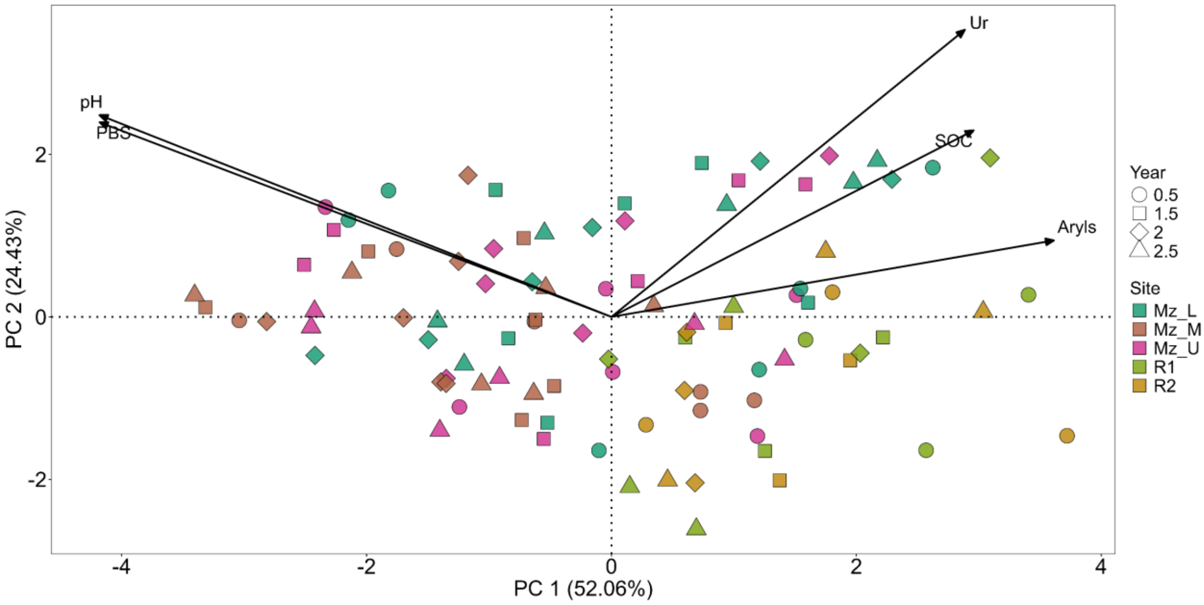

Figure 2 – PCA plot to understand the relationships between MDS, sampling points, and the PCs summarizing the data's variance.

Reference areas (R1 and R2) exhibited tight clustering in the PCA plot, suggesting internal similarity in their soil attributes. These reference samples were most strongly associated with high SOC content and elevated enzymatic activities (Aryls and Ur), as indicated by the alignment of the respective vectors (Figure 2). In contrast, samples from the rehabilitating Mz area, distributed across upper (Mz_U), middle (Mz_M), and lower (Mz_L) sections toward the Paraopeba River, were spread more broadly in the PCA space, showing heterogeneity in soil conditions. PBS and pH were associated with samples from the Mz area, with vector directions orthogonal to those of the enzymatic activities, implying different patterns of variance and potentially contrasting soil processes. The PCA thus highlighted a clear separation in chemical and biological attributes between rehabilitated and reference soils.

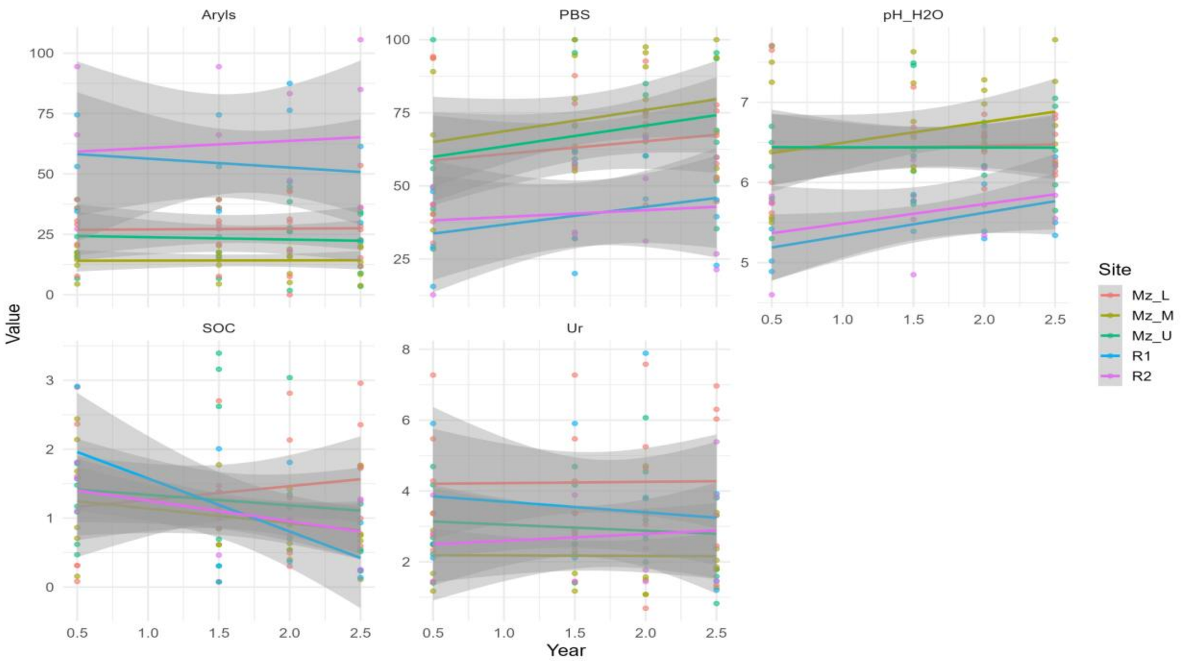

Figure 3 – Simple linear regression analyses by minimum dataset, comparing sites by year. The gray shaded area around the regression line indicates the 95% confidence interval for predicted mean values, reflecting uncertainty in the fitted relationship.

Figure 3 presents the results of simple linear regression analyses for each selected variable by site and year. Aryl's activity consistently exhibited higher values in the reference areas R1 and R2 across all sampling periods. The activity remained lower in Mz_U, Mz_M, and Mz_L, with no temporal fluctuation. PBS showed the opposite trend, with higher values observed in the Mz sections in all periods, with insignificant temporal progression, while reference sites had the lowest PBS levels. Soil pH followed a similar pattern to PBS, with higher values in the Mz sections compared to the references. SOC displayed intermediate values in Mz sectors, approaching values seen in the reference sites. Urease activity displayed a similar trend, with values in the Mz sections overlapping those in the R1 and R2 areas.

Figure 4 shows boxplots summarizing the distribution of each selected soil property across reference areas (R1 and R2) and rehabilitating Mz sections (Mz_U, Mz_M, and Mz_L). For Aryls, reference sites had higher median values and narrower interquartile ranges, indicating more consistent and elevated enzymatic activity. In contrast, all three Mz sectors showed lower medians and greater variability, with occasional outliers suggesting heterogeneity in microbial function.

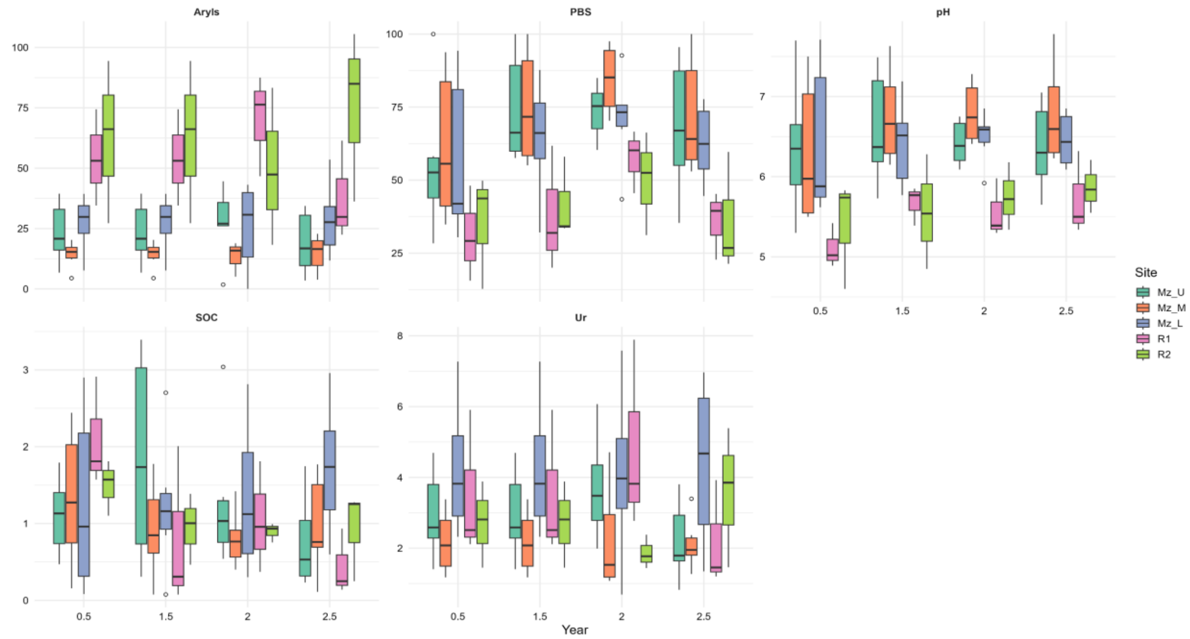

Figure 3 – Boxplots of the constructed Technosol minimum dataset values among sections of the "Marco Zero" area and the soil of the reference areas for depths of 0–20 cm.

PBS values were higher in the Mz sectors, with the highest medians and broader distributions. Reference sites exhibited lower PBS values with tight distributions. This pattern was mirrored in soil pH, which also presented higher values in the Mz sections compared to the reference areas. SOC in Mz sections was consistently similar to those in the reference sites, with more compact distributions indicating stable organic matter content. Urease activity followed a trend similar to SOC. Collectively, these results demonstrate spatial variability in soil chemical and biological attributes across the rehabilitating and reference areas. While specific properties, such as PBS and pH, were elevated in the rehabilitating soils, likely reflecting construction and amendment practices, others, like Aryls and Ur, remained consistently lower than in reference areas. SOC and Ur showed signs of partial convergence with reference levels, suggesting variable trajectories in the reestablishment of soil functions.

4. Discussion

An increasing number of studies have explored the use of Technosols constructed with diverse anthropogenic materials to address a wide range of environmental and social challenges. These include sustainable solid waste management, urban greening, food production, carbon sequestration, advancing pedogenetic understanding, and the restoration of ecosystems degraded by urbanization, mining, dam failures, and other anthropogenic disturbances (Barredo et al., 2020; Fourvel et al., 2019; Grard et al., 2025; Imbaná et al., 2024; Ruiz et al., 2023, 2022; Séré et al., 2010; Silva et al., 2024; Tarnawczyk et al., 2024; Uzarowicz et al., 2018). In restoration contexts, the design of Technosols must integrate ecological functionality to support processes such as species recruitment and faunal recolonization. This is essential whether the goal is to recreate pre-disturbance conditions or establish novel ecosystems capable of delivering ecosystem services under altered environmental regimes (Castro et al., 2023; Gastauer et al., 2020, 2019).

The lack of statistically significant trends in key soil parameters over 2.5 years of monitoring in the "Marco Zero" (Mz) area (Figure S1) highlights the inherent complexity of early-stage soil rehabilitation following the Córrego do Feijão tailings dam collapse. While some variability was expected, the absence of consistent improvement suggests that foundational soil processes—such as organic matter accumulation, nutrient cycling, and microbial activity—remain in early stages of development (Colombini et al., 2022; Ferreira et al., 2025). This reinforces the view that Technosol-driven ecological restoration follows a slow, non-linear trajectory (Zhao et al., 2024), where short-term assessments may fail to capture incipient but critical shifts in soil function, especially at the macroscale (Zhong et al., 2023). Nevertheless, the strategic integration of mineral and organic components into Technosols can enhance soil functionality, support vegetation establishment, and facilitate successional dynamics (Barredo et al., 2020; Colombini et al., 2022; Raupp et al., 2024; Song et al., 2024).

Principal component analysis was employed to interpret complex soil datasets and highlight the most informative indicators of rehabilitation progress. By comparing Mz sections (Mz_U, Mz_M, Mz_L) against reference sites (R1 and R2), PCA effectively reduced dimensionality and emphasized key gradients in soil condition (Rutledge, 2018; Wold et al., 1987). Reference areas, unaffected by the dam failure, clustered tightly and displayed high levels of soil organic carbon (SOC) and enzymatic activities (arylsulfatase and urease), biological proxies for mature microbial communities and stable nutrient cycling (Bieluczyk et al., 2025; Ferreira et al., 2025). The consistent values observed in these reference areas offer robust benchmarks for restoration evaluation. In contrast, the Mz samples were more dispersed, reflecting spatial heterogeneity in early Technosol development (Bandyopadhyay and Maiti, 2021). This variability likely stems from differences in substrate composition and amendment application (Imbaná et al., 2024; Khelifi et al., 2025). PCA vectors showed that PBS and pH were positively associated with Mz areas, likely reflecting initial liming interventions (Klajman et al., 2024; Neina, 2019; Wenyika et al., 2025), while SOC and enzymatic indicators were aligned with the reference sites.

These interpretations were supported by regression analyses, which showed consistently higher arylsulfatase activity in reference areas and lower, more variable values in Mz. As arylsulfatase activity is closely linked to microbial function and sulfur cycling, its reduced levels in Mz confirm the slower pace of biological recovery relative to chemical reconditioning (Adetunji et al., 2017; Fekete et al., 2024; Forján et al., 2024; Zine et al., 2024). Elevated PBS and pH in Mz further indicate that chemical modifications occur more rapidly through amendments, but these do not necessarily correspond with functional soil recovery (Pietrzykowski et al., 2024). SOC and urease activity in Mz sectors showed intermediate values, suggesting incipient biological improvements and potential convergence toward reference conditions. Such early shifts in microbial processes may serve as sensitive indicators of functional recovery, even before complete ecosystem restoration is achieved (Awasthi et al., 2014; Lu et al., 2022; Zhang et al., 2024).

Boxplots reinforced these trends, illustrating the stability and high biological activity of reference areas and the greater variability within Mz. While Mz showed signs of progress, particularly in SOC and enzymatic indicators, elevated PBS and pH levels remained dominant across all subsections, consistent with the impacts of chemical amendments. This highlights the need to integrate multiple indicators, biological, chemical, and physical, when assessing Technosol performance, as no single parameter can fully capture the system’s complexity. Ultimately, these findings confirm the potential of Technosols as a tool for post-mining and post-dam collapse restoration. Their engineered composition allows for targeted interventions that support both abiotic and biotic recovery. However, the disconnect observed between chemical improvements and biological limitations emphasizes the importance of integrative strategies. Restoration success requires striking a balance between nutrient availability and microbial development to foster resilient, self-sustaining ecosystems. Reference sites play a critical role not only as baselines but as dynamic functional targets. They help define restoration trajectories that are ecologically meaningful and locally feasible. Given the heterogeneity observed in the Marco Zero area, future efforts should incorporate broader ecological indicators, such as microbial diversity, vegetation structure, and soil fauna, to more comprehensively evaluate Technosol functionality and guide long-term restoration planning.

5. Conclusion

Technosols constructed in the “Marco Zero” (Mz) area after the Córrego do Feijão dam failure present chemical and biological potential for ecological restoration. However, 2.5 years of monitoring revealed no significant temporal changes in key soil properties. Arylsulfatase, urease, SOC, base saturation, and pH were identified as the most sensitive indicators for assessing soil quality trajectories.

The Mz area remains chemically distinct and biologically limited compared to reference ecosystems, reflecting the influence of initial amendment inputs and the slow pace of Technosol development. These results highlight the need for long-term monitoring, the use of multiple soil quality indicators, and the adoption of reference areas as functional benchmarks. To improve soil functionality and support ecosystem recovery, future restoration efforts must integrate chemical, physical, and biological strategies.

Acknowledgments

We thank Vale S.A. for funding and supporting the fieldwork, as well as the Coordination for the Improvement of Higher Education Personnel (CAPES) – Financial Code 001, and the National Council for Scientific and Technological Development (CNPq) – Financial Code 001, for their financial support. These contributions were essential to the success of this study.

References

Adetunji, A.T., Lewu, F.B., Mulidzi, R., Ncube, B., 2017. The biological activities of β-glucosidase, phosphatase and urease as soil quality indicators: A review. Soil Sci Plant Nutr 17, 794–807. https://doi.org/10.4067/s0718-95162017000300018

Alkmim, F.F., Marshak, S., 1998. Transamazonian Orogeny in the Southern São Francisco Craton Region, Minas Gerais, Brazil: evidence for Paleoproterozoic collision and collapse in the Quadrilátero Ferrífero. Precambrian Res 90, 29–58. https://doi.org/10.1016/S0301-9268(98)00032-1

Al-shammary, A.A.G., Kouzani, A.Z., Kaynak, A., Khoo, S.Y., Norton, M., Gates, W., 2018. Soil Bulk Density Estimation Methods: A Review. Pedosphere 28, 581–596. https://doi.org/10.1016/s1002-0160(18)60034-7

Alvares, C.A., Stape, J.L., Sentelhas, P.C., De Moraes Gonçalves, J.L., Sparovek, G., 2013. Köppen's climate classification map for Brazil. Meteorologische Zeitschrift 22, 711–728. https://doi.org/10.1127/0941-2948/2013/0507

Aphalo, P., Slowikowski, K., 2023. ggpmisc: Miscellaneous Extensions to ggplot2.

Awasthi, A., Singh, M., Soni, S.K., Singh, R., Kalra, A., 2014. Biodiversity acts as insurance of productivity of bacterial communities under abiotic perturbations. ISME Journal 8, 2445–2452. https://doi.org/10.1038/ismej.2014.91

Bandyopadhyay, S., Maiti, S.K., 2021. Application of statistical and machine learning approach for prediction of soil quality index formulated to evaluate trajectory of ecosystem recovery in coal mine degraded land. Ecol Eng 170, 106351. https://doi.org/10.1016/j.ecoleng.2021.106351

Barredo, O., Vilela, J., Garbisu, C., Besga, G., Alkorta, I., Epelde, L., 2020. Technosols made from urban and industrial wastes are a good option for the reclamation of abandoned city plots. Geoderma 377, 114563. https://doi.org/10.1016/j.geoderma.2020.114563

Bekker, A., Slack, J.F., Planavsky, N., Krapež, B., Hofmann, A., Konhauser, K.O., Rouxel, O.J., 2010. Iron formation: the sedimentary product of a complex interplay among mantle, tectonic, oceanic, and biospheric processes. Econ. Geol. 105, 467–508. https://doi.org/10.2113/gsecongeo.105.3.467

Bieluczyk, W., Duarte, M.P., Camargo, P.B. de, Noronha, N.C., Piccolo, M. de C., Tsai, S.M., 2025. Restoration of soil health by Amazonian secondary forests is severely eroded by slash-and-burn recurrence. Catena (Amst) 254, 108925. https://doi.org/10.1016/j.catena.2025.108925

Buch, A.C., Sims, D.B., de Ramos, L.M., Marques, E.D., Ritcher, S., Abdullah, M.M.S., Silva-Filho, E.V., 2024. Assessment of environmental pollution and human health risks of mine tailings in soil: after dam failure of the Córrego do Feijão Mine (in Brumadinho, Brazil). Environ Geochem Health 46, 1–23. https://doi.org/10.1007/s10653-024-01870-2

Carmo, D.L., Silva, C.A., 2012. Métodos de quantificação de carbono e matéria orgânica em resíduos orgânicos. Rev Bras Cienc Solo 36, 1211–1220. https://doi.org/10.1590/s0100-06832012000400015

Carmo, Flávio Fonseca do, Kamino, L.H.Y., Junior, R.T., Campos, I.C. de, Carmo, Felipe Fonseca do, Silvino, G., Castro, K.J. da S.X. de, Mauro, M.L., Rodrigues, N.U.A., Miranda, M.P. de S., Pinto, C.E.F., 2017. Fundão tailings dam failures: the environment tragedy of the largest technological disaster of Brazilian mining in global context. Perspect Ecol Conserv 15, 145–151. https://doi.org/10.1016/j.pecon.2017.06.002

Castro, A.F. de, Assis, I.R. de, Caldeira, C.F., Ramos, S.J., Coelho, R.R., Oliveira, G.C. de, Medeiros-Sarmento, P.S., Gastauer, M., 2023. Minimum thresholds of key ecological attributes facilitate the tracking of mineland restoration. Resources Policy 84, 103722. https://doi.org/10.1016/j.resourpol.2023.103722

Cavalcanti, J.A.D., da Silva, M.S., Schobbenhaus, C., Atencio, D., Mota de Lima, H., 2023. Geoconservation of geological and mining heritage related to banded iron formation of Itabira Group, Quadrilátero Ferrífero, Minas Gerais, Brazil: A challenging issue. International Journal of Geoheritage and Parks 11, 118–148. https://doi.org/10.1016/j.ijgeop.2022.12.002

Colombini, G., Watteau, F., Auclerc, A., 2022. Technosol rehabilitation strategies drive soil physico-chemical properties and fauna diversity on a former coking plant area. Applied Soil Ecology 177, 104542. https://doi.org/10.1016/j.apsoil.2022.104542

Dornellas, L.M.S.M., da Silva, P.G., Auler, A.S., Culver, D.C., Pipan, T., 2024. Subterranean fauna associated with mesovoid shallow substratum in canga formations from southeastern Brazil: invertebrate biodiversity of a highly threatened ecosystem. Sci Rep 14, 23211. https://doi.org/10.1038/S41598-024-75053-5

Eivazi, F., Tabatabai, M.A., 1988. Glucosidases and galactosidases in soils. Soil Biol Biochem 20, 601–606. https://doi.org/10.1016/0038-0717(88)90141-1

Eivazi, F., Tabatabai, M.A., 1977. Phosphatases in soils. Soil Biol Biochem 9, 167–172. https://doi.org/10.1016/0038-0717(77)90070-0

Embrapa, 2018. Sistema brasileiro de classificação de solos, Empresa Brasileira de Pesquisa Agropecuária.

Embrapa, 2017. Manual de métodos de análise de solo., Manual de Métodos de Análise de Solo. Brasília, DF: Embrapa, 2017.

Fabbri, D., Pizzol, R., Calza, P., Malandrino, M., Gaggero, E., Padoan, E., Ajmone-Marsan, F., 2021. Constructed Technosols: A Strategy toward a Circular Economy. Applied Sciences 11. https://doi.org/10.3390/app11083432

Fekete, R., Valkó, O., Fischer, L.K., Deák, B., Klaus, V.H., 2024. Ecological restoration and biodiversity-friendly management of urban grasslands – A global review on the current state of knowledge. J Environ Manage 368, 122220. https://doi.org/10.1016/j.jenvman.2024.122220

Fernandes-Filho, E.I., Reynaud Schaefer, C.E.G., Faria, R.M., Lopes, A., Francelino, M.R., Gomes, L.C., 2022. The unique and endangered Campo Rupestre vegetation and protected areas in the Iron Quadrangle, Minas Gerais, Brazil. J Nat Conserv 66, 126131. https://doi.org/10.1016/j.jnc.2022.126131

Ferreira, L. de S., Lima, H.S., de Castro, A.G., de Carvalho, K.B., Silva, W.M., Prado, I.G. de O., de Assis, I.R., Aniceto, D., Kasuya, M.C.M., de Paula, S.O., da Silva, C.C., 2025. Microbial community structure and nitrogen cycling in an area affected by the tailings dam collapse under a rehabilitation process. Applied Soil Ecology 209, 106045. https://doi.org/10.1016/j.apsoil.2025.106045

Forján, R., Arias-Estévez, M., Gallego, J.L.R., Santos, E., Arenas-Lago, D., 2024. Biochar-nanoparticle combinations enhance the biogeochemical recovery of a post-mining soil.

Science of The Total Environment 930, 172451. https://doi.org/10.1016/j.scitotenv.2024.172451

Fourvel, G.J., Vidal-Beaudet, L., Le Bocq, A., Thery, F., Brochier, V., Cannavo, P., 2019. Fertility of Technosols constructed with dam sediments for urban greening and land reclamation. J Soils Sediments 19, 3178–3192. https://doi.org/10.1007/s11368-018-2077-1

Gastauer, M., Caldeira, C.F., Ramos, S.J., Trevelin, L.C., Jaffé, R., Oliveira, G., Vera, M.P.O., Pires, E., Santiago, F.L. de A., Carneiro, M.A.C., Coelho, F.T.A., Silva, R., Souza-Filho, P.W.M., Siqueira, J.O., 2020. Integrating environmental variables by multivariate ordination enables the reliable estimation of mineland rehabilitation status. J Environ Manage 256, 109894. https://doi.org/10.1016/j.jenvman.2019.109894

Gastauer, M., Souza Filho, P.W.M., Ramos, S.J., Caldeira, C.F., Silva, J.R., Siqueira, J.O., Furtini Neto, A.E., 2019. Mine land rehabilitation in Brazil: Goals and techniques in the context of legal requirements. Ambio 48, 74. https://doi.org/10.1007/s13280-018-1053-8

Grard, B.J.P., Barrier-Guillot, A., Chenu, C., 2025. Early pedogenesis of a young Technosol made from organic wastes. Geoderma 459, 117343. https://doi.org/10.1016/j.geoderma.2025.117343

Guo, Y., Sun, Y., Li, Z., Feng, S., Yang, R., Qu, L., 2022. Detection, detoxification, and removal of multiply heavy metal ions using a recyclable probe enabled by click and declick chemistry. J Hazard Mater 423, 127242. https://doi.org/10.1016/j.jhazmat.2021.127242

IBGE, 2012. Manual Técnico da Vegetação Brasileira, 2 edição r. ed. Coordenação de Recursos Naturais e Estudos Ambientais, Rio de Janeiro.

Imbaná, R., Valente, F.D.A., Siqueira, R.G., Moquedace, C.M., Assis, I.R., 2024. Assessing the quality of constructed technosols enabled holistic monitoring of ecological restoration. J Environ Manage 353. https://doi.org/10.1016/j.jenvman.2024.120237

Ivashchenko, K., Lepore, E., Vasenev, V., Ananyeva, N., Demina, S., Khabibullina, F., Vaseneva, I., Selezneva, A., Dolgikh, A., Sushko, S., Marinari, S., Dovletyarova, E., 2021. Assessing Soil-like Materials for Ecosystem Services Provided by Constructed Technosols. Land (Basel) 10. https://doi.org/10.3390/land10111185

Kandeler, E., Gerber, H., 1988. Short-term assay of soil urease activity using colorimetric determination of ammonium. Biol Fertil Soils 6, 68–72. https://doi.org/10.1007/bf00257924

Kassambara, A., Mundt, F., 2020. factoextra: Extract and Visualize the Results of Multivariate Data Analyses.

Khelifi, F., Zhao, X., Dino, G.A., Padoan, E., 2025. Quality assessment of new constructed technosols: Key findings on their biogeochemical and environmental characteristics. J Hazard Mater 489, 137571. https://doi.org/10.1016/j.jhazmat.2025.137571

Klajman, K., Beckett, P., Spiers, G., Nkongolo, K., 2024. Effects of aerial liming on soil chemical and biological properties in metal contaminated and inaccessible lands in Ontario (Canada). Ecotoxicology 33, 1145–1160. https://doi.org/10.1007/s10646-024-02804-5

Klein, C., 2005. Some Precambrian banded iron-formations (BIFs) from around the world: Their age, geologic setting, mineralogy, metamorphism, geochemistry, and origins. American Mineralogist 90, 1473–1499. https://doi.org/10.2138/am.2005.1871

Lu, M., Wang, X., Li, Y., Liu, H., An, X., Lian, B., 2022. Soil microbial community structure and environmental effects of serpentine weathering under different vegetative covers in the serpentine mining area of Donghai County, China. Science of The Total Environment 835, 155452. https://doi.org/10.1016/j.scitotenv.2022.155452

Mendiburu, F., 2019. Agricolae: statistical procedures for agricultural research. cir.nii.ac.jp.

Neina, D., 2019. The Role of Soil pH in Plant Nutrition and Soil Remediation. Appl Environ Soil Sci 2019, 1–9. https://doi.org/10.1155/2019/5794869

Pietrzykowski, M., Woś, B., Likus-Cieślik, J., Pajak, M., Sierka, E., Stalmachová, B., 2024. Restoration Ecosystem Toward Spontaneous Succession on Reclaimed Mining Sites. Biodiversity and Ecosystem Services on Post-Industrial Land 97–118. https://doi.org/10.1002/9781394187416.ch4

Porsani, J.L., de Jesus, F.A.N., Stangari, M.C., 2019. GPR Survey on an Iron Mining Area after the Collapse of the Tailings Dam I at the Córrego do Feijão Mine in Brumadinho-MG, Brazil. Remote Sensing 2019, Vol. 11, Page 860 11, 860. https://doi.org/10.3390/rs11070860

Queiroz, H.M., Ferreira, A.D., Ruiz, F., Bovi, R.C., Deng, Y., de Souza Júnior, V.S., Otero, X.L., Bernardino, A.F., Cooper, M., Ferreira, T.O., 2022. Early pedogenesis of anthropogenic soils produced by the world's largest mining disaster, the "Fundão" dam collapse, in southeast Brazil. Catena (Amst) 219. https://doi.org/10.1016/j.catena.2022.106625

Raupp, P., Carrillo, Y., Nielsen, U.N., 2024. Soil Health to Enhance Ecological Restoration and Conservation. Journal of Sustainable Agriculture and Environment 3, e70022. https://doi.org/10.1002/sae2.70022

RCoreTeam, 2024. R: A Language and Environment for Statistical Computing. R Foundation for Statistical Computing.

Ruiz, F., Andrade, G.R.P., Sartor, L.R., Santos, J.C.B. dos, Souza Júnior, V.S. de, Ferreira, T.O., 2022. The rhizosphere of tropical grasses as driver of soil weathering in embryonic Technosols (SE-Brazil). Catena (Amst) 208. https://doi.org/10.1016/j.catena.2021.105764

Ruiz, F., Safanelli, J.L., Perlatti, F., Cherubin, M.R., Demattê, J.A.M., Cerri, C.E.P., Otero, X.L., Rumpel, C., Ferreira, T.O., 2023. Constructing soils for climate-smart mining. Communications Earth & Environment 2023 4:1 4, 1–6. https://doi.org/10.1038/s43247-023-00862-x

Rutledge, D.N., 2018. Comparison of Principal Components Analysis, Independent Components Analysis and Common Components Analysis. J Anal Test 2, 235–248. https://doi.org/10.1007/s41664-018-0065-5

Saes, B.M., Bisht, A., 2020. Iron ore peripheries in the extractive boom: A comparison between mining conflicts in India and Brazil. Extr Ind Soc 7, 1567–1578. https://doi.org/10.1016/j.exis.2020.09.010

Salles, D.M., Do Carmo, F.F., Jacobi, C.M., 2019. Habitat Loss Challenges the Conservation of Endemic Plants in Mining-Targeted Brazilian Mountains. Environ Conserv 46, 140–146. https://doi.org/10.1017/s0376892918000401

Séré, G., Schwartz, C., Ouvrard, S., Renat, J.C., Watteau, F., Villemin, G., Morel, J.L., 2010. Early pedogenic evolution of constructed Technosols. J Soils Sediments 10, 1246–1254. https://doi.org/10.1007/s11368-010-0206-6

Séré, G., Schwartz, C., Ouvrard, S., Sauvage, C., Renat, J.C., Morel, J.L., 2008. Soil construction: A step for ecological reclamation of derelict lands. J Soils Sediments 8, 130–136. https://doi.org/10.1065/jss2008.03.277

Silva, B.M., Queiroz, H.M., Ferreira, A.D., Ruiz, F., Ferreira, T.O., 2024. Technosols Made from Iron Mine Tailings and Construction and Demolition Waste as an Alternative for Sustainable Solid Waste Management. Land Degrad Dev 36, 208–217. https://doi.org/10.1002/ldr.5355

Song, W., Li, J., Li, X., Xu, D., Min, X., 2024. Effects of land reclamation on soil organic carbon and its components in reclaimed coal mining subsidence areas. Science of The Total Environment 908, 168523. https://doi.org/10.1016/j.scitotenv.2023.168523

Tabatabai, M.A., Bremner, J.M., 1970. Arylsulfatase Activity of Soils. Soil Science Society of America Journal 34, 225–229. https://doi.org/10.2136/sssaj1970.03615995003400020016x

Tarnawczyk, M., Uzarowicz, Ł., Kwasowski, W., Górka-Kostrubiec, B., Pędziwiatr, A., 2024. Soil-forming factors controlling Technosol formation in historical mining and metallurgical sites in the high-alpine environment of the Tatra Mountains, southern Poland. Catena (Amst) 247, 108521. https://doi.org/10.1016/j.catena.2024.108521

Thompson, F., de Oliveira, B.C., Cordeiro, M.C., Masi, B.P., Rangel, T.P., Paz, P., Freitas, T., Lopes, G., Silva, B.S., S. Cabral, A., Soares, M., Lacerda, D., dos Santos Vergilio, C., Lopes-Ferreira, M., Lima, C., Thompson, C., de Rezende, C.E., 2020. Severe impacts of the Brumadinho dam failure (Minas Gerais, Brazil) on the water quality of the Paraopeba River. Science of The Total Environment 705, 135914. https://doi.org/10.1016/j.scitotenv.2019.135914

Uzarowicz, Ł., Skiba, M., Leue, M., Zagórski, Z., Gąsiński, A., Trzciński, J., 2018. Technogenic soils (Technosols) developed from fly ash and bottom ash from thermal power stations combusting bituminous coal and lignite. Part II. Mineral transformations and soil evolution. Catena (Amst) 162, 255–269. https://doi.org/10.1016/j.catena.2017.11.005

Vergilio, C. dos S., Lacerda, D., Oliveira, B.C.V. de, Sartori, E., Campos, G.M., Pereira, A.L. de S., Aguiar, D.B. de, Souza, T. da S., Almeida, M.G. de, Thompson, F., Rezende, C.E. de, 2020. Metal concentrations and biological effects from one of the largest mining disasters in the world (Brumadinho, Minas Gerais, Brazil). Sci Rep 10, 1–12. https://doi.org/10.1038/s41598-020-62700-w

Watteau, F., Jangorzo, N.S., Schwartz, C., 2019. A micromorphological analysis for quantifying structure descriptors in a young constructed Technosol. Boletin de la Sociedad Geologica Mexicana 71, 11–20. https://doi.org/10.18268/bsgm2019v71n1a2

Wenyika, P., Enesi, R.O., Linda, ·, Gorim, Y., Dyck, · Miles, 2025. Effects of liming on soil biota and related processes in agroecosystems: a review. Discover Soil 2025 2:1 2, 1–36. https://doi.org/10.1007/s44378-025-00063-2

Wickham, H., Averick, M., Bryan, J., Chang, W., D', L., Mcgowan, A., François, R., Grolemund, G., Hayes, A., Henry, L., Hester, J., Kuhn, M., Lin Pedersen, T., Miller, E., Bache, S.M., Müller, K., Ooms, J., Robinson, D., Seidel, D.P., Spinu, V., Takahashi, K., Vaughan, D., Wilke, C., Woo, K., Yutani, H., 2019. Welcome to the Tidyverse. J Open Source Softw 4, 1686. https://doi.org/10.21105/joss.01686

Wilke, C., Wiernik, B., 2022. ggtext: improved text rendering support for ggplot2.

Wold, S., Esbensen, K., Geladi, P., 1987. Principal component analysis. Chemom Intell Lab Syst 2, 37–52. https://doi.org/10.1016/0169-7439(87)80084-9

Zhang, H., Li, Y., Xu, Y., John, R., 2024. The recovery of soil N-cycling and P-cycling following reforestation in a degraded tropical limestone mine. J Clean Prod 448, 141580. https://doi.org/10.1016/j.jclepro.2024.141580

Zhao, H., Wei, D., Wang, X., Hong, J., Wu, J., Xiong, D., Liang, Y., Yuan, Z., Qi, Y., Huang, L., 2024. Three decadal large-scale ecological restoration projects across the Tibetan Plateau. Land Degrad Dev 35, 22–32. https://doi.org/10.1002/ldr.4928

Zhong, J., Cui, L., Deng, Z., Zhang, Y., Lin, J., Guo, G., Zhang, X., 2023. Long-Term Effects of Ecological Restoration Projects on Ecosystem Services and Their Spatial Interactions: A Case Study of Hainan Tropical Forest Park in China. Environmental Management 2023 73:3 73, 493–508. https://doi.org/10.1007/s00267-023-01892-z

Zine, H., Hakkou, R., Papazoglou, E.G., Elmansour, A., Abrar, F., Benzaazoua, M., 2024. Revegetation and ecosystem reclamation of post-mined land: toward sustainable mining. International Journal of Environmental Science and Technology 2024 21:15 21, 9775–9798. https://doi.org/10.1007/s13762-024-05697-3

Supplementary material

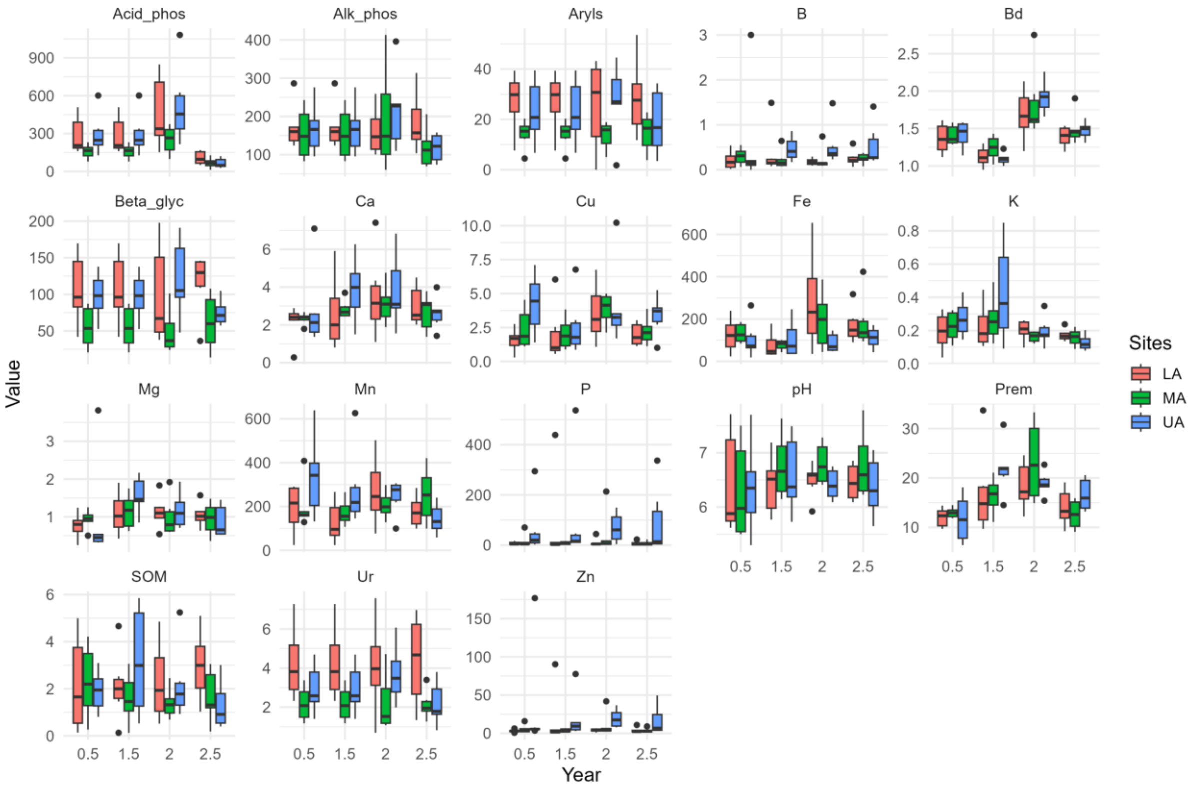

Figure S1 – Boxplots of the total dataset values among sections of the "Marco Zero" area for the depths of 0–20 cm.

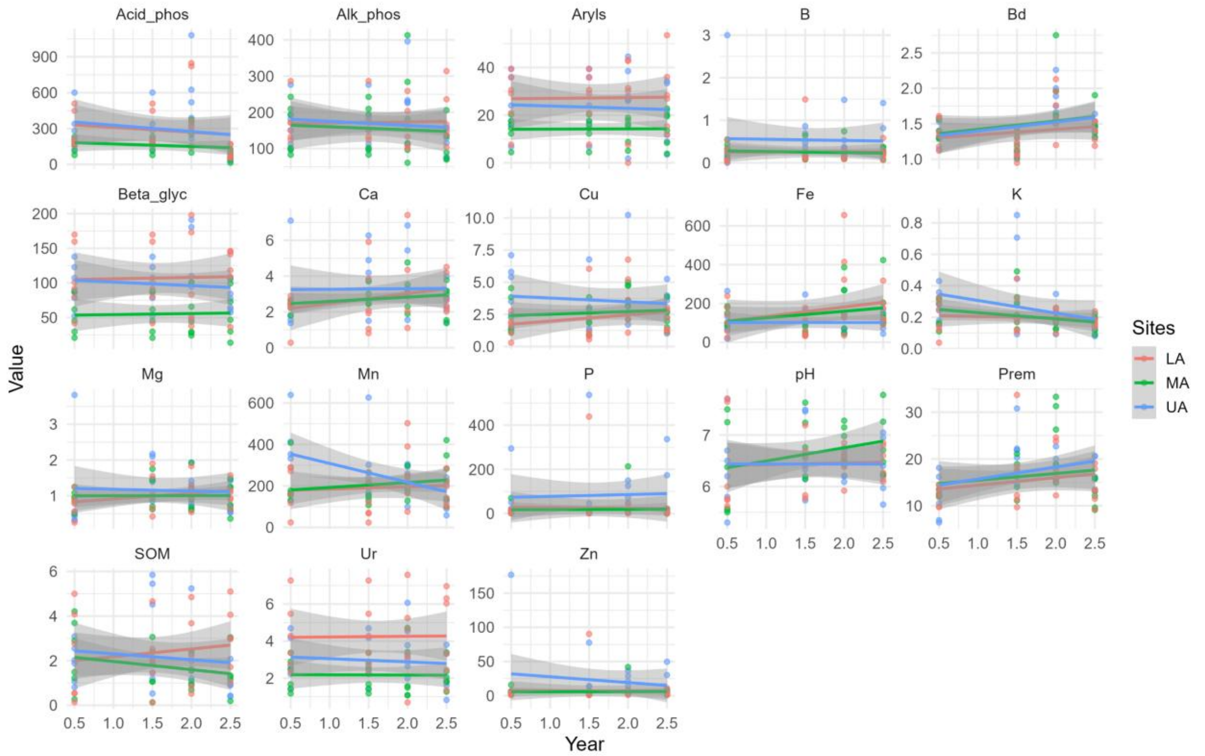

Figure S2 – Simple linear regression of the total dataset values across sections of the "Marco Zero" area for the depths of 0–20 cm.

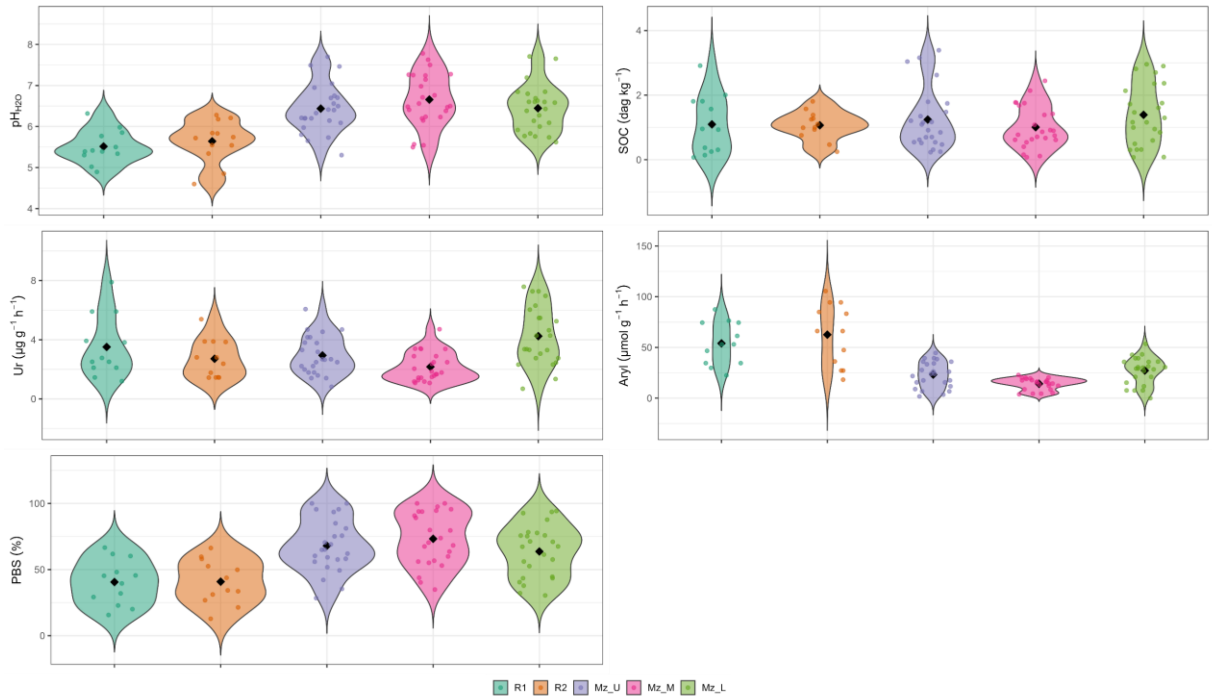

Figure S3 – Boxplots of the minimum dataset values among sections of the "Marco Zero" area (Mz_U, Mz_M, and Mz_L) and reference areas (R1 and R2) for the depths of 0–20 cm**.**

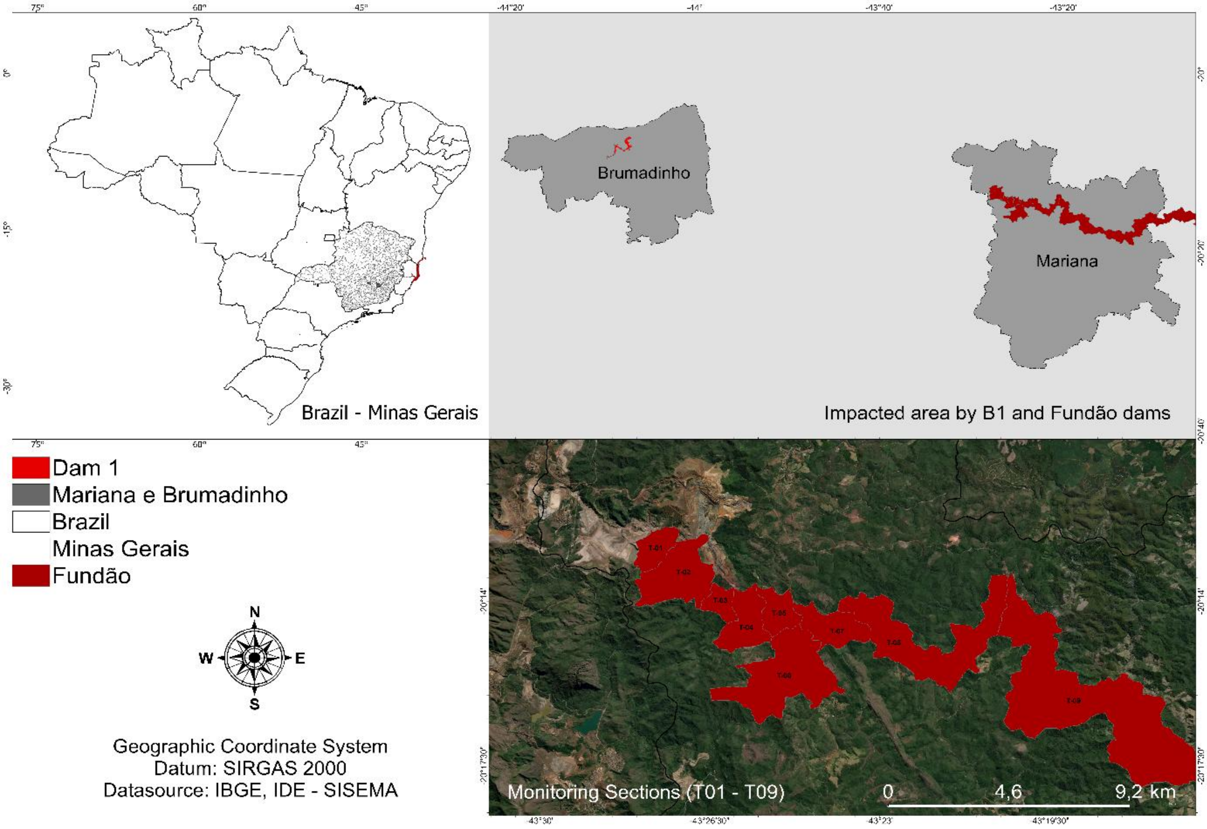

Figure S4 – An illustration depicting the regions impacted by the two significant collapses of iron mining tailings dams in the Iron Quadrangle.

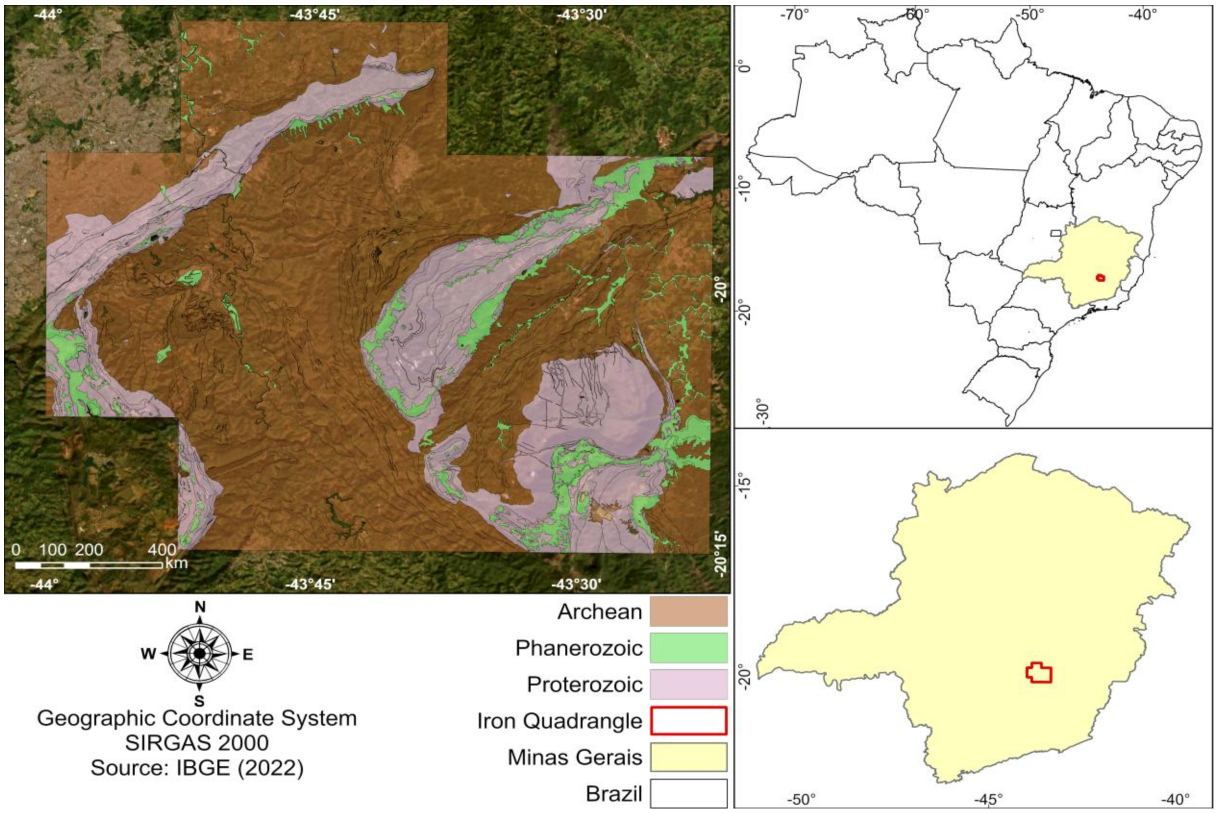

Figure S5 – The Iron Quadrangle: The geological age of its rocks within the state of Minas Gerais in southeastern Brazil.

Chapter 2: Exploring the annual seasonal impacts on the ecological restoration of post-mining sites

Rugana Imbaná[a]*, Fernanda Daniele de Almeida Valente[a], Maísa Quintiliano Alves[a], Sandro Lucio Silva Moreira[a], Fernanda Zeidan Oliveira[a], Amanda de Abreu Anunciação[a], Rosilene Rodrigues Silva[b], Felipe Tadashi Asao Coelho[b], Igor Rodrigues de Assis[a]

[a] Department of Soil Science, Universidade Federal de Viçosa, R. Purdue S/N, Campus Universitário, Viçosa, Minas Gerais, 36570-900, Brazil.

[b] Mineração Corumbaense Reunida S.A. – Vale S.A., Corumbá, Mato Grosso do Sul, Brazil, 79332-900.

E-mail addresses: rugana.imbana@ufv.br*, fernanda.daniele@ufv.br, maisa.alves@ufv.br, sandro.moreira@ufv.br, fernanda.zeidan@ufv.br, amanda.anunciacao@ufv.br, rosilene.silva@vale.com, felipe.coelho@vale.com, igor.assis@ufv.br

Abstract: Seasonal variations significantly influence post-mining restoration outcomes. In dynamic ecosystems like the Pantanal, the wet season fosters plant recruitment but also increases soil erosion risks, while the dry season limits vegetative growth yet reduces erosion. To assess these dynamics, we developed a Rehabilitation Quality Index (RQI) alongside permutation tests (resemblance), integrating field surveys and laboratory analyses to select, weigh, and score key environmental attributes. Our findings indicate that post-mining sites exhibit soil and vegetation characteristics similar to some reference areas during the rainy season, suggesting improved ecological function. However, this trend does not persist in the dry season, likely due to inadequate vegetation cover and the shallow nature of technogenic soils, which restrict water retention. Despite seasonal fluctuations, most selected attributes remained stable, reinforcing the crucial role of water and nutrient availability in driving ecosystem recovery. The RQI effectively captured these seasonal shifts, highlighting the need for tailored reclamation strategies. Reclamation efforts should prioritize site resilience, particularly during challenging dry periods, by improving soil water retention and vegetation stability to enhance long-term ecological restoration in seasonally dynamic regions.

Keywords: Functional recovery. Sustainable rehabilitation. Technogenic soils.

1. Introduction

Mining is crucial for socioeconomic development, providing jobs and enabling industrial progress. Demand for critical minerals like lithium and silver for electric vehicle batteries and electronics has recently underscored the sector's ongoing importance in driving technological innovation and global economic resilience (Grandell et al., 2016; Young et al., 2022). Nevertheless, mining imposes significant environmental burdens that can outweigh socioeconomic benefits despite its limited spatial footprint (Persico et al., 2023; Tauqeer et al., 2021). The global mining footprint has surpassed 57,000 km^2 and is rapidly expanding, causing significant ecological degradation, including deforestation, biodiversity loss, and increased carbon emissions from soil disturbance (Sonter et al., 2017; Young et al., 2022). Furthermore, mining significantly contributes to global solid waste production (Kaza et al., 2018), while its long-term impacts on biogeochemical cycles, particularly in tropical regions, are still underestimated and insufficiently mitigated.

The awareness of mining and other environmental impacts on biodiversity and climate has spurred worldwide restoration initiatives. Efforts like the United Nations Decade on Ecosystem Restoration (2021–2030), the Bonn Challenge, and the Paris Climate Agreement stress ecological restoration as a key response to climate change and biodiversity loss (Strassburg et al., 2020). Simultaneously, the introduction of frameworks such as the Mine Site Restoration Standards (MSRS) has emphasized the importance of responsible post-mining rehabilitation, regardless of local legal obligations (Young et al., 2022). Brazil exemplifies this duality: while mining sites cover more than 19% of its national territory, with 60% of this area located within the Amazon Rainforest, its biomes simultaneously hold immense ecological value and vulnerability (Gomes et al., 2019; Sonter et al., 2017). Deforestation, mercury contamination in gold-mining regions, and catastrophic tailings dam failures across multiple biomes underscore the environmental risks associated with poor mining practices (Queiroz et al., 2018; Soares et al., 2024). These threats underscore the urgent necessity for robust ecological restoration strategies backed by site-specific environmental monitoring.

Among Brazil's major ecoregions, the Pantanal biome remains critically understudied regarding post-mining ecological restoration (Brancalion et al., 2022; Guerra et al., 2020). Recognized as the world's largest tropical wetland and a global biodiversity hotspot, the Pantanal spans Bolivia, Paraguay, and parts of Brazil, covering approximately 1.76% of Brazil's territory (Alho and Silva, 2012; Scremin-Dias et al., 2011). Its confluence with surrounding biomes, including the Cerrado, Amazon, and Atlantic Forest, shapes its ecological complexity (Bergier et al., 2018). The region's flood pulse regime supports diverse landscapes of grasslands, savannas, forests, and marshes, providing vital ecosystem services like climate regulation, carbon sequestration, and water purification (Pinho et al., 2017; Ivory et al., 2019). The flooding is vital for sustaining both ecological networks and the livelihoods of local and Indigenous communities. Despite this environmental significance and socioeconomic dependence, few studies have examined the interaction between anthropogenic activities, including mining and post-mining works, and the Pantanal's unique hydrology and seasonality (Bergier, 2013; Coelho-Junior et al., 2022; Fernando et al., 2024). The Pantanal's geological history, characterized by ancient crystalline highlands and Quaternary floodplains, further adds to its complexity and mining relevance (Assine and Soares, 2004; Cohen et al., 2015). For instance, iron ore mining in the Urucum Massif, a highland region adjacent to the floodplain near Corumbá, has led to extensive local land disturbance (Pereira et al., 2019). However, little is known about restoration trajectories in such contexts. Unlike other biomes, the Pantanal's pronounced seasonal fluctuations may uniquely alter post-mining restoration dynamics. While the wet season promotes vegetation growth and nutrient availability, it can also intensify erosion and runoff. Conversely, the dry season may limit plant recruitment but reduce soil erosion. This spatiotemporal variability challenges the transferability of restoration metrics and calls for biome-specific approaches to evaluate ecosystem recovery.

This understanding aligns with recent efforts to standardize restoration practices in Brazil, mainly through Normative Instruction No. 14/2024 from the Brazilian Institute for the Environment and Renewable Natural Resources (IBAMA), which mandates post-mining reclamation planning and monitoring across all biomes using integrated assessments of soil, vegetation, and other environmental indicators. However, scientific evidence supporting such integrated approaches remains limited, especially in the Pantanal biome concerning the effects of seasonal variation on restoration outcomes. The Rehabilitation Quality Index (RQI) integrates diverse environmental factors, serving as a promising tool for monitoring restoration dynamics in seasonally wet and dry conditions. Unlike traditional soil quality indices (SQI), which typically focus on soil physicochemical or biological properties, RQI includes a multidisciplinary framework that combines soil metrics with vegetation structure and other relevant environmental parameters. This study aimed to explore post-mining ecological restoration in the Pantanal highlands using RQI and permutational multivariate analyses. We hypothesize that the Pantanal ecoregion's annual wet-to-dry season shift significantly impacts post-mining restoration performance. These contrasting effects are anticipated to create variable restoration outcomes that single-season monitoring cannot fully capture.

2. Materials and methods

2.1. Study site description

The study area is an iron ore mining complex located in Brazil's Pantanal biome highlands (Figure 1), encompassing six post-mining sites (S1–S6) and four reference areas (R1–R4). The region experiences a tropical megathermal climate (*Aw*) with distinct dry winters and rainy summers. The wet season (October to March) brings 1,000–1,400 mm of rainfall and temperatures often exceeding 30 °C, promoting vigorous vegetation growth and seasonal flooding. In contrast, the dry season (April to September) sees minimal rainfall, reduced water levels or complete drying of floodplains, cooler nights, and warm daytime temperatures. The average annual temperature is 25.1 °C, with most precipitation occurring between November and February (Alvares et al., 2013). Evaporation averages 1,400 mm/year, and daylight duration ranges from 2,400 to 2,500 hours. Relative humidity varies between 50% and 75% (Laranjeira et al., 2024). Geologically, the region comprises ancient crystalline rocks in the highlands and floodplain Quaternary sediments (Assine and Soares, 2004). Predominant soils include Litholic Neosols, Cambisols, Planosols, and Argisols (Embrapa, 2018), with occurrences of Phaeozems, Gleysols, and Chernozems (Laranjeira et al., 2024; Souza Oliveira et al., 2021). The native vegetation includes seasonal deciduous and semideciduous forests and diverse savanna formations (IBGE, 2012). Forests occur mainly along slopes and watercourses, while savannas dominate elevated areas like the Urucum Massif, where canga vegetation, adapted to iron-rich substrates, covers ore deposits (Gastauer et al., 2020). The biome hosts over 4,700 plant and animal species, including threatened endemics such as the jaguar (*Panthera onca*), giant otter (*Pteronura brasiliensis*), and hyacinth macaw (*Anodorhynchus hyacinthinus*) (Garcia et al., 2021). Its ecological connectivity with the Amazon, Cerrado, and Atlantic Forest further boosts its conservation value (Chiaravalloti et al., 2022; Wantzen et al., 2024). In addition to biodiversity, the Pantanal provides essential ecosystem services such as climate regulation, carbon sequestration, and water purification, which are crucial to both hydrological balance and local livelihoods, including those of Indigenous and traditional communities (Ivory et al., 2019). The biome also supports migratory bird populations and holds international conservation status under the Ramsar Convention and UNESCO's Biosphere Reserves (Garcia et al., 2021).

The Pantanal seasonally inundated terrain juxtaposes recent sediment dynamics with ancient geological features, including one of the oldest basement rocks on Earth (Cohen et al., 2015; Oriolo et al., 2017), which is crucial, for example, to understanding Gondwana's supercontinent formation. These lithological and structural contrasts shape the ecoregion's unique topography of highlands and wetlands (Furquim et al., 2010; Pott and Pott, 2004). For example, the Urucum Massif, near Corumbá in Mato Grosso do Sul, holds significant iron and manganese deposits (Pereira et al., 2019). Mining for iron and manganese in these highlands has caused deforestation and soil degradation in the Pantanal lowlands (Bergier, 2013). The region shifts from high plateaus (ca. 700 m) to floodplains (<120 m), influencing sediment transport and hydrological connectivity (Cohen et al., 2015; Schulz et al., 2019). The Pantanal's flood pulse governs essential ecological functions like sedimentation, nutrient cycling, and species distribution (Silveira et al., 2022). This hydrological regime supports habitats like flooded grasslands, marshes, lagoons, and savannas, promoting productivity and biodiversity (Abessa et al., 2019; Libonati et al., 2020).

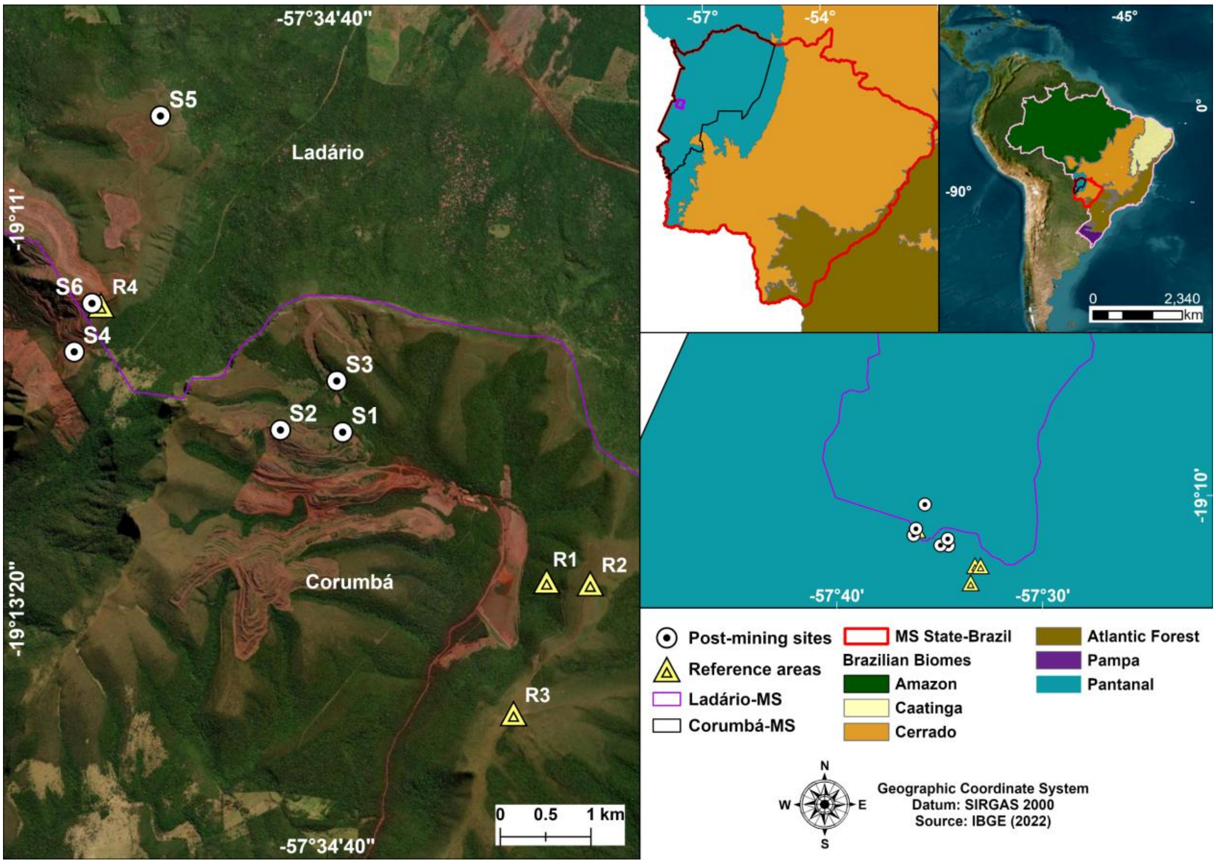

Figure 4 – From left to right: reference areas (R1–R4) and post-mining sites (S1–S6) in the Pantanal biome within the state of Mato Grosso do Sul, as well as the broader geographic context of Brazil within South America in the upper right.

To capture vegetation types in the Pantanal highlands and compare them to post-mining sites for assessing their potential to achieve a sustainable level of ecosystem functionality, we selected reference areas (R1 – R4) by prioritizing the following factors: 1) best-preserved or least disturbed areas; 2) proximity to and similar environmental conditions with the post-mining sites (S1 – S6), including weather, topography, and vegetation type; and 3) the need to avoid oversimplifying misconceptions related to ecological restoration assessments (Ramos et al., 2024). The R1 area is characterized by indigenous tree species and is distinguished by a substantial organic layer (O horizon) within the soil profile. R2 is a grassland characterized by sparse herbaceous vegetation, known as the "Campo Sujo" phytophysiognomy of the Cerrado. R3 is another grassland area, called the "Campo Limpo" phytophysiognomy of the Cerrado. R4 is another grassland classified as the "Campo Limpo" phytophysiognomy.

The post-mining site S1 exhibits a significant gradient characterized by a waste rock disposal pile, which is capped with stockpiled topsoil and is colonized mainly by indigenous plant species. The reclamation process commenced in 2013, involving the reconfiguration of the landscape through the utilization of waste mining materials and the application of stockpiled topsoil, along with the revegetation efforts of the area. The S2 site has been naturally regenerating since 2000, following the disposal of mining waste material. The absence of a nearby conserved area reduces the likelihood of propagules arriving. The S3 site has been rehabilitating since 2013, following the reconfiguration of the landscape and the afforestation with native species. However, the site is primarily dominated by exotic species, including *Melinis minutiflora* P. Beauv., which poses a significant threat to the local environment. Reclamation efforts at the S4 site commenced in 2002, following the disposal of waste material as a sterile mound. This area is predominantly occupied by invasive species, including *Melinis minutiflora* P. Beauv., *Brachiaria* sp., and *Mimosa*. The S5 site exhibits a significant prevalence of exotic species, specifically *Melinis minutiflora* P. Beauv. and *Brachiaria* sp. This site has been experiencing natural regeneration since 1997, following the deposition of mining waste materials. The reclamation process at Site S6 commenced in 2009 and encompassed the sowing of both native and exotic species, as well as the planting of indigenous species. The resulting vegetation primarily comprises native species. The restoration process at post-mining sites (S1-S6) has been significantly influenced by the annual seasonal transition from the rainy to dry season within the Pantanal biome. This is mainly due to shallow technogenic soils and a lack of stringent monitoring for potential interventions over time.

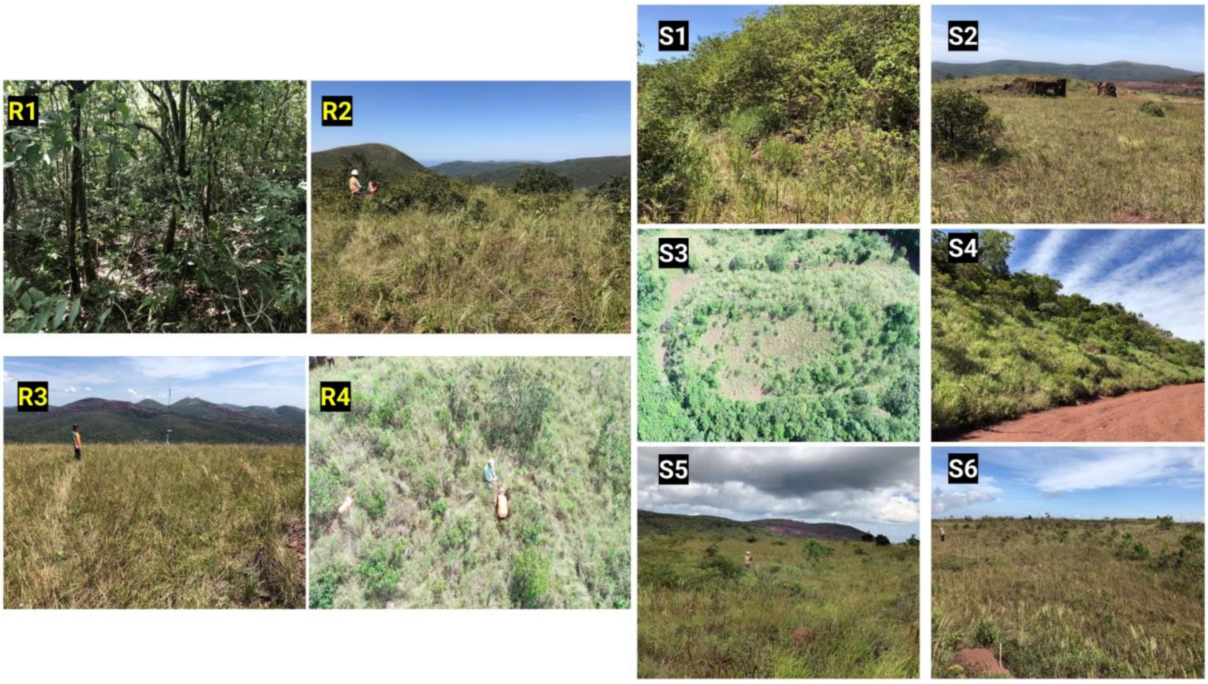

Figure 5 – The photographs taken of the sampled areas showcase the different types of vegetation found in both the reference areas (R1 – R4) and the post-mining sites (S1 – S6).

2.2. Sampling, soil, and vegetation parameters

In March (rainy) and October (dry) 2019, soil samples were collected from each post-mining site (S1–S6) and reference area (R1–R4). Four subsamples were taken from three randomly established plots of 100 m^2 at two depths: 0-2.5 cm and 2.5-10 cm, which were then combined into composite samples. Sixty soil samples were processed each season from ten sites, three plots, and two soil depths. The same sites, plots, depths, and plant variables were analyzed in each period of the year. Before laboratory analysis, soil samples were air-dried naturally in a greenhouse at 21°C to 32°C for one week. Then, the samples were sieved to obtain fine earth (soil particles ≤ 2 mm).

We assessed soil texture—coarse and fine sand, silt, and clay—using the pipette method with 0.1 M NaOH as a dispersant (Embrapa, 2017). Bulk density (Bd, g cm^{-3}) was measured using the excavation method, according to Al-Shammary et al. (2018). The particle density (Pd, g cm^{-3}) was measured using the volumetric flask method (Embrapa, 2017). Total porosity (tP, cm^3 cm^{-3}) was then calculated using the formula: $tP = [1 - (Bd/Pd)]$. We also measured the soil moisture content at a matric potential of –10 kPa, which corresponds to field capacity (FC_10, cm^3 cm^{-3}), and at a matric potential of –1500 kPa, representative of the permanent wilting point (PWP_1500, cm^3 cm^{-3}). The difference between FC_10 and PWP_1500 was used to estimate the available water content in the soil (AW, cm^3 cm^{-3}) (Embrapa, 2017).

The pH was determined in soil and deionized water suspensions (1:2.5, *w/v*). The Mehlich-1 extractant, consisting of 0.05 M HCl and 0.0125 M H_2SO_4, was used to extract available phosphorus (P, mg dm^{-3}) and potassium (K, mg dm^{-3}). We quantified K using atomic absorption spectroscopy (AAS) and P using photocolorimetry. To extract available sulfur (S, mg dm^{-3}), we employed monocalcium phosphate in acetic acid (MCPa) at pH 2.2 and determined S using sulfate turbidimetry. Potential soil acidity (H + Al, cmolc dm^{-3}) was estimated through titration with a 0.025 M NaOH solution, using phenolphthalein as an indicator, following extraction with 0.5 M Ca^{2+} buffered at pH 7.0. Exchangeable calcium (Ca^{2+}, cmolc dm^{-3}), magnesium (Mg^{2+}, cmolc dm^{-3}), and aluminum (Al^{3+}, cmolc dm^{-3}) were extracted with a 1 M KCl solution. Ca^{2+} and Mg^{2+} were determined using AAS, while Al^{3+} was quantified by titration with 0.025 M NaOH. We estimated the remaining phosphorus (Prem, mg L^{-1}) as an assessment of soil buffering capacity by shaking the soil sample with a 0.01 M $CaCl_2$ solution containing 60 mg L^{-1} of P for one hour (at a 1:10 soil-solution ratio) and analyzing it via photocolorimetry (Embrapa, 2017). The semi-total contents of arsenic (AsT), cadmium (CdT), cobalt (CoT), lead (PbT), nickel (NiT), zinc (ZnT), aluminum (AlT), manganese (MnT), and iron (FeT) were measured following the EPA 3051A procedure (USEPA, 2007). Elemental quantification was performed using inductively coupled plasma optical emission spectroscopy (ICP-OES). Each digestion batch included the certified reference sample (*SS-1 EnviroMAT™ Soil Contamination*), and the detection and quantification limits for each element were calculated following the Eurachem guidelines (Magnusson, 2014).

We determined soil organic carbon (SOC, dag kg^{-1}) using a CHNS elemental analyzer through dry combustion (Carmo and Silva, 2012). Organic matter (OM, dag kg^{-1}) was estimated by multiplying SOC by the "van Bemmelen" conversion factor of 1.724, which reflects that carbon comprises approximately 58% of organic matter (Pribyl, 2010). The Kjeldahl method was used to measure the total nitrogen (TN, dag kg^{-1}) (Bremner, 1960; Sáez-Plaza et al., 2013). The soil carbon and nitrogen microbial biomass (MBC and MBN, mg kg^{-1}) were measured using the irradiation-extraction method (Ferreira et al., 1999; Monz et al., 1991). We measured soil microbial respiration by collecting carbon dioxide (CO_2) in sealed glass jars fitted with a central rubber septum. After a 5-day incubation period, with soil moisture adjusted to 70% of field capacity, we sampled the CO_2 evolution using syringes. The quantification of CO_2 was performed using a cavity ring-down spectrometer (CRDS) (Gomez-Pelaez et al., 2019). The basal respiration (BR) value represents the average daily microbial respiration rate (mg kg^{-1} soil day^{-1}). In contrast, the C-CO_2 value indicates the microbial respiration rate accumulated after a 5-day incubation period (mg kg^{-1} soil 5-day^{-1}). The microbial quotient (qMic) is calculated as the ratio of MBC to SOC. In contrast, the metabolic quotient for CO_2 or specific respiration rate (qCO_2) is derived from the ratio of BR to MBC (Anderson and Domsch, 1993).

We integrated applied remote sensing and geographic information system (GIS) techniques to evaluate vegetative parameters, specifically vegetation cover (VC, % $plot^{-1}$) and volume (VV, m^3 $plot^{-1}$). We used a DJI Phantom 4 Professional unmanned aerial vehicle (UAV or drone) with a 4K resolution camera to capture uncontrolled small-format aerial imagery (SFAI). Images were acquired during the high sun, minimizing shadows. The georeferenced images included three spectral bands necessary for natural-color imagery: RED (0.64–0.67 μm), GREEN (0.53–0.59 μm), and BLUE (0.45–0.51 μm). These bands enhance the detection of vegetation and its features. We processed the images using Agisoft Metashape® software, which produced orthorectified images for each plot. Subsequently, we used ArcGIS® Professional software to analyze these images. The VC (% $plot^{-1}$) for each plot was determined using the Modified Photochemical Reflectance Indices (MPRI), constructed from the red and green bands of the orthorectified images (Barbosa et al., 2019). In the MPRI analysis, we categorized the image into vegetation and exposed soil. The percentage of exposed soil was calculated as the ratio of exposed soil pixels to the total number of pixels in the image. To estimate VV, we generated a digital terrain model (DTM) and a digital surface model (DSM) using Agisoft Metashape®. The VV (m^3 $plot^{-1}$) is derived from the difference between the DTM and DSM. While this method does not provide an exact measurement of plant material volume – an accurate estimate would typically require LiDAR data (Andualem et al., 2024) – it is effective for comparing plant volume differences across reclaimed and reference areas (Padró et al., 2019).

2.3. Rehabilitation Quality Index Assessment

We used a non-linear additive factorial algorithm to evaluate the RQI (Ahirwal and Maiti, 2018, 2016; Bandyopadhyay and Maiti, 2021). This assessment considers plant and soil attributes (Alves et al., 2024). We calculated the RQI in three steps, similar to the Soil Quality Index (Imbaná et al., 2024): (i) selection of key plant and soil attributes and weighing (Wj); (ii) sigmoidal scoring (Sj) based on "optimal range", "more is better", or "less is better"; and (iii) rehabilitation indexing (RQI) by summing the products of Wj and Sj for the selected attributes.

2.3.1. Attributes selection, weighing, and scoring

We adjusted the assignment of weights and the criteria for "optimal range," "more is better," and "less is better" when calculating sigmoidal scores for R1 (forest reference area).

The PCA-selected attributes received Wj and Sj values of 1, resulting in an RQI of 1 for the R1 reference area. We assumed that the soil and plant characteristics in the R1 area represent the optimal conditions within the study context that rehabilitation sites can achieve, making human intervention unnecessary regarding seasonal shifts from rainy to dry periods. Our Total Dataset (TDS) comprised forty-one standardized and dimensionless physical, chemical, and microbiological soil attributes, along with two vegetative parameters. To derive the Minimum Data Set (MDS) for the RQI, we identified attributes with loading factors of 0.85 or higher |r ≥ 85| in the first two principal components, PC1 and PC2. Each selected attribute's contribution (r^2) to PC1 and PC2 was calculated by squaring its loading factor (r). To calculate the MDS attribute weights (Wj), we followed these steps: (i) multiply the r^2 values by the eigenvalue of the corresponding principal component (PC); (ii) sum these products from PC1 and PC2 while adhering to the orthogonality principle of PCs; (iii) combined these results for each selected attribute; and (iv) divide each result by the total sum, as represented in the following equation:

$$Wj = \sum_{i=1}^{n} (r^2jiFi) / \sum_{j=1}^{n} \left[\sum_{i=1}^{n} (r^2jiFi) \right] \quad (1)$$

Wj represents the weight of the j-th attribute, ranging from 0 to 1; closer to 1 indicates a greater contribution to the total variance; "r2ji" means the j-th attribute's contribution to the i-th principal component (PC), and "Fi" is the eigenvalue of PC i.

The scores (Sj) of selected attributes were calculated using an S-shaped curve that ranks input values and assigns outputs between 0 and 1. For attributes where higher values indicate a greater contribution to ecosystem reclamation, we used a "more is better" criterion. Conversely, we applied a "less is better" criterion for attributes where lower values are preferable. An "optimal range" was used for MDS scoring when necessary.

$$Sj = \frac{a}{\left[1 + \left(\frac{X}{Xo}\right) b\right]} \quad (2)$$

Sj is the non-linear dimensionless scoring function for the j-th soil and vegetative attributes in RQI, with values from 0 to 1. The parameter "a" is the maximum output of the S-shaped curve at 1. "X" is the observed attribute value, and "Xo" is the average value. The slope, “b”, is typically close to 1, set to –2.5 for "more is better" attributes and +2.5 for "less is better" attributes (Bandyopadhyay and Maiti, 2021; Imbaná et al., 2024).

The criteria for sigmoidal scoring functions ("more is better," "less is better," and "optimal range") used in calculating the RQI are crucial for standardizing and interpreting each selected indicator. "More is better" applies to variables where higher values indicate improved ecosystem condition. For instance, organic matter, species richness, and vegetation cover should increase with ecological restoration, supporting this positive relationship. "Less is better" applies to attributes indicating ecological improvement with lower values. Indicators like bulk density and electrical conductivity fall into this category, as high values suggest compaction or salinization, which are undesirable in a recovering ecosystem. "Optimal range" is selected for variables that indicate optimal ecosystem functioning within a defined interval, where extreme values can be harmful. For example, soil pH outside a specific range may hinder nutrient availability and biological activity. The scoring curve assigns maximum scores within the target range and lower scores outside it. The categorization of each variable into these functional response types was grounded in ecological relevance, supported by evidence from literature and expert insight, guaranteeing that the scoring accurately represents realistic restoration pathways and ecosystem objectives.

We calculated the RQI by summing the products of selected attribute weights (Wj) and their corresponding scores (Sj) for each area. This approach relies on an additive non-linear factorial algorithm that is commonly used for evaluating soil quality indices (Andrews et al., 2004). It integrates various attributes for a comprehensive evaluation of land use's environmental impacts (Yu et al., 2018) and reclamation outcomes (Imbaná et al., 2024; Mukhopadhyay et al., 2016).

$$RQI=\sum_{j=1}^{n} Wj * Sj \qquad (3)$$

RQI is the rehabilitation quality index; Wj and Sj represent the dimensionless weight and score of the j-th attributes, respectively. RQI, the rehabilitation quality index, uses Wj and Sj as the weight and score of the j-th attributes. A post-mining site RQI near 1 indicates better ecological functionality and a stronger tendency for an effective restoration process.

2.4. Statistical Analyses

We conducted statistical analyses using R software. (RCoreTeam, 2024). Soil attributes and vegetational parameters for the Minimum Data Set (MDS) were selected through Principal Component Analysis (PCA) with the "FactoMineR" (Lê et al., 2008) and "Factoextra" (Kassambara and Mundt, 2020) packages. To examine relationships between post-mining sites (S1-S6) and reference areas (R1-R4) based on soil and plant-selected attributes, we conducted a Permutational Multivariate Analysis of Variance (PERMANOVA) combined with Non-Metric Multidimensional Scaling (NMDS). This was adjusted by non-parametric ordination analysis (Anderson, 2017; Anderson and Walsh, 2013), using the "permute" (Simpson, 2022), "lattice" (Sarkar, 2008), and "vegan" (Oksanen et al., 2022) packages.

3. Results

3.1. The minimum data set (MDS)

Tables S1 and S2 present all results, and Figure S2 presents MDS values for rainy and dry seasons, comparing reference areas and post-mining sites. Our MDS highlights differences in soil structure, nutrient trends, toxic exposure, and microbial activity.

During the rainy season, at a depth of 0-2.5 cm (Table S1a), bulk density (Bd) values ranged from 0.62 g cm^{-3} in the forest reference soil (R1) to 1.56 g cm^{-3} in the post-mining site (S6). This pattern aligned with the organic matter (OM) content, which varied from 32.03 dag kg^{-1} in R1 to 1.33 dag kg^{-1} in S6. Furthermore, R1 exhibited higher vegetation volume (VV), soil organic carbon (SOC), and total nitrogen (TN) values compared to other reference areas and all post-mining sites. Particle density (Pd) values ranged from 1.55 g cm^{-3} in R1 to 3.52 g cm^{-3} in S6, indicating an iron-rich lithological background. Total iron (FeT) varied from 107.7 g kg^{-1} in R1 to 310.7 g kg^{-1} in S4. Water content at field capacity (FC_10) and permanent wilting point (PWP_1500) was higher in reference areas (R1–R4) than in post-mining sites (S1–S6), as were effective (eCEC) and potential cation exchange capacity (pCEC), sulfur (S), and total nickel (NiT). However, the percentage of the base sum (PBS) pattern varied. R1 showed a higher PBS associated with lower aluminum saturation (Al_sat), while other reference sites (R2–R4) displayed lower PBS values influenced by higher Al_sat. This trend of lower PBS and higher Al_sat was noted in the post-mining sites, except for S4 (a 17-year-old developing ecosystem dominated by invasive species) and S5 (a 22-year-old reclaiming site dominated by exotic species). Similar patterns between reference areas and rehabilitation sites were observed at the 2.5-10 cm soil depth during the rainy season. Except for Al_sat, total lead (PbT), total iron (FeT), Pd, and Bd, which had lower levels in R1, all other selected attributes (Table S1a) were higher in R1 compared to other reference areas and rehabilitation sites. Notably, the values of Al_sat and PBS in R1 were similar to those found in S4 and S5. Overall, the increased availability of nutrients and water in R1 enhanced biological activity compared to other reference areas and post-mining recovery sites.

During the dry season, at a depth of 0-2.5 cm (Table S1b), R1 demonstrated higher water content at FC_10 and PWP_1500, along with increased levels of pCEC, eCEC, OM, nitrogen microbial biomass (MBN), SOC, TN, and VV compared to other reference and post-mining areas. Conversely, R2-R4 showed higher Al_sat than R1 and the reclaiming sites (S1-S6), which corresponded with lower PBS in these grassland reference areas. A similar trend was noted at a soil depth of 2.5-10 cm during the dry season (Table S1b); R2-R4 maintained higher Al_sat, while PBS values were greater in S4 and S5, followed by R1. All other measured parameters in R1 were significantly better, indicating greater water content and enhanced nutrient availability during both rainy and dry seasons.

Figure 3 (PCA results) displays the variance that the first two principal components (PC1 and PC2) explained on the axis labels. Together, these components accounted for over 90% of the total variance across all scenarios. At the 0–2.5 cm depth during the rainy season, PC1 captured 71.77% of the variance, while PC2, orthogonal to PC1, explained an additional 19.75%. For the second layer in the rainy season, PC1 and PC2 explained 77.29% and 13.65%, respectively. In the dry season, the first two components explained 76.19% and 15.63% for the 0–2.5 cm layer, and 74.54% and 17.11% for the second layer.

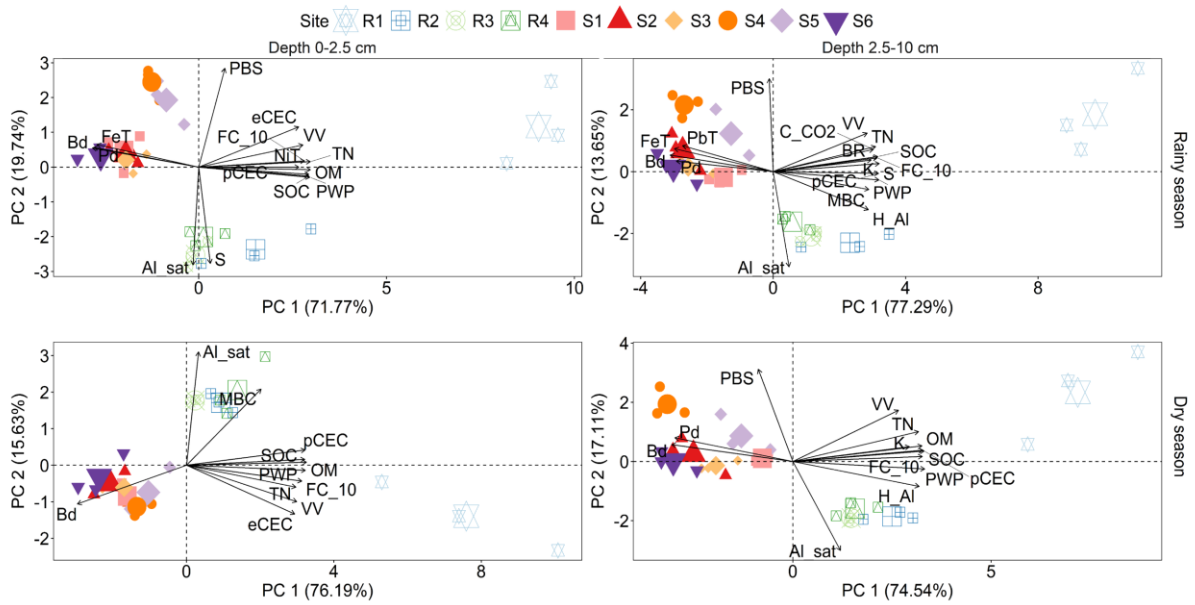

Figure 6 – PCA maps of reference (R1-R4) and post-mining sites (S1-S6) show MDS factors for rainy and dry seasons at soil depths of 0–2.5 cm and 2.5–10 cm, including vegetational parameters.

Figure 4 presents the PERMANOVA/nMDS factor maps, illustrating that during the rainy season, the selected attributes of sites S1–S6 closely resembled those of reference areas R3 and R4 at the 0–2.5 cm depth. This suggests that R3 and R4 may serve as benchmarks for post-mining sites with adequate water and nutrient conditions. However, the dry season maps showed a clear distinction between post-mining sites S1–S6 and reference areas R1–R4, indicated by no polygon overlap, emphasizing the importance of proper management during challenging seasons. Notably, R1 showed no similarity to other references or post-mining sites across all scenarios, highlighting its ecological stability in both dry and rainy seasons.

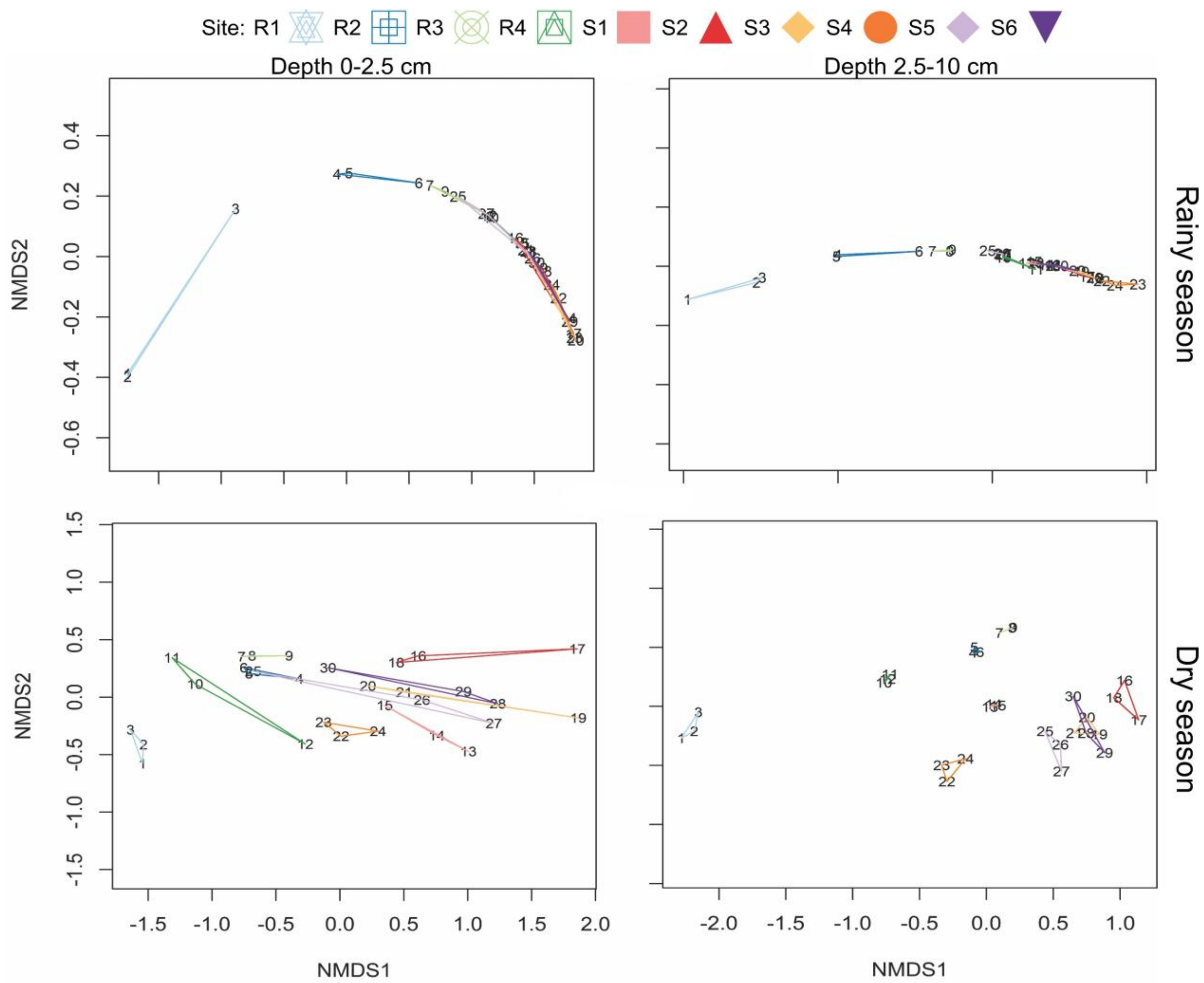

Figure 7 – PERMANOVA/nMDS factor maps of reference (R1-R4) and post-mining (S1-S6) sites based on MDS for rainy and dry seasons at the 0–2.5 and 2.5–10 cm soil depths.

PCA identified key variables (minimum dataset) that are major contributors to variability among rehabilitating sites and reference areas, particularly along PC1 and PC2. PERMANOVA confirmed whether there are statistically significant differences or similarities ($p < 0.05$), supporting the interpretation that ecosystem functionality shifts consistently with restoration progress. The nMDS ordination further illustrated this pattern, showing clear separation or junction between rehabilitating sites (S1–S6) and reference areas (R1–R4), indicating functional divergence. Together, PCA highlights the drivers of variation, while nMDS and PERMANOVA evaluate the structure and statistical significance of ecological groupings.

3.2. **R*ehabilitation quality index assessment***

Figure 5 presents the RQI for S1-S6 sites compared to the environmental quality of reference areas (R1-R4) during rainy and dry seasons at soil depths of 0–2.5 cm and 2.5–10 cm, along with vegetative parameters. The figure highlights each MDS parameter's contribution (relative weight * sigmoidal scoring). We classified the following attributes as "more is better": water content at field capacity (FC_10) and permanent wilting point (PWP_1500), effective cation exchange capacity (eCEC), potential cation exchange capacity (pCEC), percentage of base sum (PBS), soil organic carbon (SOC), organic matter (OM), vegetational volume (VV), soil carbon (MBC) and nitrogen microbial biomass (MBN), total nitrogen (TN), and available potassium (K). For sulfur (S) and total iron (FeT), we applied the criterion "optimum is better," considering local features and their influence on vegetative performance, as these nutrients are required in adequate quantities. The classification "less is better" was used for soil bulk density (Bd), particle density (Pd), aluminum saturation (Al_sat), potential acidity (H+Al), microbial respiration (C-CO_2), basal respiration (BR), total nickel (NiT), and total lead (PbT). Specifically, for C-CO_2 and BR, higher values may lead to increased metabolic quotient (qCO_2), which can indicate stress within the microbial community of an ecosystem. A decrease in qCO_2 is associated with an improvement in an ecosystem (Anderson and Domsch, 1993). Selected attributes in reclaiming sites (S1-S6) with values higher than those in R1 met the "less is better" criterion, while MDS with lower values were rated as "more is better." The MDS parameters with a higher contribution (> 0.040) for RQI (Tables S3 and S4) included soil physical and chemical attributes (pCEC, eCEC, Bd, PWP_1500, OM, TN, and NiT), highlighting soil water and nutrient availability for plant recruitment as the primary distinctions between reference areas and post-mining sites.

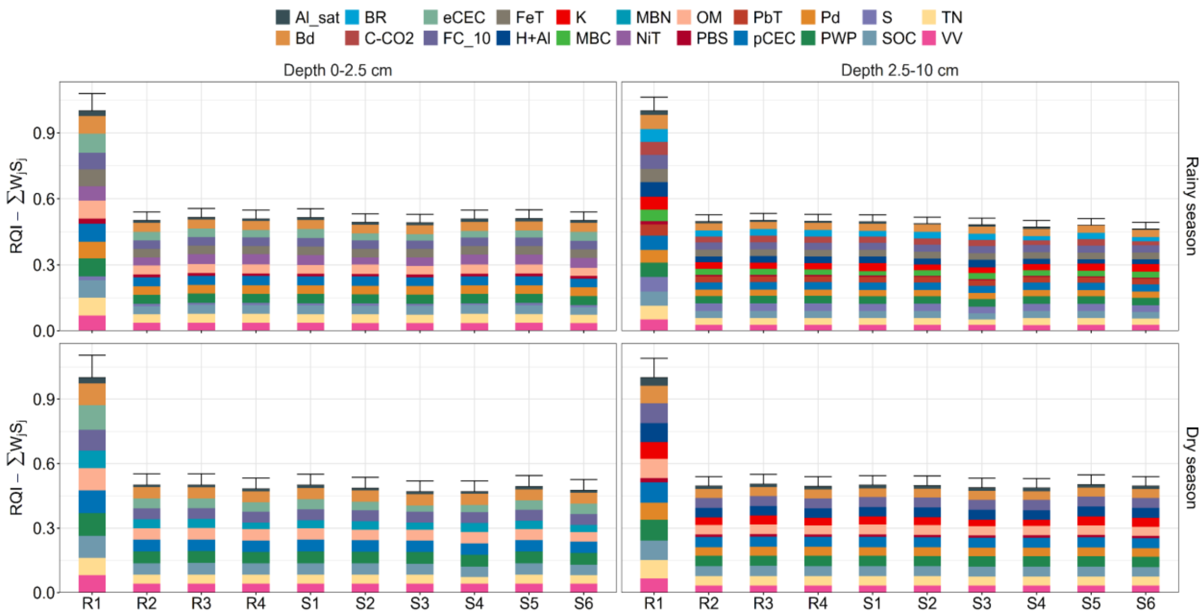

Figure 8 – Contribution of the MDS to the RQI for sites S1-S6, compared to reference sites R1-R4, during the rainy and dry seasons at soil depths of 0-2.5 cm and 2.5-10 cm.

4. Discussion

4.1. Model adaptation

The Soil Quality Index (SQI) has been widely used to evaluate ecological restoration in sites affected by mining and urbanization (Mukherjee and Lal, 2014; Séré et al., 2024), as it provides a comprehensive assessment of reclamation achievement (Imbaná et al., 2024). The Rehabilitation Quality Index (RQI) enhances this evaluation by incorporating both soil and vegetation attributes within an agronomic diagnostic framework (Alves et al., 2024; Andrews et al., 2004; Imbaná et al., 2024; Mukherjee and Lal, 2014). To refine this model, a minimum dataset (MDS) is extracted from a larger total dataset (TDS) through principal component analysis (PCA), weighted, and scored using predefined sigmoidal functions ("more is better," "less is better," and "optimal range"). While this approach simplifies data interpretation in environmental assessments, natural complexity often challenges the assumption of linear responses. Threshold effects must be considered, as slight increases beyond optimal concentration can shift effects from beneficial to toxic. For instance, although agronomic recommendations for available iron (Fe) and manganese (Mn) suggest defined optimal ranges, native vegetation may exhibit higher tolerance, indicating the need for region-specific calibrations (e.g., reference areas).

PCA and PERMANOVA analyzed variations in soil and vegetation across seasons at post-mining sites and their reference areas in the Pantanal ecoregion. PCA decreased data dimensionality and identified essential indicators of ecosystem functionality for restoration efforts. This method can facilitate the consolidation of key variables, including soil pH, bulk density, enzymatic activity, vegetation traits, and other environmental factors, into the assessment of seasonal trends via the RQI. PERMANOVA was used with a Bray-Curtis dissimilarity matrix to statistically determine the significance of multivariate differences between seasons and location categories. By employing NMDS for visual representation, these multivariate techniques provided significant insights into the timeline of ecological restoration and its success measures. Collectively, PCA and PERMANOVA establish a robust framework for tracking post-mining ecosystem responses within various spatial and temporal frameworks, thereby supporting evidence-based restoration initiatives.

By capturing the heterogeneous nature of post-mining sites and ensuring comprehensive site characterization, our sampling approach included 43 attributes (soil and vegetation parameters) selected for their affordability, ease of measurement, and ecological relevance. The dataset was obtained during both rainy and dry seasons across ten sites (four reference areas and six post-mining sites) and sampled at two soil depths (0-2.5 cm and 2.5-10 cm). This methodological rigor enabled a robust analysis of restoration dynamics in the Corumbá-Ladário region within the Pantanal biome, which features a diverse vegetation formation and where climatic dynamics influence ecological restoration. The PCA-based selection effectively establishes direct mechanistic links between MDS and ecosystem function or ecological restoration; however, this is not always the case (van Leeuwen et al., 2017). We evaluated and scored factors (0 to 1) using standardization, applying a loading threshold of $|r \geq 0.85|$ for attribute selection, while including many attributes. Our approach aligns with studies (Calzolari et al., 2020; Ungaro et al., 2022) advocating for broader assessments that incorporate ecosystem sustainability indicators beyond soil properties alone. As suggested by Séré et al. (2024), this approach is critical for post-mining soil function modeling, as it considers interactions among technogenic soil formation (Tarnawczyk et al., 2024), water infiltration, and nutrient cycling.

4.2. Site features and comparison

Rehabilitation sites (S1–S6) exhibited significant variability in ecological restoration stages, driven mainly by differences in reclamation practices and site histories. Notably, site S4, a 17-year-old waste rock pile dominated by invasive species, displayed elevated vegetation volume due to increased macronutrient availability in loamy soils. Enhanced plant growth and microbial activity in this site were linked to increased organic matter (OM) content and percentage of base sum (PBS = 51%), which facilitated metal binding and reduced bioavailability of potentially toxic elements (PTEs) such as FeT and NiT (Al-Amin et al., 2024; Esfandiar et al., 2022). Soil microbiological communities are particularly sensitive to these changes; for example, bioavailable Cr and Ni can influence microbial diversity and function (Luo et al., 2022). Although prolonged exposure to PTEs may suppress microbial activity, metal-tolerant microorganisms such as *Caulobacter* (bacteria) and *Cladosporium* and *Monocillium* (fungi) can thrive under such conditions (Czortek et al., 2020; Stefanowicz et al., 2012; Wang et al., 2021).

Root systems significantly influence pedogenesis, soil structure, and hydraulic properties through exudation and mechanical penetration (Xiao et al., 2024). For instance, the presence of vegetation can have a positive long-term effect on soil properties (Gelhardt et al., 2021; Ni et al., 2024; Zhou et al., 2025). These improvements can facilitate practical land reclamation efforts (Yu et al., 2024, 2023). However, bulk density and hydraulic limitations pose significant challenges to ecological restoration, particularly in post-mining Technosols, where compaction hinders root penetration and water movement. Our findings indicate that despite seasonal improvements, physical constraints in rehabilitated sites (S1-S6) can slow recovery, especially during the dry season. Without targeted interventions, ecosystem resilience remains vulnerable to climatic stressors. Reference sites (R1-R4), characterized by lower bulk density and higher organic matter inputs, suggest that early restoration efforts should prioritize soil structure amelioration and the establishment of diverse native plant species.

Given the potential for SOC and TN depletion in dry climates (Soares et al., 2024), managing water and organic inputs is crucial to sustaining soil fertility and microbial function during the rehabilitation of post-mining sites within climatic dynamics. In the wet season, increased soil moisture enhances vegetation cover, reducing microbial stress and improving enzymatic activity (Ahmadi et al., 2018; Dick et al., 2015). Decomposition of organic matter and nutrient mineralization accelerate key processes in soil carbon cycling. Increased vegetation adds organic inputs through litter and root exudates, fueling microbial activity (Neina et al., 2016; Stefanowicz et al., 2012). In advanced rehabilitation, these inputs restore plant–soil feedback like reference ecosystems. The interaction of vegetation structure, species richness, soil moisture, pH, and organic matter under wet conditions drives functional convergence between rehabilitated and reference sites. Thus, seasonal approximation reflects moisture availability, vegetation-driven carbon inputs, and enhanced microbial functioning—key indicators of ecosystem recovery.

Seasonal dynamics significantly shape vegetation structure and function in restoration areas, with varying impacts across vegetation types. In seasonally flooded ecosystems like the Pantanal, wet and dry periods affect species composition, plant phenology, productivity, and resilience (Ivory et al., 2019). Grasslands respond rapidly to seasonal changes; the wet season promotes biomass accumulation and species turnover, enhancing ground cover and reducing erosion. However, dry-season stress can lead to senescence and increased vulnerability to erosion and nutrient loss. In contrast, woody vegetation shows slower but more stable responses, with deep roots accessing water during dry periods, supporting year-round carbon sequestration and microclimate regulation. Prolonged droughts or altered flooding can hinder seedling recruitment and shift species composition, leading to long-term changes. Seasonal inundation patterns shape habitat heterogeneity, support diverse successional stages, and promote biodiversity, maintaining a mosaic of vegetation types that contribute to ecosystem functions like habitat provision and trophic interactions. Ultimately, restored ecosystems' resilience depends on vegetation's ability to adapt to seasonal variability. Restoration strategies should prioritize diverse plant assemblages with complementary traits for stability across hydrological cycles.

4.3. Rehabilitation quality index and a wide-ranging set of reference areas

The comparison of post-mining sites (S1-S6) with reference areas (R1-R4) using PERMANOVA and nMDS analyses was consistent with RQI evaluations, confirming distinct restoration trajectories. While sites with six years of reclamation (S1, S3) exhibited similarities to those with ten (S6), seventeen (S4), nineteen (S2), and twenty-two (S5) years of restoration during the rainy season, their ecological functions remained distinct from the biodiverse reference ecosystems (R1, R2). These differences were particularly pronounced in the dry season, highlighting the persistence of environmental stressors. Imbaná et al. (2024) reported that achieving post-mining restoration goals may require extended reclamation efforts and careful monitoring. Zhang et al. (2024) found that human intervention is essential for successful ecological restoration. Over the past decade, the Chinese government has made significant investments in projects to enhance the resilience and sustainability of local ecosystems (Song et al., 2022). These initiatives have successfully increased vegetation cover and promoted "greening" in many regions. Our findings indicate significant differences between the post-mining sites (S1-S6) and the reference areas of forest (R1) and shrubland (R2) across all scenarios studied. Additionally, we observed similarities between these post-mining sites and grasslands, specifically the "Campo Limpo" phytophysiognomy of the Cerrado (R3 and R4), in both soil depths during the rainy season. These findings support the use of diverse reference models in post-mining restoration planning. Within the study context, grassland formations like the "Campo Limpo" phytophysiognomy of the Cerrado (R3, R4) may serve as short-term benchmarks, while more complex ecosystems, such as Campo Sujo (R2) and hillside forests (R1), can inform medium- and long-term goals. The goal is not to replicate past conditions but to achieve functional ecosystems capable of self-sustaining ecological processes with minimal human intervention (Castro et al., 2023). The seasonal divergence between reference and rehabilitation sites underscores the need for dynamic management strategies that adapt to fluctuations in water availability and vegetative cover (Yu et al., 2024). RQI's ability to integrate soil and vegetation parameters into a single assessment metric enhances its applicability for long-term ecosystem monitoring, facilitating trend analysis and guiding adaptive management practices (Imbaná et al., 2024; Vasu et al., 2024).

The Rehabilitation Quality Index (RQI) and traditional Soil Quality Indices (SQIs) are important tools for evaluating ecological restoration. The RQI emphasizes ecosystem functionality and resilience over soil productivity or fertility, a typical focus of SQIs used in agriculture and land management. Both indices use principal component analysis (PCA) for variable selection and a sigmoidal scoring function to prevent misinterpretation of parameters.

The main difference is in the scope and integration of indicators. Conventional SQIs assess only soil properties, while the RQI employs a multidisciplinary framework that combines soil metrics with vegetation structure and other ecological parameters. This approach recognizes the functional interdependence of biotic and abiotic components, allowing for a more holistic assessment of restoration progress. The RQI is particularly suited for post-mining and severely degraded environments, where simultaneous recovery of vegetation and soil is crucial for ecosystem stability. In these contexts, SQIs may not effectively capture plant community structure or landscape functionality, which is essential for true ecological recovery. By including variables like species richness, vegetation cover, soil pH, and organic matter, the RQI offers a robust measure of restoration success. Its inclusive framework enhances practicality in complex restoration scenarios, where multifaceted environmental processes must be tackled. Thus, the RQI is a more comprehensive tool for monitoring and guiding rehabilitation in disturbed landscapes.

5. Conclusion

The RQI approach effectively assessed post-mining restoration in the Pantanal by integrating soil and vegetation indicators, distinguishing reference from rehabilitated sites, and identifying key restoration drivers. Using PCA to choose a minimal dataset, combined with seasonal and depth sampling, we established that restoration results differ by site and are influenced by soil characteristics and vegetation cover factors.

Although there have been advancements in certain areas, challenges such as dry-season stress and physical constraints persist. Taking early steps to enhance soil structure, encourage the growth of native species, and effectively manage organic materials is essential. Various reference models aid in restoration efforts: grasslands act as immediate objectives, whereas forests symbolize long-term aspirations. The RQI reflects these gradients and facilitates adaptive management. Future research should enhance soil models with local thresholds, improve tracking of seasonal shifts, and synchronize with native plant tolerance. Long-term monitoring and adaptable strategies are essential for resilient recovery.

Acknowledgments

We thank Vale S.A. for funding and supporting the fieldwork, as well as the Coordination for the Improvement of Higher Education Personnel (CAPES) – Financial Code 001, and the National Council for Scientific and Technological Development (CNPq) –

Financial Code 001, for their financial support. These contributions were essential to the success of this study.

References

Abessa, D., Famá, A., Buruaem, L., 2019. The systematic dismantling of Brazilian environmental laws risks losses on all fronts. Nature Ecol. Evol. 3, 510–511. https://doi.org/10.1038/s41559-019-0855-9

Ahirwal, J., Maiti, S.K., 2018. Development of Technosol properties and recovery of carbon stock after 16 years of revegetation on coal mine degraded lands, India. Catena (Amst) 166, 114–123. https://doi.org/10.1016/j.catena.2018.03.026

Ahirwal, J., Maiti, S.K., 2016. Assessment of soil properties of different land uses generated due to surface coal mining activities in tropical Sal (Shorea robusta) forest, India. Catena (Amst) 140, 155–163. https://doi.org/10.1016/j.catena.2016.01.028

Ahmadi, K., Razavi, B.S., Maharjan, M., Kuzyakov, Y., Kostka, S.J., Carminati, A., Zarebanadkouki, M., 2018. Effects of rhizosphere wettability on microbial biomass, enzyme activities and localization. Rhizosphere 7, 35–42. https://doi.org/10.1016/j.rhisph.2018.06.010

Al-Amin, A., Ryan, R.J., McKenzie, E.R., 2024. Effects of dissolved organic carbon on potentially toxic element desorption in stormwater bioretention systems. Science of The Total Environment 912, 168651. https://doi.org/10.1016/j.scitotenv.2023.168651

Alho, C.J.R., Silva, J.S.V., 2012. Effects of Severe Floods and Droughts on Wildlife of the Pantanal Wetland (Brazil)—A Review. Animals 2012, Vol. 2, Pages 591-610 2, 591–610. https://doi.org/10.3390/ani2040591

Al-shammary, A.A.G., Kouzani, A.Z., Kaynak, A., Khoo, S.Y., Norton, M., Gates, W., 2018. Soil Bulk Density Estimation Methods: A Review. Pedosphere 28, 581–596. https://doi.org/10.1016/s1002-0160(18)60034-7

Alvares, C.A., Stape, J.L., Sentelhas, P.C., De Moraes Gonçalves, J.L., Sparovek, G., 2013. Köppen's climate classification map for Brazil. Meteorologische Zeitschrift 22, 711–728. https://doi.org/10.1127/0941-2948/2013/0507

Alves, M.Q., Assis, I.R. de, Neves, J.C.L., Oliveira, F.Z., Anunciação, A. de A., Moreira, S.L.S., Stewart, R.D., 2024. Recovery quality index as a tool for monitoring the mined land reclamation. Ecological Indicators 159, 111716. https://doi.org/10.1016/j.ecolind.2024.111716

Anderson, M.J., 2017. Permutational Multivariate Analysis of Variance (PERMANOVA). Wiley StatsRef: Statistics Reference Online 1–15. https://doi.org/10.1002/9781118445112.STAT07841

Anderson, M.J., Walsh, D.C.I., 2013. PERMANOVA, ANOSIM, and the Mantel test in the face of heterogeneous dispersions: What null hypothesis are you testing? Ecol Monogr 83, 557–574. https://doi.org/10.1890/12-2010.1

Anderson, T.H., Domsch, K.H., 1993. The metabolic quotient for CO2 (qCO2) as a specific activity parameter to assess the effects of environmental conditions, such as ph, on the microbial biomass of forest soils. Soil Biol Biochem 25, 393–395. https://doi.org/10.1016/0038-0717(93)90140-7

Andrews, S.S., Karlen, D.L., Cambardella, C.A., 2004. The Soil Management Assessment Framework. Soil Science Society of America Journal 68, 1945–1962. https://doi.org/10.2136/SSSAJ2004.1945

Andualem, T.G., Peters, S., Hewa, G.A., Myers, B.R., Boland, J., Pezzaniti, D., 2024. Channel morphological change monitoring using high-resolution LiDAR-derived DEM and multi-temporal imageries. Science of The Total Environment 921, 171104. https://doi.org/10.1016/j.scitotenv.2024.171104

Assine, M.L., Soares, P.C., 2004. Quaternary of the Pantanal, west-central Brazil. Quaternary International 114, 23–34. https://doi.org/10.1016/s1040-6182(03)00039-9

Bandyopadhyay, S., Maiti, S.K., 2021. Application of statistical and machine learning approach for prediction of soil quality index formulated to evaluate trajectory of ecosystem recovery in coal mine degraded land. Ecol Eng 170, 106351. https://doi.org/10.1016/j.ecoleng.2021.106351

Barbosa, B.D.S., Ferraz, G.A.S., Gonçalves, L.M., Marin, D.B., Maciel, D.T., Ferraz, P.F.P., Rossi, G., 2019. RGB vegetation indices applied to grass monitoring: a qualitative analysis. Agronomy Research 17, 349–357. https://doi.org/10.15159/ar.19.119

Bergier, I., 2013. Effects of highland land-use over lowlands of the Brazilian Pantanal. Science of The Total Environment 463–464, 1060–1066. https://doi.org/10.1016/j.scitotenv.2013.06.036

Bergier, I., Assine, M.L., McGlue, M.M., Alho, C.J.R., Silva, A., Guerreiro, R.L., Carvalho, J.C., 2018. Amazon rainforest modulation of water security in the Pantanal wetland. Science of The Total Environment 619–620, 1116–1125. https://doi.org/10.1016/j.scitotenv.2017.11.163

Brancalion, P.H.S., de Siqueira, L.P., Amazonas, N.T., Rizek, M.B., Mendes, A.F., Santiami, E.L., Rodrigues, R.R., Calmon, M., Benini, R., Tymus, J.R.C., Holl, K.D., Chaves, R.B., 2022. Ecosystem restoration job creation potential in Brazil. People and Nature 4, 1426–1434. https://doi.org/10.1002/pan3.10370

Bremner, J.M., 1960. Determination of nitrogen in soil by the Kjeldahl method. J Agric Sci 55, 11–33. https://doi.org/10.1017/s0021859600021572

Calzolari, C., Tarocco, P., Lombardo, N., Marchi, N., Ungaro, F., 2020. Assessing soil ecosystem services in urban and peri-urban areas: From urban soils survey to providing support tool for urban planning. Land use policy 99, 105037. https://doi.org/10.1016/j.landusepol.2020.105037

Carmo, D.L., Silva, C.A., 2012. Métodos de quantificação de carbono e matéria orgânica em resíduos orgânicos. Rev Bras Cienc Solo 36, 1211–1220. https://doi.org/10.1590/s0100-06832012000400015

Castro, A.F. de, Assis, I.R. de, Caldeira, C.F., Ramos, S.J., Coelho, R.R., Oliveira, G.C. de, Medeiros-Sarmento, P.S., Gastauer, M., 2023. Minimum thresholds of key ecological attributes facilitate the tracking of mineland restoration. Resources Policy 84, 103722. https://doi.org/10.1016/j.resourpol.2023.103722

Chiaravalloti, R.M., Bolzan, F., Roque, F.D.O., Biswas, S., 2022. Ecosystem services in the floodplains: Socio-cultural services associated with ecosystem unpredictability in the Pantanal wetland, Brazil. Aquat Ecosyst Health Manag 25, 72–80. https://doi.org/10.14321/aehm.025.01.72

Coelho-Junior, M.G., Diele-Viegas, L.M., Calheiros, D.F., Silva Neto, E.C., Fearnside, P.M., Ferrante, L., 2022. Pantanal port licence would threaten the world’s largest tropical wetland. Nat Ecol Evol 6, 484–485. https://doi.org/10.1038/s41559-022-01724-z

Cohen, A., McGlue, M.M., Ellis, G.S., Zani, H., Swarzenski, P.W., Assine, M.L., Silva, A., 2015. Lake formation, characteristics, and evolution in retroarc deposystems: A synthesis of the modern Andean orogen and its associated basins. Memoir of the Geological Society of America 212, 309–335. https://doi.org/10.1130/2015.1212(16)

Czortek, P., Królak, E., Borkowska, L., Bielecka, A., 2020. Impacts of soil properties and functional diversity on the performance of invasive plant species Solidago canadensis L. on post-agricultural wastelands. Science of The Total Environment 729, 139077. https://doi.org/10.1016/j.scitotenv.2020.139077

De Pinho, J.B., Aragona, M., Hakamada, K.Y.P., Marini, M.Â., 2017. Migration patterns and seasonal forest use by birds in the Brazilian Pantanal. Bird Conserv. Int. 27, 371–387. https://doi.org/10.1017/s0959270916000290

Dick, R.P., Breakwell, D.P., Turco, R.F., 2015. Soil enzyme activities and biodiversity measurements as integrative microbiological indicators. Methods for Assessing Soil Quality 247–271. https://doi.org/10.2136/sssaspecpub49.c15

Embrapa, 2018. Sistema brasileiro de classificação de solos, Empresa Brasileira de Pesquisa Agropecuária.

Embrapa, 2017. Manual de métodos de análise de solo., Manual de Métodos de Análise de Solo. Brasília, DF: Embrapa, 2017.

Esfandiar, N., Suri, R., McKenzie, E.R., 2022. Competitive sorption of Cd, Cr, Cu, Ni, Pb and Zn from stormwater runoff by five low-cost sorbents; Effects of co-contaminants, humic acid, salinity and pH. J Hazard Mater 423, 126938. https://doi.org/10.1016/j.jhazmat.2021.126938

Fernando, A.M.E., Lopes, D.A., Mateus, L., Penha, J., Súarez, Y.R., Catella, A.C., Nunes, A.V., Arenhart, N., Chiaravalloti, R.M., 2024. The economic displacement of thousands of fishers in the Pantanal, Brazil: A telling story of small-scale fisheries marginalization worldwide. Fish and Fisheries 25, 951–958. https://doi.org/10.1111/faf.12856

Ferreira, A.S., Camargo, F.A.O., Vidor, C., 1999. Utilização de microondas na avaliação da biomassa microbiana do solo. Rev Bras Cienc Solo 23, 991–996. https://doi.org/10.1590/s0100-06831999000400026

Furquim, S.A.C., Graham, R.C., Barbiero, L., Queiroz Neto, J.P., Vidal-Torrado, P., 2010. Soil mineral genesis and distribution in a saline lake landscape of the Pantanal Wetland, Brazil. Geoderma 154, 518–528. https://doi.org/10.1016/j.geoderma.2009.03.014

Garcia, L.C., Szabo, J.K., de Oliveira Roque, F., de Matos Martins Pereira, A., Nunes da Cunha, C., Damasceno-Júnior, G.A., Morato, R.G., Tomas, W.M., Libonati, R., Ribeiro, D.B., 2021. Record-breaking wildfires in the world's largest continuous tropical wetland: Integrative fire management is urgently needed for both biodiversity and humans. J Environ Manage 293, 112870. https://doi.org/10.1016/j.jenvman.2021.112870

Gastauer, M., Caldeira, C.F., Ramos, S.J., Trevelin, L.C., Jaffé, R., Oliveira, G., Vera, M.P.O., Pires, E., Santiago, F.L. de A., Carneiro, M.A.C., Coelho, F.T.A., Silva, R., Souza-Filho, P.W.M., Siqueira, J.O., 2020. Integrating environmental variables by multivariate ordination enables the reliable estimation of mineland rehabilitation status. J Environ Manage 256, 109894. https://doi.org/10.1016/j.jenvman.2019.109894

Gelhardt, L., Dittmer, U., Welker, A., 2021. Relationship of particle density and organic content in sieve fractions of road-deposited sediments from varying traffic sites based on a novel data set. Science of The Total Environment 794, 148812. https://doi.org/10.1016/j.scitotenv.2021.148812

Gomes, L.C., Faria, R.M., de Souza, E., Veloso, G.V., Schaefer, C.E.G.R., Filho, E.I.F., 2019. Modelling and mapping soil organic carbon stocks in Brazil. Geoderma 340, 337–350. https://doi.org/10.1016/j.geoderma.2019.01.007

Gomez-Pelaez, A.J., Ramos, R., Cuevas, E., Gomez-Trueba, V., Reyes, E., 2019. Atmospheric CO2, CH4, and CO with the CRDS technique at the Izaña Global GAW station: Instrumental tests, developments, and first measurement results. Atmos Meas Tech 12, 2043–2066. https://doi.org/10.5194/amt-12-2043-2019

Grandell, L., Lehtilä, A., Kivinen, M., Koljonen, T., Kihlman, S., Lauri, L.S., 2016. Role of critical metals in the future markets of clean energy technologies. Renew Energy 95, 53–62. https://doi.org/10.1016/j.renene.2016.03.102

Guerra, A., Reis, L.K., Borges, F.L.G., Ojeda, P.T.A., Pineda, D.A.M., Miranda, C.O., Maidana, D.P.F. de L., Santos, T.M.R. dos, Shibuya, P.S., Marques, M.C.M., Laurance, S.G.W., Garcia, L.C., 2020. Ecological restoration in Brazilian biomes: Identifying advances and gaps. For Ecol Manage 458, 117802. https://doi.org/10.1016/j.foreco.2019.117802

IBGE, 2012. Manual Técnico da Vegetação Brasileira, 2 edição r. ed. Coordenação de Recursos Naturais e Estudos Ambientais, Rio de Janeiro.

Imbaná, R., Daniele de Almeida Valente, F., Siqueira, R.G., Moquedace, C.M., Rodrigues de Assis, I., 2024. Assessing the quality of constructed technosols enabled holistic monitoring of ecological restoration. J Environ Manage 353, 120237. https://doi.org/10.1016/j.jenvman.2024.120237

Ivory, S.J., McGlue, M.M., Spera, S., Silva, A., Bergier, I., 2019. Vegetation, rainfall, and pulsing hydrology in the Pantanal, the world's largest tropical wetland. Environmental Research Letters 14, 124017. https://doi.org/10.1088/1748-9326/ab4ffe

Kassambara, A., Mundt, F., 2020. factoextra: Extract and Visualize the Results of Multivariate Data Analyses.

Kaza, S., Yao, L.C., Bhada-Tata, P., Van Woerden, F., 2018. What a Waste 2.0: A Global Snapshot of Solid Waste Management to 2050. Urban Development. https://doi.org/10.1596/978-1-4648-1329-0

Laranjeira, L.T., Schiavo, J.A., de Souza Oliveira, N., Pereira, M.G., Viana de Moraes, E.M., Cirilo de Souza, A., Barros Ozório, J.M., 2024. Black soils in the southwest of the Brazilian Pantanal: Organic carbon and secondary carbonates accumulation in Phaeozems–Gleysol-Chernozem. J South Am Earth Sci 141, 104935. https://doi.org/10.1016/j.jsames.2024.104935

Lê, S., Josse, J., Husson, F., 2008. FactoMineR: An R Package for Multivariate Analysis. J Stat Softw 25, 1–18. https://doi.org/10.18637/jss.v025.i01

Libonati, R., DaCamara, C.C., Peres, L.F., Sander de Carvalho, L.A., Garcia, L.C., 2020. Rescue Brazil's burning Pantanal wetlands. Nature 588, 217–219. https://doi.org/10.1038/d41586-020-03464-1

Luo, Y., Pang, J., Li, C., Sun, J., Xu, Q., Ye, J., Wu, H., Wan, Y., Shi, J., 2022. Long-term and high-bioavailable potentially toxic elements (PTEs) strongly influence the microbiota in electroplating sites. Science of The Total Environment 814, 151933. https://doi.org/10.1016/j.scitotenv.2021.151933

Magnusson, B., 2014. The fitness for purpose of analytical methods: a laboratory guide to method validation and related topics (2014).

Monz, C.A., Reuss, D.E., Elliott, E.T., 1991. Soil microbial biomass carbon and nitrogen estimates using 2450 MHz microwave irradiation or chloroform fumigation followed by direct extraction. Agric Ecosyst Environ 34, 55–63. https://doi.org/10.1016/0167-8809(91)90093-d

Mukherjee, A., Lal, R., 2014. Comparison of Soil Quality Index Using Three Methods. PLoS One 9, e105981. https://doi.org/10.1371/journal.pone.0105981

Mukhopadhyay, S., Masto, R.E., Yadav, A., George, J., Ram, L.C., Shukla, S.P., 2016. Soil quality index for evaluation of reclaimed coal mine spoil. Science of The Total Environment 542, 540–550. https://doi.org/10.1016/j.scitotenv.2015.10.035

Neina, D., Buerkert, A., Joergensen, R.G., 2016. Microbial response to the restoration of a Technosol amended with local organic materials. Soil Tillage Res 163, 214–223. https://doi.org/10.1016/j.still.2016.06.008

Ni, J., Liu, S., Huang, Y., Gao, Y., 2024. Temperature and plant root effects on soil hydrological response and slope stability. Comput Geotech 174, 106663. https://doi.org/10.1016/j.compgeo.2024.106663

Oksanen J, Simpson G, Blanchet F, Kindt R, Legendre P, Minchin P, O'Hara R, Solymos P, Stevens M, Szoecs E, Wagner H, Barbour M, Bedward M, Bolker B, Borcard D, Carvalho G, Chirico M, De Caceres M, Durand S, Evangelista H, FitzJohn R, Friendly M, Furneaux, W.J., 2022. vegan: Community Ecology Package.

Oriolo, S., Oyhantçabal, P., Wemmer, K., Siegesmund, S., 2017. Contemporaneous assembly of Western Gondwana and final Rodinia break-up: Implications for the supercontinent cycle. Geoscience Frontiers 8, 1431–1445. https://doi.org/10.1016/j.gsf.2017.01.009

Padró, J.C., Carabassa, V., Balagué, J., Brotons, L., Alcañiz, J.M., Pons, X., 2019. Monitoring opencast mine restorations using Unmanned Aerial System (UAS) imagery. Science of The Total Environment 657, 1602–1614. https://doi.org/10.1016/j.scitotenv.2018.12.156

Pereira, C.C., Santos Soares, F. de F., Fonseca, R.S., Henriques, N.R., Arruda, D.M., 2019. Ferruginous rupestrian savannah: A floristic and structural analysis of these rare environments. Neotropical Biology and Conservation 14, 381–397. https://doi.org/10.3897/neotropical.14.e47228

Persico, F., Coulon, F., Ladyman, M., López, C.F., Temple, T., 2023. Evaluating the effect of insensitive high explosive residues on soil using an environmental quality index (EQI) approach. Science of The Total Environment 869, 161797. https://doi.org/10.1016/j.scitotenv.2023.161797

Pott, A., Pott, V.J., 2004. Features and conservation of the Brazilian Pantanal wetland. Wetl. Ecol. Manag. 12, 547–552. https://doi.org/10.1007/s11273-005-1754-1

Pribyl, D.W., 2010. A critical review of the conventional SOC to SOM conversion factor. Geoderma 156, 75–83. https://doi.org/10.1016/j.geoderma.2010.02.003

Queiroz, H.M., Nóbrega, G.N., Ferreira, T.O., Almeida, L.S., Romero, T.B., Santaella, S.T., Bernardino, A.F., Otero, X.L., 2018. The Samarco mine tailing disaster: A possible time-bomb for heavy metals contamination? Science of The Total Environment 637–638, 498–506. https://doi.org/10.1016/j.scitotenv.2018.04.370

Ramos, L., Negreiros, D., Goulart, F.F., Figueiredo, J.C.G., Kenedy-Siqueira, W., Toma, T.S.P., Justino, W. de S., Maia, R.A., de Oliveira, J.T., Oki, Y., Barbosa, M., Aguilar, R., dos Santos, R.M., Dias, H.M., Nunes, Y.R.F., Fernandes, G.W., 2024. Dissimilar forests along the Rio Doce watershed call for multiple restoration references to avoid biotic homogenization. Science of The Total Environment 930, 172720. https://doi.org/10.1016/j.scitotenv.2024.172720

RCoreTeam, 2024. R: A Language and Environment for Statistical Computing. R Foundation for Statistical Computing.

Sáez-Plaza, P., Michałowski, T., Navas, M.J., Asuero, A.G., Wybraniec, S., 2013. An Overview of the Kjeldahl Method of Nitrogen Determination. Part I. Early History, Chemistry of the Procedure, and Titrimetric Finish. Crit Rev Anal Chem 43, 178–223. https://doi.org/10.1080/10408347.2012.751786

Sarkar, D., 2008. Lattices: Multivariate Data Visualization with R, Progress in Mathematics. https://doi.org/10.1007/b11801_9

Schulz, C., Whitney, B.S., Rossetto, O.C., Neves, D.M., Crabb, L., de Oliveira, E.C., Terra Lima, P.L., Afzal, M., Laing, A.F., de Souza Fernandes, L.C., da Silva, C.A., Steinke, V.A., Torres Steinke, E., Saito, C.H., 2019. Physical, ecological and human dimensions of environmental change in Brazil's Pantanal wetland: Synthesis and research agenda. Science of The Total Environment 687, 1011–1027. https://doi.org/10.1016/j.scitotenv.2019.06.023

Scremin-Dias, E., Lorenz-Lemke, A.P., Oliveira, A.K.M., 2011. The floristic heterogeneity of the Pantanal and the occurrence of species with different adaptive strategies to water stress. Brazilian Journal of Biology 71, 275–282. https://doi.org/10.1590/s1519-69842011000200006

Séré, G., Le Guern, C., Bispo, A., Layet, C., Ducommun, C., Clesse, M., Schwartz, C., Vidal-Beaudet, L., 2024. Selection of soil health indicators for modelling soil functions to promote smart urban planning. Science of The Total Environment 924, 171347. https://doi.org/10.1016/j.scitotenv.2024.171347

Silveira, F.A.O., Ordóñez-Parra, C.A., Moura, L.C., Schmidt, I.B., Andersen, A.N., Bond, W., Buisson, E., Durigan, G., Fidelis, A., Oliveira, R.S., Parr, C., Rowland, L., Veldman, J.W., Pennington, R.T., 2022. Biome Awareness Disparity is BAD for tropical ecosystem conservation and restoration. Journal of Applied Ecology 59, 1967–1975. https://doi.org/10.1111/1365-2664.14060

Simpson, G.L., 2022. Functions for Generating Restricted Permutations of Data [R package permute version 0.9-7].

Soares, M.B., Rodrigues, R.R., Péres, L.O., Cerri, C.E.P., Alleoni, L.R.F., 2024. Impact of climatic seasons on the dynamics of carbon, nitrogen and mercury in soils of Brazilian biomes affected by gold mining. Science of The Total Environment 954, 176279. https://doi.org/10.1016/j.scitotenv.2024.176279

Song, W., Feng, Y., Wang, Z., 2022. Ecological restoration programs dominate vegetation greening in China. Science of The Total Environment 848, 157729. https://doi.org/10.1016/j.scitotenv.2022.157729

Sonter, L.J., Herrera, D., Barrett, D.J., Galford, G.L., Moran, C.J., Soares-Filho, B.S., 2017. Mining drives extensive deforestation in the Brazilian Amazon. Nature Communications 2017 8:1 8, 1–7. https://doi.org/10.1038/s41467-017-00557-w

Souza Oliveira, N., Schiavo, J.A., Cirilo de Souza, A., Laranjeira, L.T., Viana de Moraes, E.M., Pereira, M.G., 2021. Mineralogy and genesis in an alkaline soil system in the southern

Pantanal wetland, Brazil. J South Am Earth Sci 111, 103456. https://doi.org/10.1016/j.jsames.2021.103456

Stefanowicz, A.M., Kapusta, P., Szarek-Łukaszewska, G., Grodzińska, K., Niklińska, M., Vogt, R.D., 2012. Soil fertility and plant diversity enhance microbial performance in metal-polluted soils. Science of The Total Environment 439, 211–219. https://doi.org/10.1016/j.scitotenv.2012.09.030

Strassburg, B.B.N., Iribarrem, A., Beyer, H.L., Cordeiro, C.L., Crouzeilles, R., Jakovac, C.C., Braga Junqueira, A., Lacerda, E., Latawiec, A.E., Balmford, A., Brooks, T.M., Butchart, S.H.M., Chazdon, R.L., Erb, K.H., Brancalion, P., Buchanan, G., Cooper, D., Díaz, S., Donald, P.F., Kapos, V., Leclère, D., Miles, L., Obersteiner, M., Plutzar, C., Carlos, C.A., Scarano, F.R., Visconti, P., 2020. Global priority areas for ecosystem restoration. Nature 2020 586:7831 586, 724–729. https://doi.org/10.1038/s41586-020-2784-9

Tarnawczyk, M., Uzarowicz, Ł., Kwasowski, W., Górka-Kostrubiec, B., Pędziwiatr, A., 2024. Soil-forming factors controlling Technosol formation in historical mining and metallurgical sites in the high-alpine environment of the Tatra Mountains, southern Poland. Catena (Amst) 247, 108521. https://doi.org/10.1016/j.catena.2024.108521

Tauqeer, H.M., Karczewska, A., Lewińska, L.K., Fatima, M., Khan, S.A., Farhad, M., Turan, V., Ramzani, P.M.A., Iqbal, M., 2021. Environmental concerns associated with explosives (HMX, TNT, and RDX), heavy metals and metalloids from shooting range soils: Prevailing issues, leading management practices, and future perspectives. Handbook of Bioremediation: Physiological, Molecular and Biotechnological Interventions 569–590. https://doi.org/10.1016/b978-0-12-819382-2.00036-3

Ungaro, F., Maienza, A., Ugolini, F., Lanini, G.M., Baronti, S., Calzolari, C., 2022. Assessment of joint soil ecosystem services supply in urban green spaces: A case study in Northern Italy. Urban For Urban Green 67, 127455. https://doi.org/10.1016/j.ufug.2021.127455

USEPA, 2007. Method 3051A (SW-846): Microwave Assisted Acid Digestion of Sediments, Sludges, and Oils, Revision 1. Washington, DC.

van Leeuwen, J.P., A Saby, N.P., Jones, A., Louwagie, G., Micheli, E., Rutgers, M., O Schulte, R.P., Spiegel, H., Toth, G., Creamer, R.E., 2017. Gap assessment in current soil monitoring networks across Europe for measuring soil functions. Environmental Research Letters 12, 124007. https://doi.org/10.1088/1748-9326/aa9c5c

Vasu, D., Tiwary, P., Chandran, P., 2024. A novel and comprehensive soil quality index integrating soil morphological, physical, chemical, and biological properties. Soil Tillage Res 244, 106246. https://doi.org/10.1016/j.still.2024.106246

Wang, Yan, Xiong, Y., Wang, Yi, Li, Q., 2021. Long period exposure to serious cadmium pollution benefits an invasive plant (Alternanthera philoxeroides) competing with its native congener (Alternanthera sessilis). Science of The Total Environment 786, 147456. https://doi.org/10.1016/j.scitotenv.2021.147456

Wantzen, K.M., Assine, M.L., Bortolotto, I.M., Calheiros, D.F., Campos, Z., Catella, A.C., Chiaravalotti, R.M., Collischonn, W., Couto, E.G., da Cunha, C.N., Damasceno-Junior, G.A., da Silva, C.J., Eberhard, A., Ebert, A., de Figueiredo, D.M., Friedlander, M., Garcia, L.C., Girard, P., Hamilton, S.K., Ikeda-Castrillon, S., Libonati, R., Lourival, R., de Azevedo Macedo, H., Junior, J.M., Mateus, L., Morato, R.G., Mourão, G., Muniz, C.C., Nunes, A.V., de Oliveira, M.D., da Rosa Oliveria, M., Junior, E.S.O., Padovani, C.R., Penha, J., Ribeiro, D.B., de Oliveira Roque, F., Silva, A., Soriano, B.M.A., Sousa Junior, W.C., Tomas, W.M., Tortato, F.R., Urbanetz, C., 2024. The end of an entire biome? World's largest wetland, the Pantanal, is menaced by the Hidrovia project which is uncertain to sustainably support large-scale navigation. Science of The Total Environment 908, 167751. https://doi.org/10.1016/j.scitotenv.2023.167751

Xiao, T., Li, P., Fei, W., Wang, J., 2024. Effects of vegetation roots on the structure and hydraulic properties of soils: A perspective review. Science of The Total Environment 906, 167524. https://doi.org/10.1016/j.scitotenv.2023.167524

Young, R.E., Gann, G.D., Walder, B., Liu, J., Cui, W., Newton, V., Nelson, C.R., Tashe, N., Jasper, D., Silveira, F.A.O., Carrick, P.J., Hägglund, T., Carlsén, S., Dixon, K., 2022. International principles and standards for the ecological restoration and recovery of mine sites. Restor Ecol 30. https://doi.org/10.1111/rec.13771

Yu, P., Liu, J., Tang, H., Ci, E., Tang, X., Liu, S., Ding, Z., Ma, M., 2023. The increased soil aggregate stability and aggregate-associated carbon by farmland use change in a karst region of Southwest China. Catena (Amst) 231, 107284. https://doi.org/10.1016/j.catena.2023.107284

Yu, P., Liu, S., Zhang, L., Li, Q., Zhou, D., 2018. Selecting the minimum data set and quantitative soil quality indexing of alkaline soils under different land uses in northeastern China. Science of The Total Environment 616–617, 564–571. https://doi.org/10.1016/j.scitotenv.2017.10.301

Yu, P., Wang, H., Hu, J., Shi, W., Xia, X., Sun, X., Tang, H., Huang, Y., 2024. Vegetation degradation reduces aggregate associated carbon by reducing both labile and stable carbon fraction in Northeast China. Science of The Total Environment 954, 176789. https://doi.org/10.1016/j.scitotenv.2024.176789

Zhang, Y., Zhao, X., Gong, J., Luo, F., Pan, Y., 2024. Effectiveness and driving mechanism of ecological restoration efforts in China from 2009 to 2019. Science of The Total Environment 910, 168676. https://doi.org/10.1016/j.scitotenv.2023.168676

Zhou, J., Ni, J., Liu, S., Wang, Y., Choi, C.E., 2025. Influence of plant root aging on water percolation in three earthen landfill cover systems: A numerical study. J Hydrol (Amst) 655, 132916. https://doi.org/10.1016/j.jhydrol.2025.132916

Supplementary Material

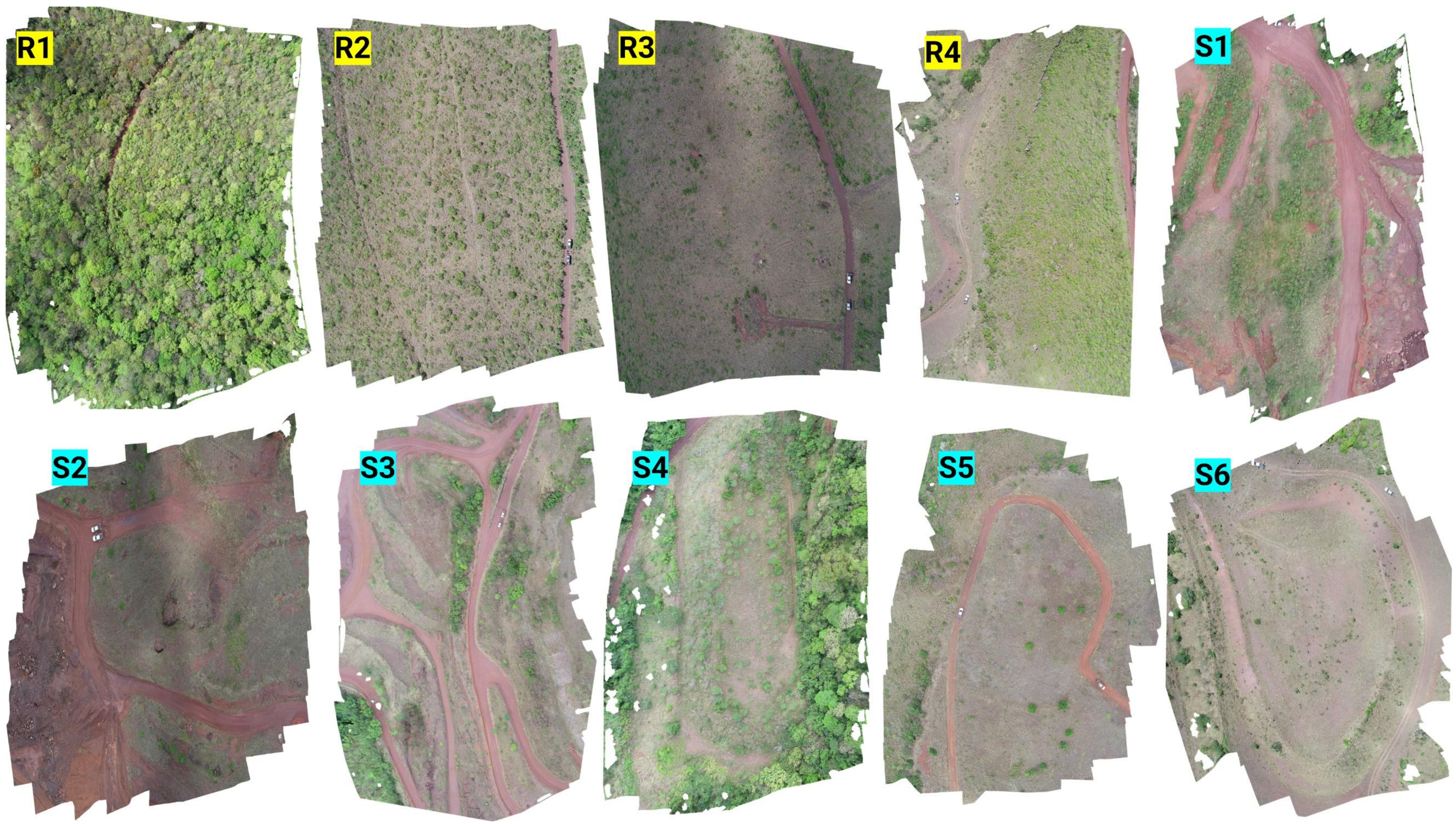

Figure S1 – Orthomosaic (high-resolution aerial photographs) of reference areas (R1–R4) and post-mining sites (S1–S6)

Table S1 – Summary statistics of the total data set for the rainy season

			Rainy Season										
Depth	Attributes	Units	R1	R2	R3	R4	S1	S2	S3	S4	S5	S6	CV (%)
	Coarse sand	$g\ g^{-1}$	0.24bc	0.22c	0.26abc	0.42ab	0.22c	0.21c	0.37abc	0.46a	0.39abc	0.38abc	21.24
	Fine sand	$g\ g^{-1}$	0.06	0.06	0.08	0.11	0.07	0.09	0.10	0.06	0.09	0.09	29.47
	Silt	$g\ g^{-1}$	0.3bc	0.18de	0.15e	0.2cde	0.345ab	0.42a	0.27bcd	0.29bcd	0.25bcde	0.31abc	14.74
	Clay	$g\ g^{-1}$	0.4ab	0.54a	0.51a	0.27bcd	0.37bc	0.28bcd	0.26cd	0.2d	0.26bcd	0.22d	14.63
	Bd	$g\ cm^{-3}$	0.62d	0.99c	1.16bc	1.22abc	1.52a	1.47ab	1.56a	1.38a	1.34ab	1.56a	9.22
	Pd	$g\ cm^{-3}$	1.55e	2.51d	2.70cd	2.91bc	3.25ab	3.27ab	3.34a	3.42a	2.91bc	3.52a	4.27
	tP	$cm^3\ cm^{-3}$	0.60	0.61	0.57	0.58	0.53	0.55	0.53	0.60	0.54	0.56	6.3
	FC_10	$cm^3\ cm^{-3}$	0.55a	0.35b	0.29bc	0.33bc	0.25bc	0.34bc	0.2bc	0.29bc	0.28bc	0.23c	11.46
	PWP_1500	$cm^3\ cm^{-3}$	0.44a	0.20b	0.18b	0.19b	0.12c	0.12c	0.11c	0.10c	0.12c	0.09c	12.2
	AW	$cm^3\ cm^{-3}$	0.368a	0.148bcd	0.104d	0.147bcd	0.127cd	0.220b	0.144bcd	0.193bc	0.161bcd	0.140bcd	17.44
	pH	—	5.6a	4.8bc	4.7bc	4.6c	5.4a	5.2ab	5.3a	5.7a	5.6a	5.2ab	3.42
	H+Al	$cmol_c\ dm^{-3}$	17.3a	14.6a	13.1a	14.6a	5.4b	4.7b	6.8b	5.2b	5.6b	3.4b	20.76
	P	$mg\ dm^{-3}$	8.1	2.03	1.7	3.7	0.9	0.43	1.43	20.73	0.93	1.37	174.58
	Prem	$mg\ L^{-1}$	10.3e	11.5de	10.3e	14.17cde	12.2cde	16.9bcd	15.7cde	32.7a	18.5bc	23.2b	13.5
	K	$mg\ dm^{-3}$	166a	77.7bcd	62cde	81bcd	109.7b	50de	54.7de	89bc	60cde	45.3e	14.04
	S	$mg\ dm^{-3}$	17.63abcd	28.33ab	28.73a	26.23ab	18.93abc	14.5cde	21.63abc	5.6e	6.9de	17.4bcd	20.88
	Ca^{2+}	$cmol_c\ dm^{-3}$	12.7a	1.08b	0.62b	0.93b	1.54b	1.04b	1.95b	4.34b	3.19b	0.9b	48.53
	Mg^{2+}	$cmol_c\ dm^{-3}$	3.54a	0.29b	0.2b	0.3b	0.41b	0.23b	0.3b	0.9b	1.55b	0.19b	59.84

	Al^{3+}	$cmol_c\ dm^{-3}$	0.12c	1.57ab	1.39b	2a	0.19c	0.28c	0.25c	0c	0.06c	0.28c	27.23
	eCEC	$cmol_c\ dm^{-3}$	16.8a	3.14b	2.36b	3.43b	2.43b	1.68b	2.65b	5.48b	4.96b	1.47b	40.49
	pCEC	$cmol_c\ dm^{-3}$	34.01a	16.17b	14.11bc	16.05b	7.64de	6.13de	9.2cde	10.71cd	10.49cd	4.56e	14.13
0-2.5 cm	BS	$cmol_c\ dm^{-3}$	16.7a	1.6b	1b	1.45b	2.24b	1.4b	2.4b	5.48b	4.89b	1.19	48.03
	PBS	%	48.63ab	9.53cde	6.87e	9.03de	29.47bc	22.67cde	25.8cde	51a	48.07ab	27.27cd	24.97
	Al_sat	%	1c	50.93a	59.3a	57.9a	8.5bc	16.03bc	9.93bc	0c	1.4c	18.9b	25.99
	AlT	$g\ kg^{-1}$	45.1b	77.3a	78.8a	39.26b	42.41b	37.28b	34.7bc	18.4c	49.2b	17.5c	14.42
	AsT	$mg\ kg^{-1}$	0.0	0.23	0.016	0.0	0.0	0.0	0.0	0.0	0.17	0.0	366.15
	CoT	$mg\ kg^{-1}$	0.0	0.2	1.17	0.18	0.09	0.0	0.0	4.35	0.0	1.03	360.89
	FeT	$g\ kg^{-1}$	107.7d	186.6c	224.5bc	252.5abc	282.6ab	292ab	295.7ab	310.8a	247abc	290.4ab	10.58
	MnT	$mg\ kg^{-1}$	777.4	90.83	91.08	406.82	558.18	471.73	863.03	4746.87	397.81	1551.59	186.79
	NiT	$mg\ kg^{-1}$	3.52a	1.65ab	0.59b	0.08b	0.01b	0.00b	0.42b	0.15b	0.48b	0.00b	99.14
	PbT	$mg\ kg^{-1}$	2.84c	7.15bc	11abc	18.83a	18.25ab	17.55ab	18.23ab	19.94a	15.04ab	18.46ab	26.9
	ZnT	$mg\ kg^{-1}$	26.15ab	24.72b	31.76ab	35.19ab	38.26ab	39.41ab	37.62ab	45.32a	36.27ab	38ab	19.56
	SOC	$dag\ kg^{-1}$	17.78a	7.89b	4.67bc	4.94bc	1.31c	1.35c	1.83c	2.96c	2.2c	0.85c	32.3
	OM	$dag\ kg^{-1}$	30.66a	13.60b	8.05cd	8.52bc	2.26e	2.33de	3.16de	5.1cde	3.79de	1.47e	19.36
	TN	$dag\ kg^{-1}$	1.44a	0.4b	0.24bcd	0.29bc	0.06d	0.06d	0.1cd	0.18cd	0.13cd	0.05d	22.56
	MBC	$mg\ kg^{-1}$	1143a	932ab	599abc	771abc	483bc	460bc	219c	412bc	199c	296c	39.31
	MBN	$mg\ kg^{-1}$	131.08	110.48	88.57	104.18	16.62	50.93	62.85	81.17	92.56	65.11	57.04
	BR	$mg\ kg^{-1}\ day^{-1}$	21.24a	17.07ab	10.99bc	11.27bc	3.03c	4.7c	3.6c	18.26ab	4.23c	2.07c	35.71
	$C\text{-}CO_2$	$mg\ kg^{-1}\ 5\text{-}day^{-1}$	106.2a	85.38ab	54.93bc	56.37bc	15.14c	23.48c	17.94c	91.32ab	21.18c	10.34c	35.71

qMic	—	0.66	1.29	1.28	1.6	3.8	3.8	1.2	1.39	0.88	4.83	91.96
qCO_2	—	0.02ab	0.02ab	0.02ab	0.015ab	0.01b	0.02ab	0.014ab	0.044a	0.03ab	0.01b	59.86
VC	% plot^{-1}	100a	78.33abc	85.73ab	91.86a	81.61ab	85.89ab	51.90cd	49.66d	44.66d	61.42bcd	13.05
VV	m^3 plot^{-1}	1427a	81.2d	39.2d	296.07b	98.57d	21.47d	54.9d	182c	61.83d	53.57d	12.29
Coarse sand	g g^{-1}	0.245c	0.218c	0.263c	0.365bc	0.221c	0.305bc	0.380bc	0.549a	0.439ab	0.363bc	17
Fine sand	g g^{-1}	0.061b	0.077ab	0.102ab	0.144a	0.072ab	0.108ab	0.096ab	0.051b	0.086ab	0.10ab	31.55
Silt	g g^{-1}	0.255bc	0.167cd	0.146d	0.198cd	0.319ab	0.373a	0.304ab	0.249bcd	0.222bcd	0.316ab	14.23
Clay	g g^{-1}	0.439bc	0.537a	0.490ab	0.293d	0.388c	0.214de	0.22de	0.151e	0.253d	0.222de	9.19
Bd	g cm^{-3}	0.73f	1.11e	1.28de	1.38cde	1.51abcd	1.69ab	1.63abc	1.73ab	1.45bcd	1.74a	6.82
Pd	g cm^{-3}	1.95e	2.83d	2.93cd	3.34abcd	3.31abcd	3.89ab	3.68abc	4.02a	3.15bcd	3.64abc	8.32
tP	cm^3 cm^{-3}	0.622a	0.604ab	0.562ab	0.583ab	0.544ab	0.565ab	0.556ab	0.570ab	0.539ab	0.523b	5.43
FC_10	cm^3 cm^{-3}	0.60a	0.31b	0.28bc	0.29bc	0.23bc	0.23bc	0.22bc	0.20c	0.23bc	0.22bc	13.18
PWP_1500	cm^3 cm^{-3}	0.34a	0.20b	0.18bc	0.18bc	0.13cd	0.1de	0.1de	0.7e	0.11de	0.09de	12.9819
AW	cm^3 cm^{-3}	0.261a	0.114b	0.107b	0.113b	0.102b	0.134b	0.127b	0.128b	0.118b	0.129b	16.81
pH	—	5.4ab	4.7cd	4.7cd	4.5d	5.2abc	5.2abc	5.3abc	5.7a	5.6a	4.9bcd	4.12
H+Al	cmol$_c$ dm^{-3}	20.27a	14.67b	12.93b	14.63b	6.3c	3.8c	5.83c	3.63c	5.2c	2.83	20.05
P	mg dm^{-3}	6.8a	1.4a	1.03a	2.8a	0.6a	6.83a	0.87a	13.53a	0.43a	1.57a	132.29
Prem	mg L^{-1}	34.83a	35.8a	33.37a	30.33ab	23.53abc	16.27bcd	26.37ab	8.03d	9.63cd	16.73bcd	22.58
K	mg dm^{-3}	145.7a	75.33b	60bcd	72bc	73bc	33.33de	24e	58.7bcd	45.33cde	26e	16.38
S	mg dm^{-3}	24.83a	9.75b	6.87bc	7.32b	1.77d	1.42d	1.60d	2.44d	2.70cd	0.7d	24.55
Ca^{2+}	cmol$_c$ dm^{-3}	7.65a	0.44b	0.35b	0.53b	0.96b	0.83b	1.04b	2.42ab	2.22ab	0.49b	112.25

	Mg^{2+}	$cmol_c\ dm^{-3}$	2.47a	0.18b	0.13b	0.24b	0.22b	0.16b	0.12b	0.48b	1.09b	0.10b	86.1
	Al^{3+}	$cmol_c\ dm^{-3}$	0.57b	1.83a	1.58a	2.14a	0.47b	0.15b	0.28b	0.0b	0.09b	0.28b	35.14
	pCEC	$cmol_c\ dm^{-3}$	30.8a	15.5b	13.6bc	15.6b	7.7d	4.9d	7.06d	6.7d	8.63cd	3.48d	16.64
2.5-10 cm	BS	$cmol_c\ dm^{-3}$	10.5a	0.82b	0.63b	0.95b	1.36b	1.07b	1.23b	3.06b	3.43b	0.65b	98.86
	PBS	%	32.63abc	5.23d	4.63d	6.17d	17.83bcd	21.9bcd	17.4cd	46.43a	41.6ab	1917bcd	39.28
	Al_sat	%	8.27bc	69.33a	71.93a	69.17a	26.2b	12.73bc	19.03bc	0c	2.87c	27.7b	24.13
	AlT	$mg\ kg^{-1}$	0.57b	1.83a	1.58a	2.14a	0.47b	0.15b	0.28b	0b	0.09b	0.28b	35.14
	AsT	$mg\ kg^{-1}$	0.0	0.0	0.0	0.0	0.0	0.0	0.0	0.0	0.40	0.0	539.86
	CoT	$mg\ kg^{-1}$	0.0	0.025	0.0	0.0	0.0	0.0	0.0	0.0	0.0	0.045	402.08
	FeT	$g\ kg^{-1}$	131.9f	177.3e	211.9de	248.6c	260.7bc	288.5ab	287ab	316.7a	238.6cd	274.4bc	5.12
	MnT	$mg\ kg^{-1}$	665.09ab	54.18b	48.12b	104.08b	811.51ab	502.4ab	806.17ab	1,455.2a	176.13ab	1,027.4ab	79.77
	NiT	$mg\ kg^{-1}$	2.76a	0.30b	0.0b	0.0b	0.0b	0.0b	0.46b	0.0b	0.0b	0.0b	112.65
	PbT	$mg\ kg^{-1}$	4.79d	6.33d	9.28cd	16.59ab	14.16ab	17.08ab	16.30ab	18.27a	13.19bc	17.11ab	12.12
	ZnT	$mg\ kg^{-1}$	25.44c	25.14c	26.36c	32.63b	35.56ab	40.43a	38.22ab	40.47a	32.49b	33.31b	6.13
	SOC	$dag\ kg^{-1}$	15.67a	4.94b	3.73bc	4.46b	1.13cd	0.86d	1.21cd	1.38cd	1.65cd	0.46d	25.88
	OM	$dag\ kg^{-1}$	27.02a	8.52b	6.43bc	7.69b	1.95cd	1.48d	2.09cd	2.38cd	2.84cd	0.79d	96.55
	TN	$dag\ kg^{-1}$	1.21a	0.27b	0.18bcd	0.24bc	0.05cd	0.02d	0.05cd	0.08bcd	0.1bcd	0.03d	31.99
	MBC	$mg\ kg^{-1}$	1.334.1a	838.98ab	643bcd	748.63bc	257.52cde	113.08de	117.35de	300bcde	240cde	80.2e	40.35
	MBN	$mg\ kg^{-1}$	117.7a	123.7a	108.8a	122.5a	7.34a	27a	61.6a	69.27a	54.02a	10.73a	61.97
	BR	$mg\ kg^{-1}\ day^{-1}$	22.58a	6.26b	7.14b	2.56b	0.73b	2.97b	1.21b	2.69b	3.39b	0.59b	47.7
	$C\text{-}CO_2$	$mg\ kg^{-1}\ 5\text{-}day^{-1}$	112.9a	31.32b	35.72b	12.82b	3.64b	14.87b	6.03b	13.44b	16.93b	2.94b	47.7

qMic	—	0.88	1.76	1.72	1.73	2.22	1.33	1.04	2.38	1.42	2.20	56.97
qCO_2	—	0.02	0.01	0.01	0.005	0.01	0.03	0.01	0.01	0.015	0.01	72.37
VC	% $plot^{-1}$	100a	78.33abc	85.73ab	91.86a	81.61ab	85.89ab	51.9cd	49.66d	44.66d	61.42bcd	13.05
VV	m^3 $plot^{-1}$	1427a	81.2d	39.2d	296.07b	98.57d	21.47d	54.9d	182c	61.83d	53.57d	12.29

R1: Hillside Forest; **R2:** Grassland with sparse herbaceous vegetation, known as the "Campo Sujo" phytophysiognomy of the Cerrado; **R3 and R4:** Grasslands, referred to as the "Campo Limpo" phytophysiognomy of the Cerrado; **S1:** 6-year-old rehabilitating site; **S2:** 19-year-old rehabilitating site; **S3:** 6-year-old rehabilitating site; **S4:** 17-year-old rehabilitating site; **S5:** 22-year-old rehabilitating site; **S6:** 10-year-old rehabilitating site; **Bd:** bulk density; **Pd:** particle density; **FC_10:** field capacity at –10 kPa; **PWP:** permanent wilting point; **H+Al:** Potential soil acidity; **pCEC:** potential cation exchange capacity (BS + H + Al); **eCEC:** effective cation exchange capacity (BS + Al^{3+}); **PBS:** percentage of bases sum (BS/pCEC * 100); **Al_sat:** aluminum saturation (Al^{3+}/eCEC * 100); **K:** available potassium; **S:** available sulfur; **SOC:** soil organic carbon; **OM:** organic matter (SOC * 1.724); **TN:** total nitrogen; **VV**: vegetation volume; **C-CO_2:** microbial respiration rate accumulated after a 5-day incubation period; **BR:** soil basal respiration rate per day; **MBC and MBN:** soil carbon and nitrogen microbial biomass; **NiT, FeT, and PbT:** semi-total content of nickel, iron and lead. The attributes highlighted in bold within the tables met both ANOVA assumptions. Distinct lowercase letters indicate significant differences at $p < 0.05$ (Tukey test) among the sites (S1-S6) and reference areas; CV = coefficient of variation.

a) For the rainy season, focusing on a soil depth of 0-2.5 cm, the MDS for the RQI includes the following parameters: Bd, Pd, FC_10, PWP, eCEC, pCEC, PBS, Al_sat, S, OM, NiT, FeT, SOC, TN, and VV.
b) In contrast, during the dry season at the same depth, the MDS consists of Bd, FC_10, PWP, pCEC, eCEC, Al_sat, OM, MBN, SOC, TN, and VV.
c) For the 2.5-10 cm soil depth during the rainy season, the MDS for RQI includes Bd, Pd, FC_10, PWP, K, H+Al, pCEC, PBS, Al_sat, S, PbT, FeT, C-CO_2, BR, MBC, SOC, TN, and VV.
d) On the other hand, during the dry season at this depth, the retained parameters are Bd, Pd, FC_10, PWP, K, H+Al, pCEC, PBS, Al_sat, OM, SOC, TN, and VV.

Table S2 – Summary statistics of the total data set for the dry season

			Dry Season										
Depth	Attributes	Units	R1	R2	R3	R4	S1	S2	S3	S4	S5	S6	CV
	Coarse sand	g g^{-1}	0.254	0.254	0.287	0.313	0.233	0.253	0.322	0.404	0.322	0.307	22.17
	Fine sand	g g^{-1}	0.065b	0.066b	0.079ab	0.122a	0.077ab	0.08ab	0.079ab	0.043b	0.085ab	0.087ab	24.37
	Silt	g g^{-1}	0.303abc	0.178de	0.168e	0.192cde	0.342ab	0.39a	0.289abcd	0.323ab	0.256bcde	0.338ab	14.49
	Clay	g g^{-1}	0.378bc	0.502a	0.467ab	0.373bc	0.347cd	0.277de	0.31cde	0.230e	0.338cd	0.267de	9.35
	Bd	g cm^{-3}	0.73d	1.07cd	1.2bc	1.06cd	1.4abc	1.52ab	1.5ab	1.62a	1.42abc	1.55ab	9.54
	Pd	g cm^{-3}	2.23e	2.52de	2.70cde	2.6cde	3.23abcd	3.54ab	3.31abc	3.94a	3.03bcd	3.68ab	8.26
	tP	cm^3 cm^{-3}	0.67a	0.58ab	0.55b	0.59ab	0.56b	0.57ab	0.55b	0.59ab	0.53b	0.58ab	6.01
	FC_10	cm^3 cm^{-3}	0.63a	0.34b	0.29b	0.37b	0.26b	0.25b	0.25b	0.25b	0.3b	0.23b	20.44
	PWP_1500	cm^3 cm^{-3}	0.44a	0.2b	0.17bcd	0.19bc	0.12bcd	0.09cd	0.11bcd	0.08d	0.12bcd	0.08d	21.84
	AW	cm^3 cm^{-3}	0.18	0.14	0.12	0.18	0.14	0.16	0.15	0.16	0.18	0.15	20.21
	pH_H_2O	—	5.6bc	5.2cd	5.2cd	5.1d	5.8b	5.9b	6ab	6.5a	5.9b	5.8b	3.17
	H+Al	cmolc dm^{-3}	16a	15.2a	13.4a	17a	5.8b	4.6b	6.7b	3.7b	6.2b	3.5b	22.21
	P	mg dm^{-3}	7.47	1.53	1.53	4.9	0.9	5.83	1.47	8.3	0.87	1.63	103.63
	Prem	mg L^{-1}	10.83d	9.67d	9.37d	13.33cd	16.2cd	21.77bc	15cd	35.6a	18.17cd	30.4ab	18.89
	K	mg dm^{-3}	194.67a	104.3cd	83cd	99cd	170.67ab	61.67d	61d	122.33bc	71cd	65.67d	18.7
	S	mg dm^{-3}	0.0c	0.0c	0.0c	14.13ab	7.37bc	11.27ab	12.77ab	9.1abc	5.23bc	18.33a	48.09
	Ca^{2+}	cmolc dm^{-3}	13.38a	1.07b	0.81b	1.34b	2.36b	1.36b	2.3b	3.45b	3.23b	1.03b	71.97
	Mg^{2+}	$cmol_c$ dm^{-3}	2.8a	0.39c	0.27c	0.39c	0.6c	0.29c	0.36c	0.96bc	1.67b	0.22c	37.58
	Al^{3+}	$cmol_c$ dm^{-3}	0.19c	1.58ab	1.26b	2.16a	0.06c	0.22c	0.22c	0.0c	0.06c	0.26c	34.36

0-2.5 cm	eCEC	$cmol_c\ dm^{-3}$	16.87a	3.32b	2.55b	4.15b	3.47b	2.03b	3.04b	4.73b	5.14b	1.68b	50.5
	pCEC	$cmol_c\ dm^{-3}$	32.7a	16.9bc	14.66bcd	18.98b	9.2def	6.41ef	9.55def	8.46ef	11.25cde	4.89f	15.17
	BS	$cmol_c\ dm^{-3}$	16.68a	1.74b	1.29b	1.98b	3.4b	1.81b	2.82b	4.73b	5.08b	1.43b	60.16
	PBS	%	49.83ab	10.27c	8.77c	10.5c	36.8ab	28.07bc	28.93bc	55.83a	46.77ab	29.83bc	27.02
	Al_sat	%	1.93b	47.63a	49.6a	52.6a	2.3b	11.47b	8.5b	0b	1.23b	15.23b	28.12
	AlT	$g\ kg^{-1}$	52.3b	86.3a	87.2a	42.7b	41.2b	36.8b	36.5b	16.5c	46.7b	14.6c	13.95
	AsT	$mg\ kg^{-1}$	0.0	0.0	0.0	0.0	0.0	0.0	0.0	0.0	0.03	0.0	537.2
	CoT	$mg\ kg^{-1}$	3.46b	3.78b	3.85b	7.54a	6.74a	6.8a	8.03a	7.8a	6.09ab	8a	15.96
	FeT	$g\ kg^{-1}$	101.7b	115.3ab	117.7ab	154.7a	149.8a	145.4a	152.4a	150.6a	143.8ab	147.7a	10.79
	MnT	$g\ kg^{-1}$	0.73ab	0.11b	0.92b	0.24b	0.49b	0.58b	0.85ab	2.3a	0.45b	1.4ab	79.72
	NiT	$mg\ kg^{-1}$	3.77a	2.03ab	1.17ab	0.11b	0.31ab	0.0b	0.17b	0.0b	0.29ab	0.0b	154.58
	PbT	$mg\ kg^{-1}$	12.9bc	12.01c	8.65c	29.53ab	24.83abc	23.27abc	24.43abc	22.4abc	32.05a	23.51abc	27.96
	ZnT	$mg\ kg^{-1}$	31.84a	23.0ab	20.74ab	25.63ab	20.93ab	26.86ab	18.84b	18.62b	23.0ab	18.29b	18.95
	SOC	$dag\ kg^{-1}$	13.06a	5.53b	5.31b	5.19b	1.55b	1.46bc	1.75bc	2.42bc	2.22bc	0.94c	36.14
	OM	$dag\ kg^{-1}$	25.27a	10.08bc	7.76bcd	10.53b	2.49d	3.08d	3.15cd	3.55bcd	4.21bcd	1.66d	33.65
	TN	$dag\ kg^{-1}$	1.19a	0.35b	0.33b	0.33b	0.09b	0.1b	0.11b	0.42b	0.13b	0.05b	60.3
	MBC	$mg\ kg^{-1}$	884.56ab	767.09ab	775.7ab	1,030.33a	174.55b	181.23b	202.42b	336.03ab	378.72ab	240.08b	52.85
	MBN	$mg\ kg^{-1}$	205a	55b	30b	29.32b	29.53b	22.96b	5.08b	15.6b	18b	15.36b	62.94
	BR	$mg\ kg^{-1}\ day^{-1}$	5.07	5.4	4.8	4.95	4.86	4.71	8.1	8.1	5.7	7.22	91
	$C\text{-}CO_2$	$mg\ kg^{-1}\ 5\text{-}day^{-1}$	25.34	26.99	23.83	24.73	24.28	23.54	40.52	40.29	28.64	36.1	91
	qMic	—	0.76	1.43	1.49	2.02	1.16	1.17	1.14	1.70	1.53	2.59	61.79

qCO_2	—	0.006	0.008	0.005	0.005	0.039	0.086	0.113	0.024	0.043	0.050	180.57
VC	% $plot^{-1}$	100a	78.33abc	85.73ab	91.86a	81.61ab	85.89ab	51.9cd	49.66d	44.66d	61.42bcd	13.05
VV	m^3 $plot^{-1}$	1427a	81.2d	39.2d	296.07b	98.57d	21.47d	54.9d	182c	61.83d	53.57d	12.29
Coarse sand	g g^{-1}	0.265b	0.237b	0.278b	0.340ab	0.253b	0.287b	0.284b	0.465a	0.323ab	0.316b	16.74
Fine sand	g g^{-1}	0.066bc	0.08bc	0.1b	0.142a	0.079bc	0.069bc	0.08bc	0.04c	0.082b	0.074bc	17.61
Silt	g g^{-1}	0.234cde	0.185de	0.160e	0.165e	0.297abc	0.365a	0.328ab	0.296abc	0.259bcd	0.320abc	11.73
Clay	g g^{-1}	0.435ab	0.499a	0.462a	0.352cd	0.371bc	0.279e	0.307cde	0.198f	0.335cde	0.290de	7.14
Bd	g cm^{-3}	1.02e	1.15de	1.28cd	1.50bc	1.48bc	1.66ab	1.56b	1.81a	1.52bc	1.68ab	5.92
Pd	g cm^{-3}	2.27f	2.65ef	2.74e	2.9de	3.23cd	3.63c	3.48bc	4.16a	2.9de	3.8ab	5.04
tP	cm^3 cm^{-3}	0.551a	0.566a	0.533a	0.481a	0.542a	0.543a	0.550a	0.563a	0.471a	0.555a	6.21
FC_10	cm^3 cm^{-3}	0.41a	0.3b	0.28bc	0.29bc	0.24bcd	0.22cd	0.23bcd	0.19d	0.26bcd	0.2d	9.69
PWP_1500	cm^3 cm^{-3}	0.26a	0.19b	0.17bc	0.15cd	0.12de	0.08efg	0.104efg	0.062g	0.113def	0.076fg	10.99
AW	cm^3 cm^{-3}	0.151	0.110	0.112	0.138	0.123	0.135	0.128	0.123	0.143	0.124	13.16
P	mg dm^{-3}	5.23	1.5	1.07	2.97	0.60	7.73	1.0	17.9	0.50	1.70	225.68
Prem	mg dm^{-3}	5.67d	7.37d	7.9d	8.7d	11.6cd	21.3abc	12.3bcd	32.8a	15.27bcd	24.07	27.76
K	mg dm^{-3}	151.33a	93b	73.67bc	75.67bc	96.33b	34de	20e	55cd	34.33	26.67de	14.91
S	mg dm^{-3}	0.0b	0.0b	3.8ab	7.5ab	6.13ab	14.6ab	9.53ab	13.43ab	3ab	20.55a	77.94
pH	—	5.5def	5.2fg	5.3efg	5.05g	5.6cde	5.9bcd	5.96bc	6.4a	6.07ab	5.6cde	2.47
H+Al	$cmol_c$ dm^{-3}	19.47a	14.77b	12.97b	15.43b	6.9c	3.73cd	5.6cd	3.13d	5.57cd	2.63d	14.31
Ca^{2+}	$cmol_c$ dm^{-3}	7.65a	0.45b	0.42b	0.61b	1.35b	0.98b	1.13b	1.99b	2.14b	0.62b	108.37
Mg^{2+}	$cmol_c$ dm^{-3}	1.73a	0.21c	0.16c	0.2c	0.3c	0.14c	0.14c	0.43bc	1.01b	0.11c	54.01

	Al^{3+}	$cmol_c\ dm^{-3}$	0.71cd	1.84ab	1.52bc	2.36a	0.39d	0.22d	0.26d	0.0d	0.16d	0.27d	37.06
	eCEC	$cmol_c\ dm^{-3}$	10.47a	2.74b	2.28b	3.36b	2.28b	1.44b	1.58b	2.56b	3.4b	1.05b	59.49
	pCEC	$cmol_c\ dm^{-3}$	29.23a	15.67b	13.73bc	16.44b	8.79cd	4.95d	6.92d	5.97d	8.81cd	3.43d	19.74
	BS	$cmol_c\ dm^{-3}$	9.76a	0.9b	0.77b	1.0b	1.89b	1.21b	1.32b	2.56b	3.24b	0.79b	88.95
2.5-10 cm	PBS	%	31.27ab	5.77c	5.57c	6.07c	21.5bc	24.83abc	18.83bc	45.63a	37.8ab	23.43abc	35.65
	Al_sat	%	13.43bc	67.1a	66.47a	70.33a	17.2bc	16.57bc	17.2bc	0c	5.03bc	24.27b	25.3
	AlT	$g\ kg^{-1}$	66.5a	75.36a	65.6a	43.31bc	46.64b	33.68bc	29.98c	13.26d	43.5bc	13.9d	12.77
	AsT	$mg\ kg^{-1}$	0.0	0.0	0.0	0.0	0.0	0.0	0.0	0.0	0.04	0.0	536.8
	CoT	$mg\ kg^{-1}$	3.89b	5.11ab	5.77ab	7.03a	6.61a	6.61a	5.99ab	5.73ab	5.58ab	7.21a	13.27
	FeT	$g\ kg^{-1}$	109.73b	141.04ab	150.35a	152.8a	149.13a	143.96a	141.02ab	135.16ab	142.7a	144.58a	7.8
	MnT	$g\ kg^{-1}$	0.548abc	0.02c	0.007c	0.040bc	0.452abc	0.589abc	0.502abc	1.4a	0.180bc	1.07ab	74.58
	NiT	$mg\ kg^{-1}$	4.55a	0.04b	0.0b	0.0b	0.0b	0.23b	0.0b	0.0b	0.0b	0.0b	139.75
	PbT	$mg\ kg^{-1}$	13.5b	18.89ab	20.46ab	28.39a	23.74ab	22.02ab	23.81ab	22.07ab	26.15a	21.42ab	16.29
	ZnT	$mg\ kg^{-1}$	26.18a	19.7abc	18.8abc	24.23ab	24.08ab	25.18a	14.82bc	11.15c	18.88abc	21.17abc	17.36
	SOC	$dag\ kg^{-1}$	8.1a	4.17b	3.27bc	4.29b	1.47cd	1.01d	1.17d	1.19d	1.60cd	0.49d	26.53
	OM	$dag\ kg^{-1}$	16.85a	7.76b	7.09b	5.12bc	2.13c	1.31c	1.82c	1.15c	2.26c	0.6c	35.35
	TN	$dag\ kg^{-1}$	0.73a	0.25b	0.19bc	0.24b	0.09bc	0.06bc	0.07bc	0.06bc	0.09bc	0.02c	40.94
	MBC	$g\ kg^{-1}$	0.72abcd	0.87ab	0.78abc	1.02a	0.19de	0.17de	0.05e	0.22cde	0.3bcde	0.089e	44.4
	MBN	$mg\ kg^{-1}$	111.68a	52.52b	30.97b	45.46b	6.7b	8.4b	8.5b	18.02b	8.38b	12.83b	59.25
	BR	$mg\ kg^{-1}\ day^{-1}$	10.73	3.83	5.97	5.02	1.62	6.2	1.53	5.79	5.1	1.01	112.22
	$C\text{-}CO_2$	$mg\ kg^{-1}\ 5\text{-}day^{-1}$	53.64	19.17	29.89	25.1	8.09	16	7.65	28.96	25.81	5.04	112.22

qMic	—	0.95	2.06	2.42	2.35	1.40	1.72	0.41	1.91	1.72	1.84	41.84
qCO_2	—	0.015	0.004	0.008	0.006	0.015	0.117	0.047	0.025	0.029	0.013	235.79
VC	% $plot^{-1}$	100a	78.33abc	85.73ab	91.86a	81.61ab	85.89ab	51.9cd	49.66d	44.66d	61.42bcd	13.05
VV	m^3 $plot^{-1}$	1427a	81.2d	39.2d	296.07b	98.57d	21.47d	54.9d	182c	61.83d	53.57d	12.29

Figure S2 – Distribution and variation of the MDS across reference areas and post-mining sites during rainy and dry seasons for depths of 0–2.5 cm and 2.5–10 cm.

Table S3 – Summarization of rehabilitation quality index assessment for reference areas (R1 – R4) and post-mining sites (S1 – S6) during the rainy season at 0-2.5 cm and 2.5-10 cm soil depth

		Rainy season									
Depth		R1	R2	R3	R4	S1	S2	S3	S4	S5	S6
	Attributes	Wj*Sj	Wj*Sj	Wj*Sj	Wj*Sj	Wj*Sj	Wj*Sj	Wj*Sj	Wj*Sj	Wj*Sj	Wj*Sj
0-2.5 cm	Al_sat	0.023	0.009	0.009	0.009	0.010	0.010	0.010	0.013	0.013	0.010
	Bd	0.080	0.041	0.041	0.041	0.041	0.041	0.041	0.041	0.041	0.041
	eCEC	0.087	0.040	0.039	0.033	0.041	0.031	0.030	0.031	0.033	0.042
	FC_10	0.075	0.038	0.039	0.039	0.039	0.039	0.038	0.039	0.039	0.038
	FeT	0.077	0.038	0.038	0.038	0.038	0.038	0.038	0.038	0.038	0.038
	NiT	0.065	0.037	0.046	0.046	0.046	0.033	0.038	0.046	0.046	0.046
	OM	0.083	0.041	0.042	0.041	0.040	0.042	0.039	0.041	0.041	0.038
	PBS	0.022	0.012	0.012	0.012	0.012	0.012	0.012	0.012	0.012	0.012
	pCEC	0.082	0.042	0.042	0.042	0.042	0.042	0.040	0.042	0.041	0.040
	Pd	0.077	0.039	0.039	0.039	0.039	0.039	0.039	0.039	0.039	0.039
	PWP	0.081	0.041	0.042	0.042	0.042	0.042	0.042	0.042	0.041	0.041
	S	0.018	0.010	0.010	0.010	0.010	0.010	0.010	0.008	0.009	0.009
	SOC	0.079	0.038	0.041	0.040	0.040	0.040	0.039	0.041	0.040	0.036
	TN	0.081	0.039	0.041	0.041	0.040	0.039	0.038	0.041	0.041	0.037
	VV	0.070	0.036	0.036	0.036	0.036	0.035	0.036	0.035	0.036	0.036
	RQI = ∑	1.000	0.501	0.515	0.508	0.514	0.493	0.490	0.508	0.510	0.501
	Al_sat	0.018	0.007	0.007	0.007	0.008	0.003	0.007	0.008	0.000	0.004
	Bd	0.064	0.033	0.033	0.033	0.033	0.033	0.033	0.033	0.033	0.033

2.5-10 cm	BR	0.059	0.027	0.030	0.029	0.027	0.030	0.028	0.020	0.029	0.019
	C-CO2	0.059	0.027	0.030	0.029	0.027	0.030	0.028	0.020	0.029	0.019
	FC_10	0.064	0.032	0.033	0.033	0.032	0.033	0.032	0.033	0.033	0.032
	FeT	0.060	0.031	0.030	0.030	0.030	0.030	0.030	0.030	0.030	0.030
	H+Al	0.066	0.026	0.029	0.030	0.029	0.027	0.034	0.024	0.018	0.022
	K	0.059	0.031	0.029	0.029	0.036	0.025	0.026	0.028	0.032	0.036
	MBC	0.053	0.027	0.028	0.025	0.020	0.026	0.027	0.027	0.026	0.027
	PBS	0.015	0.006	0.006	0.006	0.006	0.004	0.005	0.004	0.004	0.004
	PbT	0.051	0.028	0.026	0.026	0.026	0.026	0.026	0.026	0.026	0.026
	pCEC	0.066	0.034	0.034	0.034	0.034	0.034	0.032	0.033	0.033	0.033
	Pd	0.056	0.029	0.028	0.028	0.028	0.029	0.028	0.028	0.028	0.028
	PWP	0.067	0.034	0.034	0.034	0.034	0.034	0.034	0.034	0.034	0.034
	S	0.066	0.033	0.034	0.034	0.033	0.033	0.030	0.034	0.033	0.031
	SOC	0.064	0.033	0.033	0.033	0.033	0.033	0.030	0.032	0.032	0.030
	TN	0.062	0.031	0.031	0.032	0.031	0.031	0.024	0.031	0.031	0.028
	VV	0.052	0.027	0.027	0.027	0.027	0.027	0.027	0.026	0.027	0.027
	RQI = ∑	1.000	0.496	0.502	0.498	0.495	0.486	0.481	0.471	0.479	0.463

Table S4 – Summarization of rehabilitation quality index assessment for reference areas (R1 – R4) and post-mining sites (S1 – S6) during the dry season at 0-2.5 cm and 2.5-10 cm soil depth.

		Dry season									
Depth		R1	R2	R3	R4	S1	S2	S3	S4	S5	S6
	Attributes	Wj*Sj	Wj*Sj	Wj*Sj	Wj*Sj	Wj*Sj	Wj*Sj	Wj*Sj	Wj*Sj	Wj*Sj	Wj*Sj
0-2.5 cm	Al_sat	0.027	0.010	0.010	0.010	0.014	0.010	0.011	0.010	0.014	0.010
	Bd	0.101	0.051	0.051	0.051	0.051	0.051	0.051	0.051	0.051	0.051
	eCEC	0.114	0.047	0.046	0.044	0.047	0.041	0.030	0.034	0.043	0.048
	FC_10	0.096	0.050	0.051	0.049	0.050	0.050	0.050	0.050	0.050	0.050
	MBN	0.084	0.042	0.042	0.031	0.038	0.041	0.034	0.042	0.039	0.034
	OM	0.103	0.054	0.054	0.053	0.052	0.048	0.050	0.053	0.052	0.045
	pCEC	0.105	0.054	0.054	0.053	0.054	0.053	0.053	0.053	0.053	0.052
	PWP	0.106	0.055	0.055	0.054	0.055	0.054	0.055	0.055	0.055	0.055
	SOC	0.102	0.053	0.053	0.052	0.053	0.053	0.052	0.048	0.053	0.049
	TN	0.080	0.042	0.042	0.042	0.042	0.042	0.041	0.032	0.041	0.038
	VV	0.082	0.042	0.042	0.042	0.042	0.042	0.042	0.041	0.042	0.042
	RQI = ∑	1.000	0.500	0.500	0.481	0.499	0.485	0.468	0.469	0.493	0.476
	Al_sat	0.038	0.014	0.014	0.014	0.014	0.015	0.014	0.014	0.014	0.014
	Bd	0.082	0.041	0.041	0.041	0.041	0.041	0.041	0.041	0.041	0.041
	FC_10	0.093	0.047	0.047	0.047	0.047	0.046	0.047	0.047	0.047	0.046
	H+Al	0.087	0.044	0.044	0.044	0.044	0.045	0.046	0.046	0.045	0.045
	K	0.078	0.034	0.042	0.035	0.038	0.037	0.031	0.028	0.043	0.043

OM	0.089	0.045	0.045	0.042	0.046	0.045	0.043	0.043	0.044	0.042
PBS	0.021	0.011	0.011	0.011	0.011	0.011	0.011	0.011	0.011	0.011
pCEC	0.093	0.048	0.048	0.047	0.048	0.047	0.045	0.047	0.047	0.046
Pd	0.081	0.041	0.041	0.041	0.041	0.041	0.041	0.041	0.041	0.041
PWP	0.095	0.048	0.048	0.048	0.048	0.047	0.048	0.048	0.048	0.048
SOC	0.092	0.046	0.047	0.047	0.046	0.047	0.046	0.046	0.046	0.044
TN	0.086	0.044	0.045	0.045	0.044	0.044	0.042	0.042	0.043	0.041
VV	0.065	0.033	0.033	0.033	0.033	0.033	0.033	0.032	0.033	0.033
RQI = ∑	1.000	0.495	0.504	0.494	0.499	0.498	0.487	0.486	0.502	0.496

Manuscript 3: Micromorphological indicators of pedogenesis in Technosols developed from mine wastes and tailings containing iron sulphides

Rugana Imbaná[1,2], Łukasz Uzarowicz[1]*, Zbigniew Zagórski[1], Mateusz Stolarczyk[3], Wojciech Szymański[3]

[1] Warsaw University of Life Sciences SGGW, Institute of Agriculture, Department of Soil Science, Nowoursynowska Str. 159, building no. 37, 02-776 Warsaw, Poland

[2] Universidade Federal de Viçosa, Department of Soil Science, R. Purdue S/N, Campus Universitário, Viçosa, Minas Gerais, 36570-900, Brazil

[3] Jagiellonian University in Cracow, Institute of Geography and Spatial Management, Gronostajowa Str. 7, 30-387 Kraków, Poland

* Corresponding author: Łukasz Uzarowicz, lukasz_uzarowicz@sggw.edu.pl

ORCID iD:

https://orcid.org/0000-0001-6476-2571 (R. Imbaná)

https://orcid.org/0000-0002-7982-404X (Ł. Uzarowicz)

https://orcid.org/0000-0001-6342-1847 (Z. Zagórski)

https://orcid.org/0000-0001-8317-2315 (M. Stolarczyk)

https://orcid.org/0000-0002-5894-5176 (W. Szymański)

Research highlights

Pedofeatures were identified in Technosols developed from Fe sulphide mine waste.

Crumb microstructure developed in the topsoil of biologically active soils.

Hypocoatings and quasicoatings formed by Fe oxide translocation and precipitation.

Clay and Fe oxide coatings indicated active colloidal fraction translocation.

Gypsum crystals crystallised in the soil groundmass.

Abstract: The study aimed to use soil micromorphology to reveal the microscopic effects of soil-forming processes in young (up to about 200 years) Spolic Technosols developed from mine wastes containing iron (Fe) sulphides. Thin sections were analysed under petrographic microscopes. Three soil profiles developed from sulphide-rich mine wastes and tailings were studied in two abandoned pyrite mines in Rudki and Wieściszowice, south Poland. Morphological observations showed that the studied profiles were poorly developed. However, microscopic investigations allowed for the identification of a set of pedogenic features as follows: (1) pedogenic structure (in particular in the topsoil) being an effect of soil organic matter accumulation and physical and biological alteration of technogenic parent material; (2) Fe oxide hypocoatings and quasicoatings, which are the result of Fe mobilisation in the strongly acidic soil environment, followed by translocation in pore waters, incorporation and precipitation of Fe oxides inside a soil groundmass; (3) clay and Fe oxide coatings and infillings along pores which are the result of clay translocation in strongly acidic soils; (4) pedogenic gypsum in a form of rosettes or single crystals dispersed in the groundmass as an effect of crystallisation from pore waters rich in Ca and sulphate ions; and (5) bioturbations (e.g., root channels) being an effect of biota activity. The study showed that despite their young age and initial stage of soil profile development, the Technosols under investigation are subject to natural soil-forming processes on the microscale that transform technogenic parent materials into functioning soils.

Keywords: Technogenic soils; Soil-forming processes; Soil micromorphology; Microstructure; Iron oxide hypocoatings; Iron oxide quasicoatings; Clay coatings

1. Introduction

Soil micromorphology, which includes the microscopic analysis of soil thin sections (Poch and Stoops, 2023), offers valuable insights into pedogenic processes (McKeague and Sheldrick, 1980; Mermut et al., 1985; Stoops, 2021; Chen et al., 2024) and the mineral transformations across diverse ecosystems (Schaefer et al., 2008; Uzarowicz, 2013; Lopes et al., 2022; Ruiz et al., 2022; Mor and Ravindra, 2023). It elucidates soil genesis based on the microscale effects of soil-forming processes, such as, for example, soil microstructure, void arrangement, groundmass features, and the formation of pedofeatures (Stoops, 2003, 2014). Consequently, thin-section analyses are essential for understanding the complex formation processes of Technosols (Adderley et al., 2010; Howard and Orlicki, 2016). The formation of Technosols is essentially influenced by human activities such as mining, deposition of industrial wastes on the land surface, and urbanisation. However, natural soil-forming processes significantly affect Technosol formation (Schad, 2018). These processes initiate when mine and industrial wastes are deposited on the land surface. Further evolution of Technosols is controlled by a few soil-forming factors, from which vegetation developing on reclaimed disposal sites or post-industrial areas plays a significant role (Watteau et al., 2018; Queiroz et al., 2022; Tarnawczyk et al., 2024; Uzarowicz et al., 2025).

Micromorphological analysis has proven effective in identifying early evidence of pedogenesis in Technosols and monitoring their development under different conditions (Itkin et al., 2018; Watteau et al., 2019; Colombini et al., 2020; Romanis et al., 2021; Ruiz et al., 2022). However, few studies have concentrated on the micromorphological characterisation of technogenic soils derived from sulphide-bearing mine waste (Uzarowicz and Skiba, 2011). Greater emphasis has been placed on the effects of sulphide transformations on soil properties and mineral composition (Néel et al., 2003; Uzarowicz, 2013) and the influence of reclamation processes on soil biological properties (Stępniewska et al., 2020; Uzarowicz et al., 2020; Wolińska et al., 2020; Kolařík et al., 2021). Generally, iron (Fe) sulphide minerals such as pyrite, marcasite, and their precursors undergo oxidation in the presence of water and oxygen, often facilitated by microbial activity (Fanning et al., 2002; Uzarowicz and Skiba, 2011). This oxidation leads to acidic conditions that primarily promote the formation of gypsum and jarosite (Uzarowicz, 2013; Sánchez-Marañón et al., 2015; Pohl et al., 2021). Other consequences of this acidic environment include the transformation of inherited phyllosilicates (e.g., mica and chlorite) into swelling clays such as smectite and vermiculite, as well as the dissolution of less resistant clay minerals (Krasil'nikov, 1997; Uzarowicz et al., 2008; 2011; 2012).

Micromorphological features of acid sulphate soils (i.e., soils naturally rich in Fe sulphides occurring, for example, in coastal areas worldwide) have been well-recognised (Fanning et al., 2002; Poch et al., 2009). Common pedofeatures that result from Fe sulphide transformation in these soils include bright yellow jarosite coatings, Fe oxide pseudomorphs after Fe sulphides, and microlaminated silica coatings on fine sand (Poch et al., 2004; 2009; Fanning et al., 2017). The micromorphological and submicromorphological effects of Fe sulphide transformation in Technosols have been investigated by Uzarowicz (2013), who studied the chronosequence of Technosols alongside natural soils, such as Leptosols and Cambisols, derived from sulphide-rich parent materials in Poland. This study revealed poorly crystalline ferrihydrite, cubic jarosite crystals, euhedral or subhedral gypsum, and secondary Fe oxide coatings and infillings resulting from pyrite weathering.

Several studies revealing the micromorphological features of Technosols were published recently. For instance, Acosta et al. (2011) stressed integrating micromorphological evidence of faunal activity with metal partitioning data in assessing ecological functions of contaminated soils, as total metal concentrations alone could not explain soil fauna limitations, especially in industrial sites, where high Pb and Zn associations with organic matter caused the most severe functional impairments. Arocena et al. (2010, 2012), and Zanuzzi et al. (2009) studied Technosols amended with pig manure, sewage sludge, and marble waste in acid, metal-contaminated mine sites in south-eastern Spain. Results showed these amendments improved soil chemical properties and microstructure, promoting granular structure formation and enhancing biological activity, thus improving the potential for reclaiming degraded areas into productive ecosystems. Watteau et al. (2018) demonstrated that Technosols can rapidly develop key soil functions through bioturbation and the formation of porosity. Their study reinforced the value of micropedology as a tool for understanding early pedogenetic changes and for guiding Technosol management. Moreover, the microscopic evidence of soil microaggregation and pedogenic carbonate formation was found in Technosols developed on surfaces of thermal power station ash disposal sites (Uzarowicz et al. 2017; Konstantinov et al., 2020). Colombini et al. (2020) described Technosols formed on a former coking plant site containing 10–20% technogenic coal. Microfeatures in these soils include a crumb microstructure, subrounded peds, channel voids, and finely distributed organic matter. Queiroz et al. (2022) reported that Fundão tailings in Brazil, derived from iron-rich itabirite rocks primarily composed of hematite, goethite, and kaolinite, exhibited hypo- and quasicoatings impregnation as key pedofeatures. Ortega et al. (2022) examined Technosols developed from iron mine tailings aged 0, 15, and 40 years, alongside a natural reference soil. They found that between 15 and 40 years, the

Technosols exhibited advanced structural development and nutrient content comparable to those of natural soils. This rapid soil formation was attributed to the high clay content in the applied conglomerate layer, underscoring the effectiveness of this approach for the reclamation of mine tailings. Ruiz et al. (2022, 2023) studied Technosols developed from mine wastes rich in calcium, magnesium, and pyrite under various vegetation covers in Brazil, including sugarcane and grasslands. They identified angular blocky aggregates, Fe oxide concretions, and a dark brown microaggregate groundmass with strong organic–mineral associations, indicative of active pedogenic processes. Recently, Watteau et al. (2025) revealed the early pedogenetic micromorphological effects in soils of abandoned rare earth element mining sites undergoing reclamation in south China.

Despite these advances in the micromorphology of technogenic soils, there is a lack of comprehensive studies addressing Technosols derived from various industrial wastes, particularly those containing Fe sulphides. In particular, little is known about the initiation of pedogenic processes at the microscale and their effects on soil substrate organisation and pedofeature formation in such technogenic environments. This study aims to (i) determine the micromorphological characteristics of Technosols developed from Fe sulphide-bearing tailings and mine wastes, as well as (ii) identify the major pedogenic features in the studied soils and explain their origin. We hypothesise that a micromorphological analysis can reveal the microscopic effects of early-stage pedogenic processes in immature technogenic soils.

2. Material and methods

2.1. Study area

We studied three Technosol profiles (R1, R2, and W1) developed from Fe sulphide-rich mine wastes and tailings in Poland (Figs. 1 and 2). Profiles R1 and R2 were located in post-mining areas of the abandoned "Staszic" Fe sulphide mine in Rudki village, Holy Cross Mountains (Góry Świętokrzyskie), S Poland (profile R1 – 50°53'48.9"N, 21°05'57.5"E; profile R2 – 50°53'36.0"N, 21°04'49.9"E), which operated from the 1920s until 1971 (Uzarowicz and Skiba, 2011; Migaszewski et al., 2015a; 2015b; Gałuszka et al., 2016). In contrast, profile W1 was developed from pyrite-bearing mine wastes in Wieściszowice village, Western Sudeten Mountains, SW Poland (50°49'51.5"N, 15°58'18.9"E), where the exploitation continued between 1785 and 1925 (Uzarowicz and Skiba, 2011).

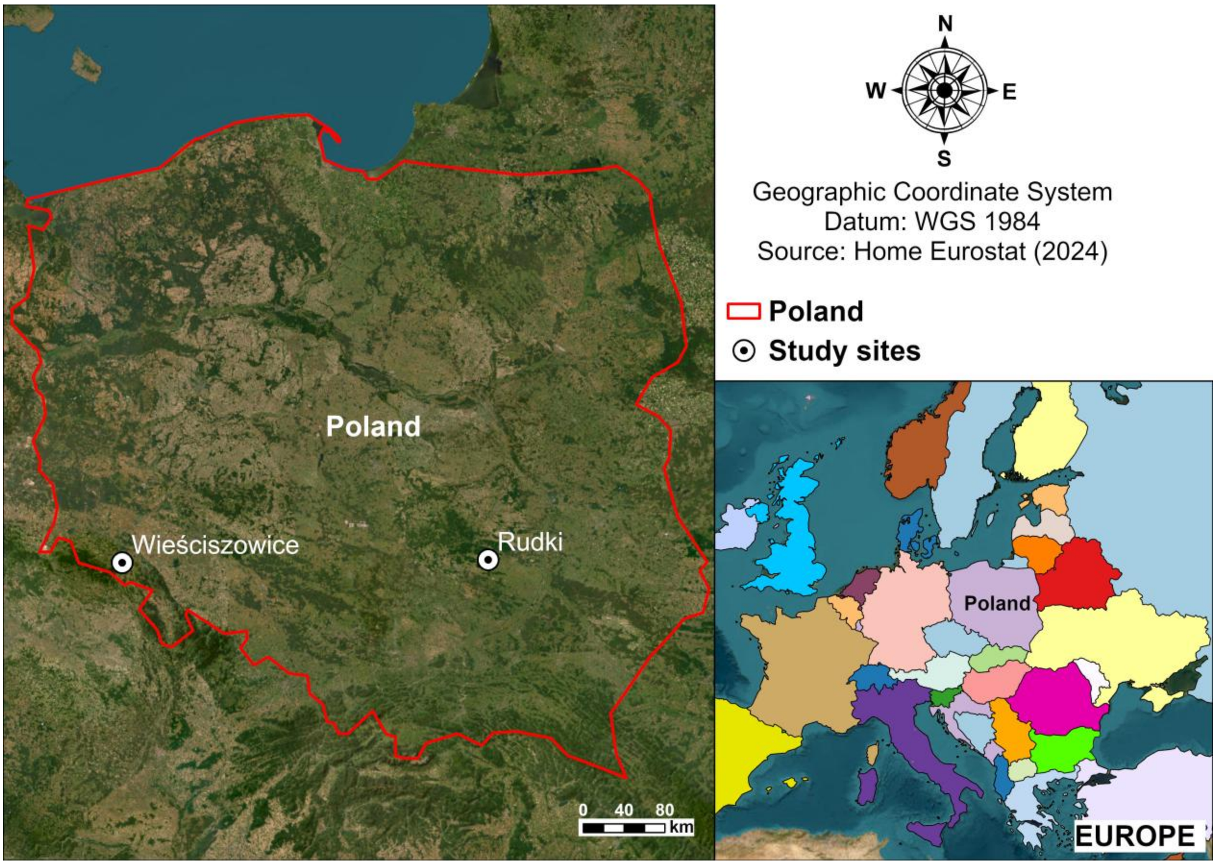

Figure 1 – Location of the study area and studied soil profiles.

The "Staszic" mine in Rudki produced two main types of industrial wastes: (1) carbonate- and Fe sulphide-rich tailings (flotation sludge) deposited in settling ponds and (2) loamy, sulphide-rich mine wastes deposited on the so-called "Serwis" dump. After mining cessation, reclamation works in the 1970s affected the properties and morphology of the studied soils. Profile R1 was formed on a reclaimed settling pond. The profile had a layer of dolomite- and Fe sulphide-rich tailings in the subsoil at a depth of 45–110 cm (Fig. 2). The topsoil of profile R1 (depth of 0–45 cm) comprised a layer composed of loamy mine waste material which was deposited on tailings during reclamation works. The covering layer contained elevated concentration of trace elements (e.g., Pb, Tl, As, U, Th) (Uzarowicz, 2011). Meadow vegetation, including *Medicago* sp., *Calamagrostis epigejos*, *Hypericum perforatum*, and *Rubus* sp. was developed on the land surface near profile R1. Profile R2 was located on the "Serwis" dump where strongly acidic (pH ~2–3) Fe sulphide-rich mine wastes were deposited. Reclamation works conducted in the 1970s involved lime application and planting grasses and legumes, although incomplete neutralisation left patches with acidic ground and limited vegetation. Profile R2 was located on the border of such a patch. Over time, these patches have been gradually colonised by *Calamagrostis epigejos*. The age of profiles R1 and R2 can be estimated at about 50–100 years.

Profile W1 was developed on a settling pond developed during the operation of the mine in Wieściszowice. This profile consisted of layers of silty (or silty loamy) material alternating with layers of sandy material (Fig. 2) derived from crushed pyrite-bearing mica-chlorite schists. The disposal site in Wieściszowice was covered with a sparse birch (*Betula pendula* Roth) and Scots pine (*Pinus silvestris* L.) forest. The site was not reclaimed, and the vegetation appeared due to natural plant succession. The approximate age of the W1 profile is 100–200 years.

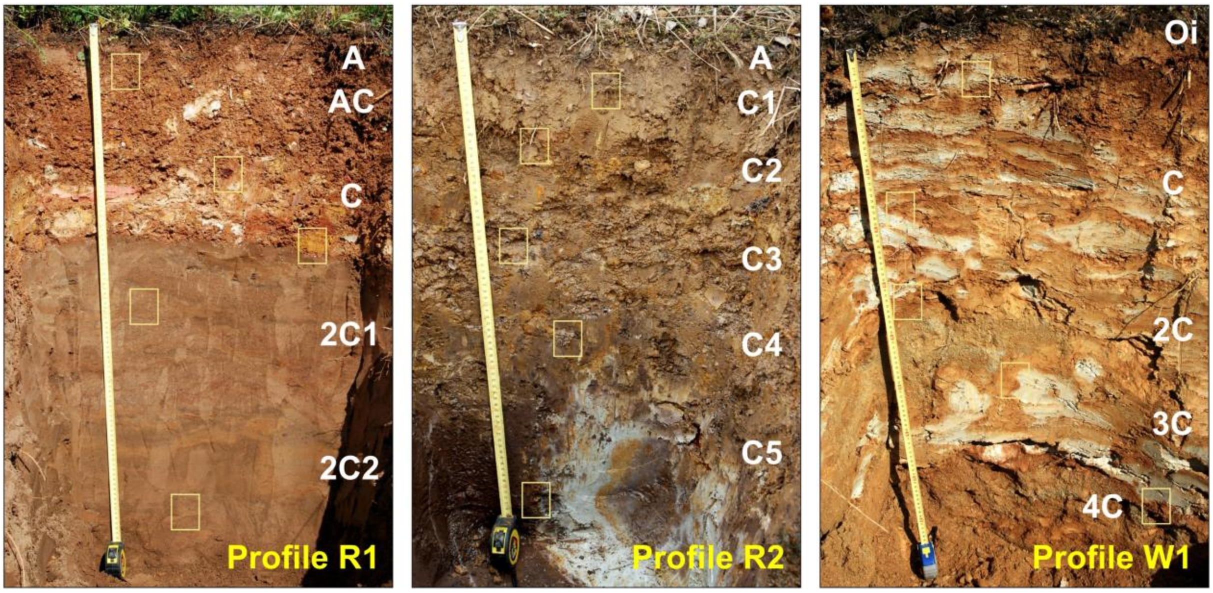

Figure 2 – Investigated soil profiles. The rectangles show areas from which Kubiëna boxes were taken for micromorphological studies.

2.2. Soil properties analyses

We described and classified technogenic soils represented by profiles R1, R2, and W1 according to the WRB classification system (IUSS Working Group WRB, 2022). Soil samples were collected from each soil horizon identified in the field. Roots and plant residues were removed before sample air-drying at room temperature. Fine earth (soil particles <2 mm) was obtained for each sample by dry sieving. The percentage of rock fragments was calculated using the masses of fine earth and rock fragments (>2 mm). Soil physical and chemical properties were analysed based on fine earth, following the pedological methods outlined by Pansu and Gautheyrou (2006). Soil texture was determined using the Bouyoucos-Casagrande hydrometer method modified by Prószyński (Warzyński et al., 2018). We determined soil texture classes based on the guidelines provided in USDA Handbook 18 (Soil Science Division Staff, 2017). The soil pH was measured using a potentiometer in deionised water and 1M KCl using a soil-solution ratio of 1:2.5 (w/v). The carbonate concentration was determined as calcium carbonate equivalent using the Scheibler volumetric method (reagent: 10% HCl). The total organic carbon (TOC), total nitrogen (TN), and total sulphur (TS) contents were measured through dry combustion using a CHNS elemental analyser (Vario Microcube, Elementar) (Pansu and Gautheyrou, 2006). To determine the TOC content in carbonate-bearing soil samples, inorganic carbon, calculated based on carbonate concentration, was subtracted from the carbon concentration based on CHNS analyses. The C/N ratio was calculated using the results for TOC and TN.

2.3. Soil thin section preparation and observations

The undisturbed soil samples were collected from selected horizons in the studied profiles using Kubiëna boxes (Fig. 2). They were air-dried and impregnated with the Araldite 2020 epoxy resin. Polished thin sections were prepared from the impregnated soil blocks according to the standard procedures (Stoops, 2021; Verrecchia and Trombino, 2021). These thin sections were examined in transmitted and reflected light through petrographic microscopes (Olympus SZX Z10, Olympus BX41). The micromorphological system and terminology given by Stoops (2021) and Verrecchia and Trombino (2021) were applied.

3. **Results**

3.1. Soil morphology and properties

The studied Technosols were poorly developed technogenic soils (Fig. 2). The only effect of pedogenesis visible in soil morphology was the accumulation of soil organic matter (SOM) in surface horizons. The majority of the soil substrate was composed of industrial wastes.

Profile R1 was a bipartite Technosol (Fig. 2). The subsoil (2C1 and 2C2 horizons) comprised dolomitic-pyritic tailings having sandy loam texture, high consistency and clear lamination of soil material. Despite containing sulphides, the subsoil was only slightly acidic (pH_{H2O} of 6.6 and 6.1 in 2C1 and 2C2 horizons, respectively) due to a high carbonate content of up to 54% in the 2C1 horizon (Table 1). The topsoil of profile R1 (A, AC, and C horizons) was a loamy material. The A and AC horizons had a granular structure. They contained many roots (Fig. 2). The C horizon was composed of mineral materials characterised by different colours (e.g., brown, red, orange, greyish), weakly affected by root activity. The A horizon was thin (0–3 cm) yet contained the highest total organic carbon (TOC) at 4.1% and total nitrogen (TN) at 0.37% in comparison with profiles R2 and W1 (Table 1).

Table 5. Selected physical and chemical properties of the studied Technosols.

Horizon	Depth (cm)	% of fraction			Soil texture class (USDA)	pH_{H2O}	pH_{KCl}	eq. of $CaCO_3$ (%)	TOC (%)	TN (%)	C/N	TS (%)
		2–0.05 mm	0.05–0.002 mm	<0.002 mm								
R1 profile – *Spolic Technosol (Pantoeutric, Epiloamic, Endoarenic, Endodolomitic, Endofluvic, Humic, Hyperartefactic, Raptic, Endohyposulfidic, Toxic)*												
A	0–3	66	24	10	Sandy Loam	7.4	6.9	1.8	4.10	0.37	11.1	0.59
AC	3–15	52	26	22	Sandy Clay Loam	7.8	7.1	0.3	1.75	0.17	10.1	0.57
C	15–45	38	29	33	Clay Loam	7.1	6.4	0.2	0.35	0.05	9.3	–
2C1	45–80	75	23	2	Loamy Sand	6.6	6.4	54.1	0	0.02	–	4.15
2C2	80–110	74	24	2	Loamy Sand	6.1	6.3	48.0	0	0.02	–	3.18
R2 profile – *Spolic Technosol (Epiarenic, Endoloamic, Ochric, Hyperartefactic, Thionic, Toxic)*												
Oi	1–0	–	–	–	–	–	–	–	–	–	–	
A	0–5	90	9	1	Sand	5.5	4.1	0	1.12	0.09	12.2	0.19
C1	5–15	71	18	11	Sandy Loam	4.9	4.5	0	0.76	0.07	11.7	0.25
C2	15–25	43	55	2	Silt Loam	3.7	3.5	0	0.42	0.05	8.2	1.34
C3	25–40	46	53	1	Silt Loam	3.2	3.0	0	0.58	0.06	9.3	1.50
C4	40–55	52	46	2	Sandy Loam	2.9	2.7	0	0.47	0.06	7.5	3.93
C5 grey and rusty	55–80	22	59	19	Silt Loam	3.7	3.3	0	0.14	0.07	2.1	0.57

C5 brown	55–80	73	17	10	Sandy Loam	4.0	3.4	0	0.10	0.03	3.0	0.26
W1 profile – *Stagnic Spolic Technosol (Polyloamic, Polyarenic, Dystric, Ochric, Hyperartefactic)*												
Oi	1–0	–	–	–	–	–	–	–	–	–	–	
C grey	0–45	4	78	18	Silt Loam	4.7	4.3	0	0.11	0.02	4.9	0.26
C rusty	0–45	19	66	15	Silt Loam	4.8	4.6	0	0.09	0.02	4.6	0.59
2C	45–60	92	7	1	Sand	4.7	4.4	0	0.05	0.02	2.8	0.45
3C grey	60–80	2	87	11	Silt	4.8	4.6	0	0.10	0.03	3.8	0.18
3C rusty	60–80	7	81	12	Silt Loam	4.6	4.2	0	0.10	0.02	4.6	0.24
4C	80–95	87	12	1	Sand	4.9	4.3	0	0.08	0.02	4.2	0.70

Explanations: 0 – below detection limit; – not analysed; TOC – total organic carbon; TN – total nitrogen; C/N ratio – the relationship between TOC and TN; TS – total sulphur.

Most soil horizons in profile R2 (A, C1, C2, C3, C4 horizons) were composed of brown loamy material with orange concentrations. However, the C5 horizon was composed of dark brown, greyish and orange mineral substrates differing in soil texture (Table 1). There were no carbonates throughout profile R2. It showed a strongly acidic reaction (pH_{H2O} 3.0–5.5) due to sulphide weathering. Fragments of sulphide rock several centimetres in size were frequently observed during fieldwork. Profile R2 contained lower TOC and TN concentrations in the topsoil (A horizon contained 1.12% of TOC and 0.09% of TN) and subsurface horizons (C1–C5 horizons) compared to profile R1.

Profile W1 was characterised by an alternation of massive silty loamy material with sandy layers or patches (Fig. 2). Internal parts of silty loamy materials had greyish colours suggesting the effects of stagnic properties. Most of the soil material had orange or rusty colours. Profile W1 had a weakly developed Oi horizon, reflecting minimal SOM accumulation at the soil surface. The profile was acidic (pH_{H2O} of 4.6–4.9) and entirely carbonate-free (Table 1).

3.2. Micromorphological features

Profile R1 displayed apparent differences in microstructural features between its topsoil (A, AC, and C horizons) and the subsoil (2C1 and 2C2 horizons) (Fig. 3 and 4; Table 2). The topsoil horizons of profile R1 showed subangular blocky microstructure in the C horizon and complex microstructure with crumbs in the A horizon (Fig. 3A–D). The crumbs in the A horizons were well developed and sized up to a few millimetres. The groundmass in the crumbs was characterised by a porphyric c/f related distribution pattern (Fig. 3A and B; Fig. 4A and B). The coarse components of the groundmass in the topsoil consisted of Fe-bearing rocks, sandstone/siltstone, and quartz grains (Fig. 3C and D; Fig. 4G and H). Micromass in the A horizon was a material rich in SOM and clay. It exhibited an undifferentiated or speckled birefringence fabric (b-fabric). In contrast, the C horizon contained a micromass rich in kaolinite clay with a striated b-fabric (Fig. 4C and D).

A combination of alternating layers with single-grain and massive microstructures characterised the subsoil of profile R1 (2C1 and 2C2 horizons), i.e., the tailings sedimented in former tanks (Fig. 3E and F). The groundmass of the subsoil was characterised by the fine monic (in fine-grained layers) and the coarse monic (in coarse-grained layers) c/f related distribution. The coarse components occurred as carbonate and Fe sulphide grains, with minimal presence of micromass constituting poorly crystalline Fe oxides in micro-laminae in fine-grained layers (Fig. 4I and J). Subhedral gypsum crystals were the major pedofeatures found in profile R1 (Fig. 4E and F; Table 2). Gypsum rosettes were found in the C horizon (Fig. 4E and F). However, single gypsum crystals dispersed in the groundmass occurred in the subsoil horizons (Fig. 4I and J). Pedoturbations due to root activity (e.g. a wedge formed by the roots) were found in the A horizon (Fig. 4A–D).

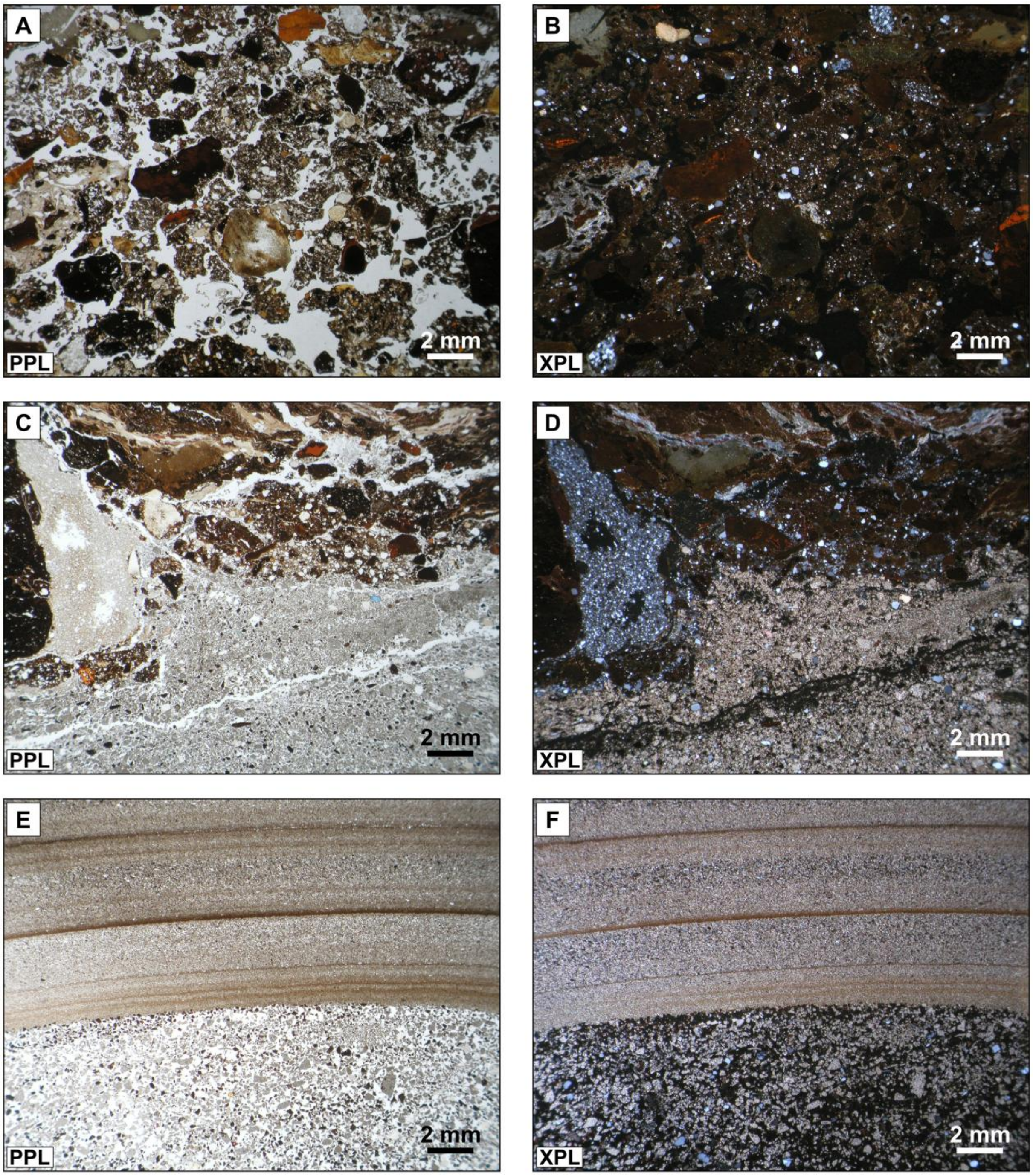

Figure 3 – Micromorphological features of R1 profile at low magnification. A and B – a complex microstructure within the A horizon, characterised by aggregates and rock fragments (Fe-bearing rocks, carbonate rocks, sandstones, siltstones) separated by compound packing voids. C and D – the transitional zone between the loamy C horizon (top) and the 2C1 horizon (bottom) comprising dolomitic-pyritic tailings (post-flotation sludge). Note a heterogeneity of

soil material in the C horizon composed of soil aggregates, Fe-rich rock fragments, siliceous sandy material, and massive clay aggregations. E and F – dolomitic-pyritic tailings (post-flotation sludge) in the subsoil of profile R1 (2C1 horizon), featuring coarse-grained material with single-grain microstructure and fine-grained laminated material exhibiting a massive microstructure. Soil micromass containing Fe oxides occurs in dark laminas. Coarse-grained material contains Fe sulphides (black particles in the E image). Explanations: PPL – plane-polarized light, XPL – cross-polarized light.

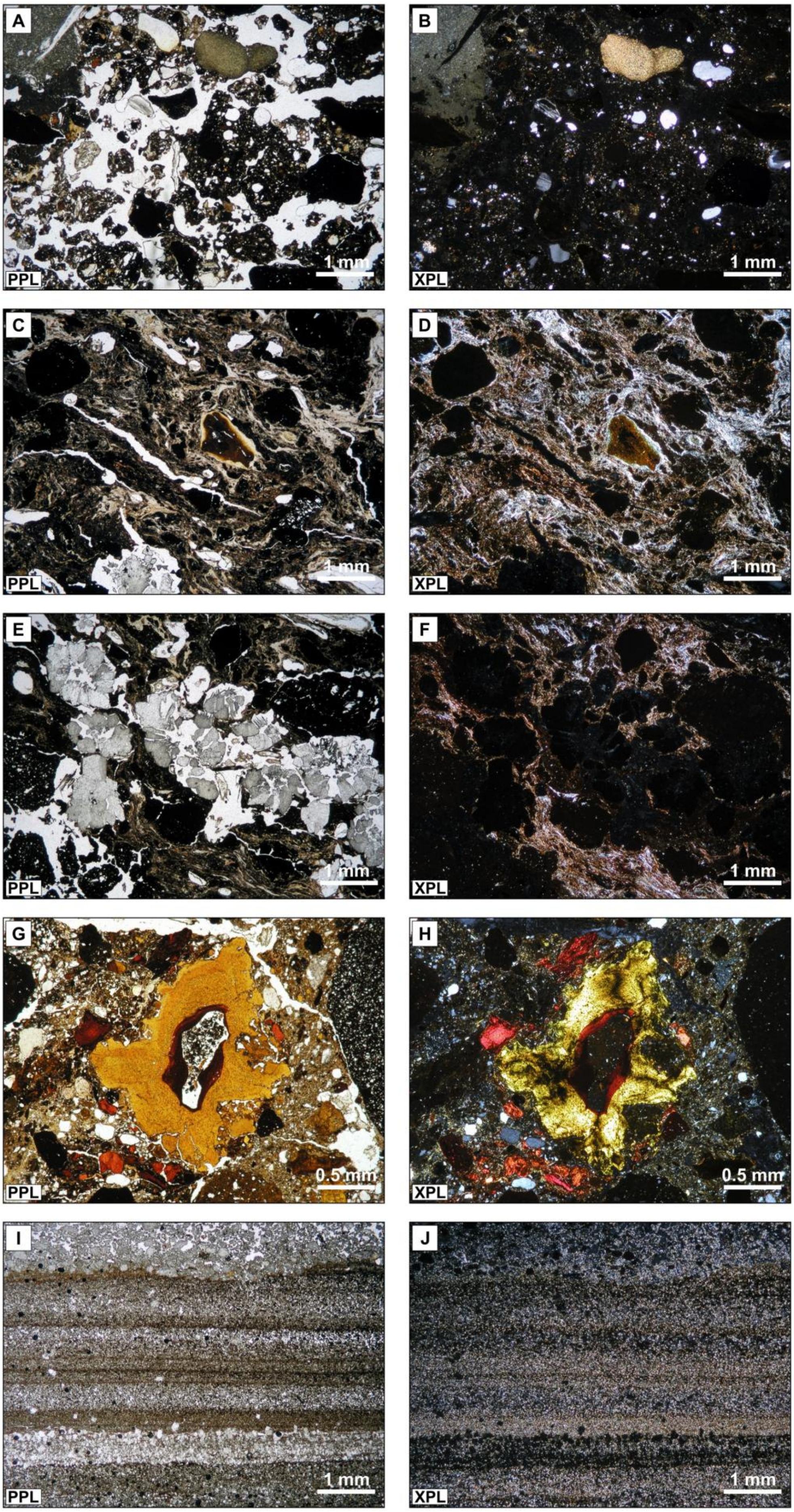
A
PPL
1 mm
B
XPL
1 mm
C
PPL
1 mm
D
XPL
1 mm
E
PPL
1 mm
F
XPL
1 mm
G
PPL
0.5 mm
H
XPL
0.5 mm
I
PPL
1 mm
J
XPL
1 mm

Figure 4 – Detailed micromorphological features of profile R1. A and B – a soil material with complex microstructure composed of aggregates (crumbs) and rock fragments (Fe-bearing rocks, carbonate rocks, siltstones) separated by compound packing voids in the A horizon. Micromass in aggregates have an undifferentiated or speckled b-fabric. Note the occurrence of a wedge (top left) formed in a rock fragment due to root activity. C and D – massive microstructure in the C horizon. The micromass is most likely composed of kaolinite-rich clay and is characterised by the striated b-fabric. Rounded root channels are developed in the soil material. E and F – Subhedral gypsum crystals arranged in rosettes in the C horizon (the crystals are so thin that the interference colours are not visible under XPL). G and H – Clay and Fe oxide particles in the C horizon most likely inherited from the technogenic parent material. I and J – A laminated dolomitic-pyritic tailings (post-flotation sludge) in the 2C1 horizon. Soil micromass containing Fe oxides occurs in dark laminas. Part of the black spots in the J image are most likely gypsum crystals, which are so thin that the interference colours are not visible under XPL. Explanations: PPL – plane-polarized light, XPL – cross-polarized light.

Soil material in a 0–55 cm layer in profile R2 was dominated by weakly developed subangular blocky microstructure with partially accommodated or unaccommodated planar voids separating soil aggregates (Fig. 5A and B; Table 2). The subsoil (C5 horizon) revealed a lenticular microstructure (Fig. 5C and D). However, subangular blocky aggregates separated by planar voids also occurred in the soil material of the C5 horizon (not shown). In profile R2, a porphyric c/f-related distribution pattern of the groundmass was observed, with quartz grains as the predominant coarse components. The micromass was composed of clay minerals and Fe oxides, and it exhibited a speckled or striated b-fabric (Fig. 6A and B; Fig. 6E and F).

Profile R2 displayed a variety of distinct pedofeatures (Fig. 6A–F; Table 2). Iron oxide hypocoatings along pore surfaces were common (Fig. 6A and B). In the C5 horizon, well-developed clay coatings and infillings occurred within the pores (Fig. 6C and D). Part of the coatings have orange/rusty colours, indicating that the coatings contain an admixture of Fe oxides. Additionally, subhedral gypsum crystals arranged in rosettes were found in the C4 horizon (Fig. 6E and F). Pedoturbations due to root activity were occasionally found across the soil groundmass (not shown).

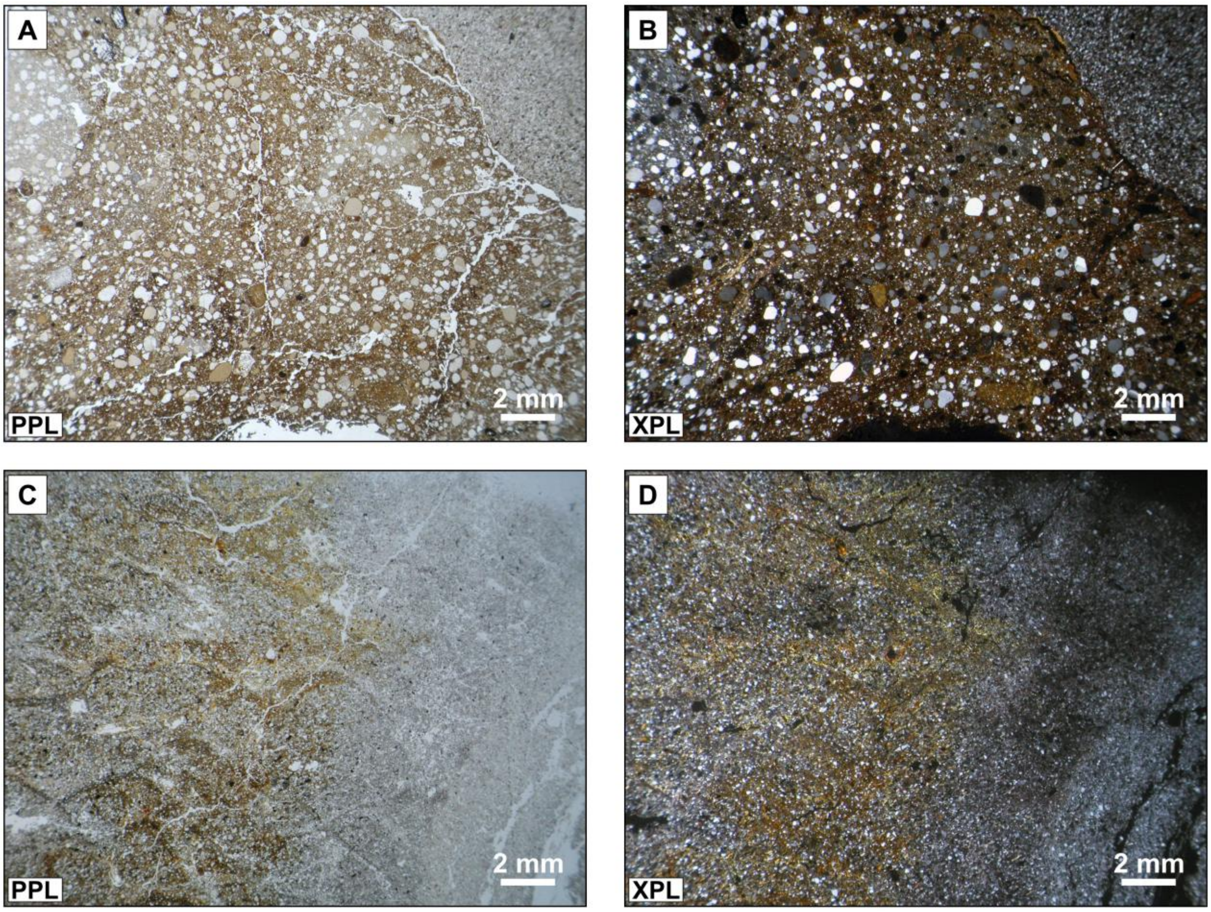

Figure 5 – Micromorphological features of profile R2 at low magnification. A and B – A weakly developed angular blocky microstructure in the C3 horizon. The aggregates have a groundmass with a porphyric c/f-related distribution. C and D – A transitional zone between grey material (on the right) and brown material in the C5 horizon, displaying a lenticular microstructure with a porphyric c/f-related distribution of the groundmass and a speckled b-fabric of micromass. Explanations: PPL – plane-polarized light, XPL – cross-polarized light.

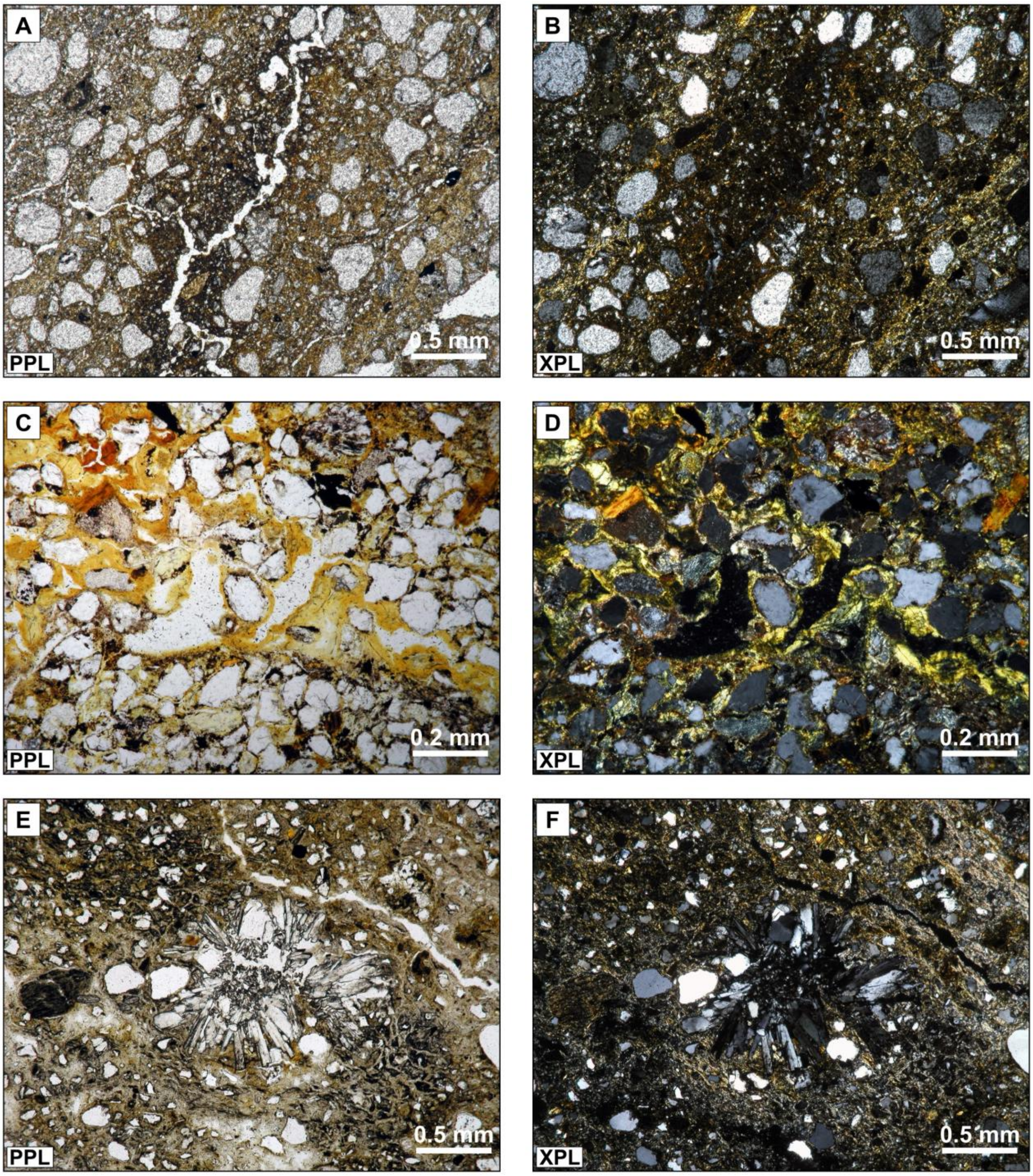

Figure 6 – Detailed micromorphological features of profile R2. A and B – Iron oxide hypocoatings along the planar void in the C3 horizon. The groundmass has a porphyric c/f-related distribution. The micromass is characterised by a speckled or striated b-fabric. C and D – Clay and iron oxide coatings and infillings occurring inside soil pores in the C5 horizon. E and F – Subhedral and euhedral gypsum crystals arranged in rosettes in the C4 horizon. The groundmass has a porphyric c/f-related distribution. The micromass is characterised by a speckled or striated b-fabric. Explanations: PPL – plane-polarized light, XPL – cross-polarized light.

Profile W1 exhibited massive microstructure in silty loamy layers (C and 3C horizons) and single-grain microstructure in sandy layers (2C and 4C horizons) (Fig. 7 and 8; Table 2). This contrast emphasises the profile's textural variability and depositional dynamics during the waste deposition in a disposal site. The groundmass of profile W1 was characterised by fine monic and coarse monic c/f related distribution in silty loamy layers and sandy layers, respectively (Fig. 7A–D). Coarse components were mineral grains (represented chiefly by quartz and phyllosilicates such as mica and chlorite) that originated by grinding the pyrite-bearing chlorite-mica metamorphic schists. The micromass in this profile was rich in clay minerals and Fe oxides, and it displayed a speckled b-fabric (Fig. 7 and 8). However, the muscovitic crystallitic b-fabric could be recognised in the micromass at higher magnification (Fig. 8F). Micromass was a minor constituent of sandy layers.

Typical pedofeatures in profile W1 included well-developed Fe oxide hypocoatings and quasicoatings formed on surfaces of the fine-grained (silty) material (Fig. 7A and B; Fig. 8A–D; Table 2). These features developed parallel to the transition zone between coarse-grained (sandy) and fine-grained (silty loamy) material. The further the quasicoatings occurred from the hypocoating, the less distinct and blurrier the Fe oxide rims were. Hypocoatings were more rusty and richer in Fe oxides than quasicoatings. Additionally, single subhedral or euhedral gypsum crystals dispersed in the groundmass were frequently found within silty layers (Fig. 8E and F). The soil substrate also contained pedoturbations due to root activity (Fig. 7A and B).

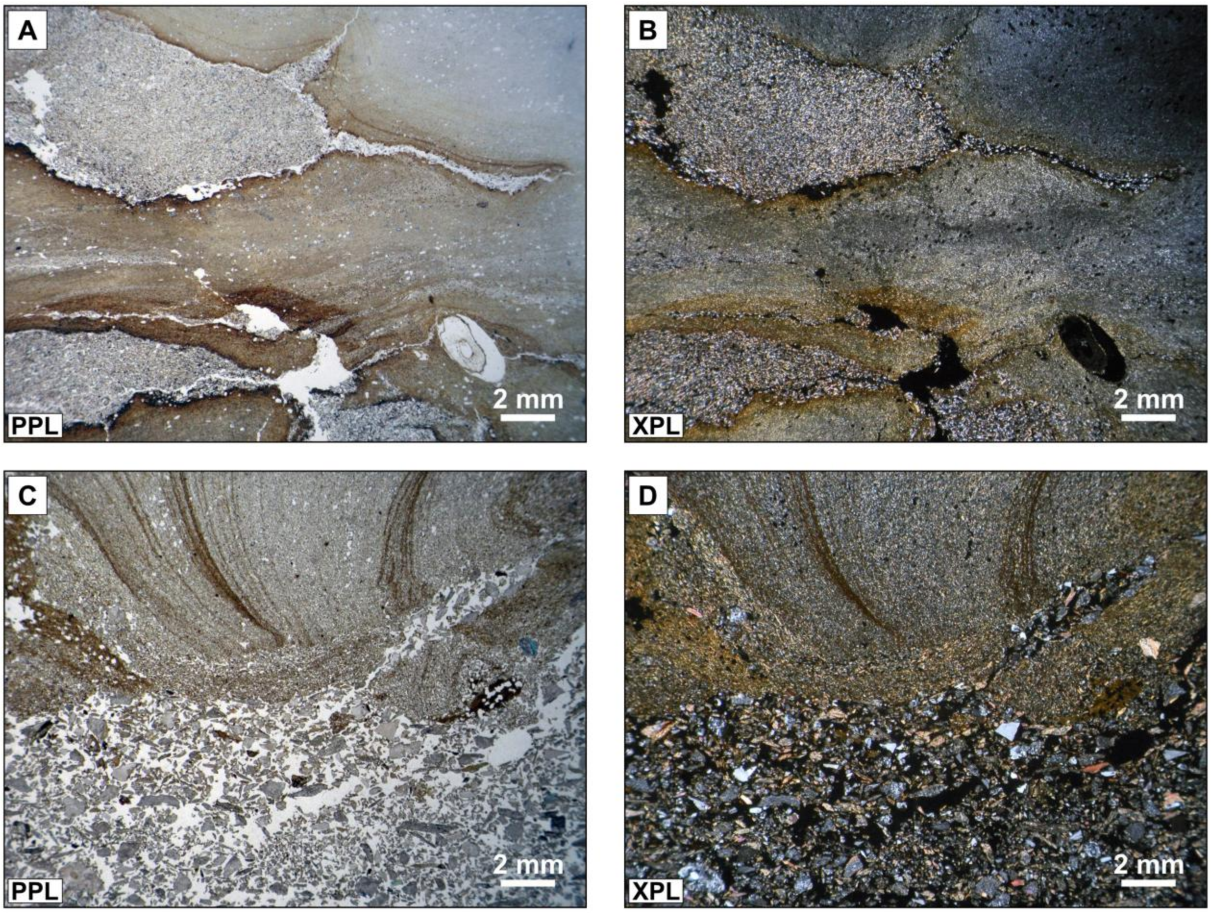

Figure 7 – Micromorphological features of profile W1 at low magnification. A and B – Patches of fine-grain (silty) and coarse-grain (sandy) materials with Fe oxide hypocoatings on the edges of fine-grain material, the transition between C and 2C horizons. A root channel is developed in fine-grained material (bottom right). C and D – Contact of coarse-grain (sandy) material with a laminated fine-grain (silty) material, the transition between C and 2C horizons. Explanations: PPL – plane-polarized light, XPL – cross-polarized light.

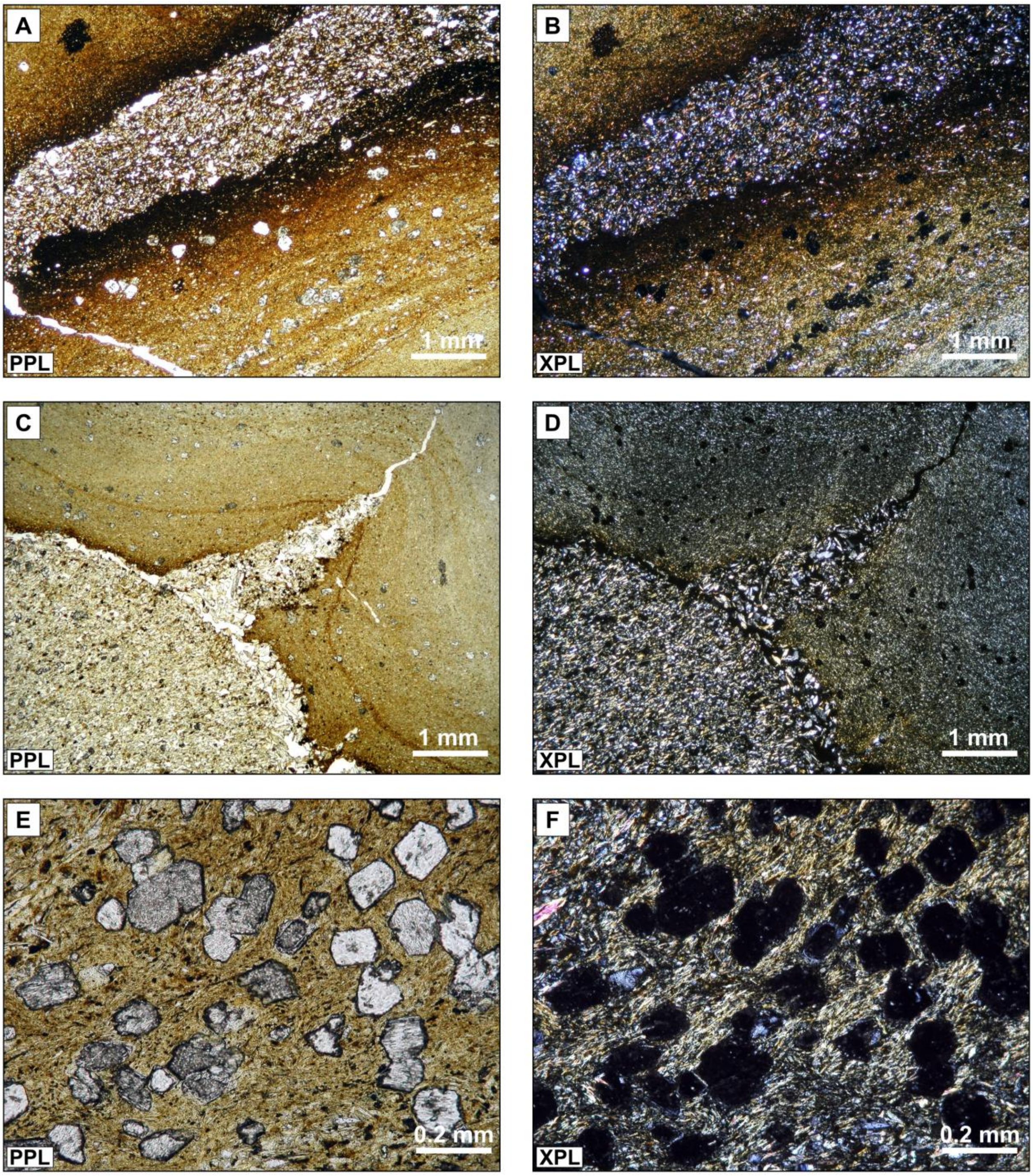

Figure 8 – Detailed micromorphological features of profile W1. A and B – The Fe oxide hypocoatings developed on the edge of fine-grained (silty) material divided by coarse-grained (sandy) material in the C horizon. C and D – The Fe oxide hypocoatings and a few generations of quasicoatings developed in the transition zone between coarse-grained (sandy) and fine-grained (silty) material, the C horizon. E and F – Subhedral and euhedral gypsum crystals dispersed in fine-grained (silty) material with muscovitic crystallitic b-fabric (the gypsum crystals are so thin that the interference colours are not visible under XPL), the C horizon. Explanations: PPL – plane-polarized light, XPL – cross-polarized light.

Table 6. Micromorphological features of the studied Technosols.

Soil profile	Part of the soil profile	Microstructure	Voids	Groundmass			Organic matter not included in the groundmass or pedofeatures	Pedogenic features
				c/f related distribution	Coarse components	Micromass (colour, nature, b-fabric)		
R1	Upper part of the reclamation layer (A and AC horizons at a depth of 0–15 cm)	Complex microstructure with crumbs and rock/mineral fragments	Complex packing voids	Porphyric (inside the crumbs)	Fe-bearing rock fragments, sandstone, siltstone, and quartz grains; occasional carbonate rock fragments	Dark-brown SOM-rich micromass with undifferentiated and speckled b-fabric	Occasional roots	Pedoturbations due to root activity
R1	Lower part of the reclamation layer (C horizon at a depth of 15–45 cm)	Subangular blocky microstructure	Packing voids, planar voids	Porphyric Fine monic	Fe-bearing rock fragments, sandstone, and quartz grains	White, grey, and brown clay micromass with striated or speckled b-fabric Part of the micromass is brown loamy material with undifferentiated b-fabric	Occasional roots	Gypsum rosettes Pedoturbations due to root activity
R1	A layer of tailings (2C1 and 2C2 horizons at a depth of 45–110 cm)	Separate fine-grained layers with massive microstructure and coarse-	Simple packing voids (in coarse-	Fine monic (in fine-grained layers)	Carbonate and Fe sulphide grains	Brown micromass rich in Fe oxides occurs only in micro-laminae in fine-grained layers	–	Single gypsum crystals dispersed within soil groundmass

		grained layers with single-grain microstructure	grained layers)	Coarse monic (in coarse-grained layers)				
R2	Topsoil (A, C1, C2, C3, C4 horizons at a depth of 0–55 cm)	Subangular and angular blocky microstructure	Planar voids	Porphyric	Quartz grains	Brown loamy micromass with speckled and striated b-fabric	Occasional roots	Fe oxide hypocoatings along planar voids Gypsum rosettes Pedoturbations due to root activity
R2	Subsoil (C5 horizon at a depth of 55–80 cm)	Lenticular microstructure, occasional subangular blocky aggregates	Planar voids	Porphyric	Quartz grains	Grey and brown loamy micromass with speckled b-fabric	–	Clay and Fe coatings and infillings in soil pores
W1	Silty loamy and silty layers (C and 3C horizons)	Massive microstructure	–	Fine monic	Quartz and phyllosilicate grains	Grey and brown silty and loamy micromass with speckled b-fabric	Occasional roots	Hypocoatings and quasicoatings on the surface of fine-grained (silty) layers Single gypsum crystals dispersed within soil groundmass Pedoturbations due to root activity
W1	Sandy layers (2C and 4C horizons)	Single-grain microstructure	Simple packing voids	Coarse monic	Quartz and phyllosilicate grains	–	Occasional roots	Pedoturbations due to root activity

Explanations: – lack of the feature, or a feature was difficult to recognise.

4. Discussion

This study presents micromorphological evidence of pedogenic processes in Spolic Technosols developed from mine wastes and tailings containing Fe sulphides. Although the studied soils were relatively young formations (up to about 200 years), they exhibited distinct microscale effects of pedogenic transformation and reorganisation of soil substrate. We identified the following micromorphological effects of pedogenesis in the investigated Technosols: (1) formation of pedogenic microstructure in the topsoil; (2) formation of Fe oxide hypocoatings and quasicoatings; (3) formation of clay and Fe coatings and infillings in soil pores; (4) crystallization of gypsum assemblages or single crystals; (5) pedoturbations due to biota activity.

Pedogenic microstructure formation was particularly evident in the A horizon of profile R1, which exhibited the highest biota activity compared to the other studied profiles. It was confirmed during field studies by a granular structure and a net of roots growing in the topsoil (Fig. 2). High biological activity in the profile R1 topsoil was confirmed by the previous studies in that area (Stępniewska et al., 2020; Uzarowicz et al., 2020; Wolińska et al., 2020). The microstructure in the A horizon of profile R1, characterised by crumbs separated by compound packing voids, most likely resulted from the combined effects of biological factors such as root and soil fauna activity (Stoops et al., 2018), along with physical processes such as shrinking-swelling and freezing-thawing affecting the studied soil (Özgan et al., 2015; Bryk et al., 2017; Van Vliet-Lanoë and Fox, 2018; Li et al., 2022). These biological and physical processes simultaneously altered the original material fabric (most likely characterised initially by a massive structure formed immediately after land reclamation in that area), leading to the development of an aggregated structure. Moreover, the generation of granular structure (and crumb microstructure) in the A horizon of profile R1 was also related to SOM accumulation (Table 1). Therefore, this highlights the considerable role of SOM in aggregation in Technosols, also confirmed in the previous studies of technogenic soils (Badin et al., 2009; Monserie et al., 2009; Séré et al., 2010; Uzarowicz et al., 2017).

In contrast to the topsoil horizons, the lower parts of the studied soil profiles were not affected much by structure-forming processes. The original distribution of soil components related to the deposition of mine wastes and tailings in disposal sites is maintained in the subsoil. Therefore, lamination and layering are typical of the subsoil of the R1 profile and throughout the W1 profile, as technogenic materials were deposited on the land surface as a slurry. Lamination and layering are characteristics of soil parent materials (both natural and anthropogenic) subject to sedimentation in water conditions (Uzarowicz et al., 2018; Al-Mufti et al., 2024; Łachacz et al., 2024). Furthermore, the occurrence of lenticular microstructure in the subsoil of profile R2 (Fig. 5C and D) is intriguing and not easy to explain. Such a microstructure is typical for frost-affected soils in polar regions or high-mountain areas (Van Vliet-Lanoë and Fox, 2018). Frost-generated microstructures, including lenticular forms, typically develop in moist, silt- and clay-rich materials by ice lens growth during freeze-thaw cycles (Van Vliet-Lanoë and Fox, 2018). We hypothesise that the mine waste material, which nowadays constitutes the subsoil of profile R2, in the past was deposited on the land surface during cold winter. Thus, the lenticular microstructure was developed in that material. Then, a new portion of the mine waste was most likely deposited on this material, which was frozen. Therefore, the lenticular microstructure was conserved in that material. Another explanation can be that the lenticular microstructure in the studied soils is a result of clay shrinking and swelling processes. The formation of lenticular microstructure is likely associated with the volume changes in the clay matrix during drying and wetting cycles (Boivin et al., 2004; Qi et al., 2022).

Iron oxide hypocoatings and quasicoatings are common pedofeatures in strongly acidic profiles R2 and W1 (Fig. 6A and B; Fig. 8A–D). Both are impregnative pedofeatures that appear as zones of amorphous or poorly crystalline Fe oxides within the soil matrix (Stoops, 2021; Verrecchia and Trombino, 2021). The identified hypocoatings are Fe oxide accumulations impregnating the soil groundmass directly adjoining the void edge (in profile R2) or occurring on the contact of fine-grained (silty loamy) and coarse-grained (sandy) materials (in profile W1). The formation of Fe oxide hypocoatings and quasicoatings in the studied Technosols is likely driven by the Fe release during Fe sulphide weathering, movement of acidic Fe-rich soil water in pores (profile R2) or layers/patches of permeable (sandy) materials (profile W1), and the subsequent impregnation of adjacent groundmass with Fe oxides. Quasicoatings were identified only in profile W1, and they have a form of rhythmic Fe oxide rims more or less parallel to a hypocoating. Quasicoatings found in profile W1 resemble Liesegang rings in some sedimentary rocks (Shahabpour, 1998; Plath, 2022; Quasim et al., 2023).

Based on soil morphology (Fig. 2), properties (Table 1), and micromorphological features (Fig. 7 and 8), we propose the following mechanism of hypocoating and quasicoating formation in profile W1: (1) the rainwater percolates through the soil profile and flows preferentially by permeable sandy layers/patches; (2) the water rich in Fe infiltrates into slowly permeable silty loamy material and Fe oxides crystallize at the contact of sandy and silty loamy groundmass; (3) once the amount of water flowing through the soil profile is small, majority of Fe oxides crystalizes as hypocoatings at the contact of sandy and silty loamy materials; (4) once the amount of water flowing through the soil profile is big, water most likely stagnate in sandy patches for some time leading to the formation of reducing conditions in which Fe^{3+} transforms into Fe^{2+} and in this state at the excess of water infiltrates more profound into the silty loamy groundmass; at some distance from the contact of sandy and silty loamy groundmass, redox conditions most likely changes into oxic ones and Fe oxides crystallize as quasicoating; as the amount of water in soil vary, the depth of Fe-rich water infiltration can differ, and therefore a group of rhythmic quasicoatings develops.

Other micromorphological features found in the studied soils are clay coatings and infillings (Fig. 6C and D) enriched in Fe oxides, which are the effects of colloidal fraction illuviation (Kühn et al., 2018; Queiroz et al., 2022). They were identified in the 5C horizon in profile R2, characterised by lenticular microstructure. Profile R2 has a very low pH, and the 5C horizon contains about 20% of the clay fraction in soil texture (Table 1), creating suitable conditions for clay dispersion and translocation within the profile. The presence of clay coatings and infillings suggests adequate water movement to carry and redeposit dispersed fine particles (clay minerals and Fe oxides), which is a process typical of well-developed soils (Alves et al., 2022; Kühn et al., 2018; Kumari, 2024; Stoops, 2021). Our findings indicate that clay and Fe oxide coatings can form not only in mature natural soils (for example in Podzols, Luvisols, and other soil containing argic horizon) (Kabała, 2023; Olifir et al., 2024), but they can originate in the groundmass of young (50–100 years old) technogenic soils as well.

Another important micromorphological evidence of pedogenic processes in the studied technogenic soils is gypsum crystallisation. Gypsum was previously confirmed in the studied soils based on scanning electron microscope observations (Uzarowicz and Skiba, 2011; Uzarowicz, 2013); however, we show micromorphological images of gypsum crystals in the present paper. Gypsum is a mineral frequently found in soils developed from gypsum rocks (Casby-Horton et al., 2015) and acid sulphate soils (Jennings and Driese, 2014). The presence of gypsum in the investigated Technosols indicates that this mineral forms in a pedogenetic cycle, involving sulphide weathering, release sulphate ions to the soil, precipitation of sulphate minerals (including gypsum and jarosite), and subsequent alternating dissolution and recrystallization of sulphates (Casby-Horton et al., 2015; Kowalska et al., 2019). In general, Fe sulphides such as pyrite or marcasite typically react with oxygen and water in the presence of microorganisms, releasing Fe^{2+}, SO_4^{2-}, and H^+ (Uzarowicz and Skiba, 2011; Uzarowicz, 2013; Xu et al., 2021; Bhat et al., 2023; Muñoz et al., 2023; Cruz Muñoz et al., 2024). Without soil buffering agents such as carbonates, this process decreases the soil pH (e.g., in profiles R2 and W1), promoting the alteration of soil components, including clay minerals (Uzarowicz et al., 2011; Uzarowicz and Skiba, 2011), and resulting in the formation of various authigenic minerals (formed *in situ*) including sulphates (Mees and Stoops, 2018). Gypsum precipitates when sulphates react with calcium in the soil (Poch et al., 2018). This model explains the observed gypsum crystallisation in the C2 horizon of profile R1, the 4C horizon of profile R2 (as crystal assemblages in the form of rosettes), and the silty loamy layers of profile W1 (as single crystals). The gypsum crystals in profile R1, found alongside carbonate and under high pH conditions (Uzarowicz and Skiba, 2011), align with the observation that gypsum precipitation kinetics are not directly dependent on pH (Amathieu and Boistelle, 1988; Ziegenheim et al., 2021). However, as pH decreases, the precipitation rate of gypsum significantly increases (Rosenberg et al., 2012).

The Technosols investigated contained examples of bioturbations due to the presence of roots (Fig. 4A–D; Fig. 7A and B). Many of these features were found in the topsoil of profile R1, characterised by the thickest net of roots compared with the other soil profiles (Fig. 2). We found a root channel in the form of a wedge in a sedimentary rock fragment (Fig. 4A and B), which indicates that the roots in the studied Technosols contribute to the biological weathering of rocks.

The pH of soil primarily influences the micromorphological differences among the profiles. The presence of carbonate causes the high pH (~7) in R1 to promote clay coagulation, limiting clay and Fe translocation and resulting in fewer pedogenic features apart from topsoil aggregation and gypsum crystallisation. In contrast, the acidic conditions in profiles R2 and W1 encourage clay dispersion, leading to coating formation, Fe translocation resulting in hypocoating and quasicoating occurrence, and gypsum crystal formation.

5. Conclusions

1. Although the Technosols developed from mine wastes and tailings containing Fe sulphides were relatively young (up to 200 years) and characterised by poorly developed soil profiles, early pedogenic processes are evident at the microscale.
2. A crumb microstructure was formed in the topsoil of the profile, which was characterised by the highest biological activity. This pedogenic structure was formed due to a combination of soil composition (e.g. loamy texture, relatively high SOM content), biological factors (e.g. root activity), and most likely physical factors (shrinking-swelling and freezing-thawing cycles).
3. Fe oxide hypocoatings and quasicoatings were frequently found in strongly acidic soils. These features were developed due to the release of Fe to soil solution by Fe sulphide weathering, translocation of Fe within the soil profile in acidic pore waters and the impregnation of the groundmass by precipitation of poorly crystalline Fe oxides along pores or on the contact between permeable and weakly permeable materials.
4. Clay coatings were identified in a strongly acidic soil profile. These features indicate the colloidal fraction translocation and deposition in voids. The presence of clay coatings in the studied Technosols shows that clay illuviation is characteristic not only in mature native soils (e.g. Luvisols or Podzols) but also in relatively young and acidic technogenic soils.
5. Pedogenic gypsum crystallisation was a common process in the studied Technosols regardless of the soil pH. Gypsum crystallised as rosettes or single crystals dispersed in the soil groundmass.
6. The biological activity of soils led to the origin of bioturbations, such as root channels and biogenic wedges in coarse components of the groundmass.

Acknowledgements

The investigation was financially supported by the Polish Ministry of Science and Higher Education, grant no. N305 3251 33. The publication was (co)financed by the Science Development Fund of the Warsaw University of Life Sciences – SGGW. Grzegorz Widlicki (University of Warsaw, Faculty of Geology, Poland) is acknowledged for his support during the preparation of thin sections.

Conflict of interest

The authors declare no conflict of interest. They have no known competing financial interests or personal relationships that could have influenced the work reported in this paper. This research did not involve human or animal subjects.

CRediT authorship contribution statement

Rugana Imbaná: Writing original draft, Writing– review & editing, Visualisation, Validation, Methodology, Investigation, Data curation. **Łukasz Uzarowicz:** Writing original draft, Writing– review & editing, Visualisation, Validation, Project administration, Methodology, Investigation, Funding acquisition, Data curation, Conceptualisation. **Zbigniew Zagórski:** Writing– review & editing, Methodology. **Mateusz Stolarczyk:** Writing– review & editing, Methodology. **Wojciech Szymański:** Writing– review & editing, Methodology.
All authors read and approved the final manuscript.

References

Acosta, J.A., Martinez-Martinez, S., Faz, A., Mourik, J.M. Van, Arocena, J.M., 2011. Micromorphological and Chemical Approaches to Understand Changes in Ecological Functions of Metal-Impacted Soils under Various Land Uses. Appl Environ Soil Sci 2011, 521329. https://doi.org/10.1155/2011/521329

Adderley, W.P., Wilson, C.A., Simpson, I.A., Davidson, D.A., 2010. Anthropogenic Features. Interpretation of Micromorphological Features of Soils and Regoliths, 569–588. https://doi.org/10.1016/b978-0-444-53156-8.00025-8

Al-Mufti, O.N., William, R., Arnott, C., William, R., 2024. The origin of planar lamination in fine-grained sediment deposited by subaqueous sediment gravity flows. The Depositional Record, 496–514. https://doi.org/10.1002/dep2.257

Alves, D.S. de J., Ladeira, F.S.B., Batezelli, A., 2022. Development of an argillic horizon in polygenetic paleosols in the Marília Formation (Maastrichtian), Brazil: Precautions for paleoenvironmental interpretation. Catena, 105896. https://doi.org/10.1016/j.catena.2021.105896

Amathieu, L., Boistelle, R., 1988. Crystallization kinetics of gypsum from dense suspension of hemihydrate in water. Journal of Crystal Growth, 88(2), 183–192. https://doi.org/10.1016/0022-0248(88)90275-8

Arocena, J.M., van Mourik, J.M., Schilder, M.L.M., Faz Cano, A. 2010. Initial soil development under pioneer plant species in metal mine waste deposits. Restoration Ecology, 18, 244–252. https://doi.org/10.1111/j.1526-100X.2009.00582.x 807

Arocena, J.M., van Mourik, J.M., Faz Cano, A., 2012. Granular soil structure indicates reclamation of degraded to productive soils: A case study in southeast Spain. Canadian Journal of Soil Science, 92, 243–251. https://doi.org/10.4141/cjss2011-017

Badin, A.L., Méderel, G., Béchet, B., Borschneck, D., Delolme, C., 2009. Study of the aggregation of the surface layer of Technosols from stormwater infiltration basins using grain size analyses with laser diffractometry. Geoderma, 153(1-2), 163–171. https://doi.org/10.1016/j.geoderma.2009.07.022

Bhat, M.A., Xu, S., Fan, D., Dar, T., Li, S.L., 2023. Chemical weathering processes impacted by pyrite oxidation in the upper Indus River basin, Western Himalaya. Journal of Asian Earth Sciences, 245, 105573. https://doi.org/10.1016/j.jseaes.2023.105573

Boivin, P., Garnier, P., Tessier, D., 2004. Relationship between clay content, clay type, and shrinkage properties of soil samples. Soil Science Society of America Journal, 68(4), 1145-1153. https://doi.org/10.2136/sssaj2004.1145

Bryk, M., Kołodziej, B., Słowińska-Jurkiewicz, A., Jaroszuk-Sierocińska, M., 2017. Evaluation of soil structure and physical properties influenced by weather conditions during autumn-winter-spring season. Soil and Tillage Research, 170, 66–76. https://doi.org/10.1016/j.still.2017.03.004

Casby-Horton, S., Herrero, J., Rolong, N.A., 2015. Gypsum Soils – their morphology, classification, function, and landscapes. Advances in Agronomy, 130, 231–290. https://doi.org/10.1016/bs.agron.2014.10.002

Chen, D., Pang, J., Zhang, Y., Huang, C.C., Zhou, Y., Zha, X., Li, Y., Xiao, Q., Zhao, X., 2024. Micromorphological characteristics and environmental significance of the Holocene aeolian loess-paleosol section in the Zoige Basin. Catena, 246, 108415. https://doi.org/10.1016/j.catena.2024.108415

Colombini, G., Auclerc, A., Watteau, F., 2020. Techno-moder: A proposal for a new morpho-functional humus form developing on Technosols revealed by micromorphology. Geoderma, 375, 114526. https://doi.org/10.1016/j.geoderma.2020.114526

Cruz Muñoz, E., Gosetti, F., Andò, S., Ballabio, D., Garzanti, E., 2024. Oxidative weathering of pyrite in acidic environments: Data-driven experimental evaluation coupled with Raman hyperspectral imaging. Science of The Total Environment, 953, 176284. https://doi.org/10.1016/j.scitotenv.2024.176284

Fanning, D.S., Rabenhorst, M.C., Burch, S.N., Islam, K.R., Tangren, S.A., 2002. Sulfides and sulfates, in: Dixon, J.B., Schulze, D.G. (Eds.), Soil Mineralogy with Environmental Applications. SSSA, Madison, pp. 229–260.

Fanning, D.S., Rabenhorst, M.C., Fitzpatrick, R.W., 2017. Historical developments in the understanding of acid sulfate soils. Geoderma, 308, 191–206. https://doi.org/10.1016/j.geoderma.2017.07.006

Gałuszka, A., Migaszewski, Z., Duczmal-Czernikiewicz, A., Dołęgowska, S., 2016. Geochemical background of potentially toxic trace elements in reclaimed soils of the abandoned pyrite–uranium mine (south-central Poland). International Journal of Environmental Science and Technology, 13, 2649–2662. https://doi.org/10.1007/s13762-016-1095-z

Howard, J.L., Orlicki, K.M., 2016. Composition, micromorphology and distribution of microartifacts in anthropogenic soils, Detroit, Michigan, USA. Catena, 138, 103–116. https://doi.org/10.1016/j.catena.2015.11.016

Itkin, D., Crouvi, O., Curtis Monger, H., Shaanan, U., Goldfus, H., 2018. Pedology of archaeological soils in tells of the Judean foothills, Israel. Catena, 168, 47–61. https://doi.org/10.1016/j.catena.2018.03.014

IUSS Working Group WRB, 2022. World Reference Base for Soil Resources. International soil classification system for naming soils and creating legends for soil maps. 4th edition. ed, cir.nii.ac.jp. Viena, Austria.

Jennings, D.S., Driese, S.G., 2014. Understanding barite and gypsum precipitation in upland acid-sulfate soils: An example from a Lufkin Series toposequence, south-central Texas, USA. Sedimentary Geology, 299, 106–118. https://doi.org/10.1016/j.sedgeo.2013.10.010

Kabała, C., 2023. Luvisols and related clay-illuvial soils (gleby płowe) – soils of the year 2023. Current view of their origin, classification and services in Poland. Soil Science Annual, 74(4), 177034, 1–16. https://doi.org/10.37501/soilsa/177034

Krasil'nikov, P.V., 1997 Transformation of phyllosilicates in the course of oxidation of sulfide-containing soil-forming rocks Eurasian Soil Science, 30, 1117–1126.

Kolařík, M., Stępniewska, H., Jankowiak, R., 2021. Taxonomic revision of the acidophilic genus *Acidiella* (Dothideomycetes, Capnodiales) with a description of new species from Poland. Plant Systematics and Evolution, 307, 38. https://doi.org/10.1007/s00606-021-01753-4

Konstantinov, A., Novoselov, A., Konstantinova, E., Loiko, S., Kurasova, A., Minkina, T., 2020. Composition and properties of soils developed within the ash disposal areas originated from peat combustion (Tyumen, Russia). Soil Science Annual, 71(1), 3–14. https://doi.org/10.37501/soilsa/121487

Kowalska, J.B., Zaleski, T., Józefowska, A., Mazurek, R., 2019. Soil formation on calcium carbonate-rich parent material in the outer Carpathian Mountains – A case study. Catena, 174, 436–451. https://doi.org/10.1016/j.catena.2018.11.025

Kühn, P., Aguilar, J., Miedema, R., Bronnikova, M., 2018. Textural Pedofeatures and Related Horizons. In: G. Stoops, V. Marcelino, F. Mees (eds.), Interpretation of Micromorphological Features of Soils and Regoliths, 377–423. https://doi.org/10.1016/b978-0-444-63522-8.00014-0

Kumari, A., 2024. Reconstructing Paleolandscape and Soil Catena of the Dinosaur-Bearing Lameta Formation, Central India. Eurasian Soil Science, 57, 30–49. https://doi.org/10.1134/s106422932360197x

Łachacz, A., Glina, B., Kalisz, B., Mendyk, Ł., Sowiński, P., 2024. Holocene lake sediments as the parent material of soil. Soil Science Annual, 75(4), 202472. https://doi.org/10.37501/soilsa/202472

Li, Y., Wang, L., Zhang, S., Tian, L., Ou, Y., Yan, B., Cui, H., Bao, M., Liang, A., 2022. Freeze-thaw cycles increase the mobility of phosphorus fractions based on soil aggregate in restored wetlands. Catena, 209, 105846. https://doi.org/10.1016/j.catena.2021.105846

Lopes, D. do V., Soares de Oliveira, F., Pereira, T.T.C., Schaefer, C.E.G.R., 2022. Pedogeomorphology and weathering at Snow Island, Maritime Antarctica. Catena, 217, 106515. https://doi.org/10.1016/j.catena.2022.106515

McKeague, J.A., Sheldrick, B.H., 1980. Micromorphology and Energy-Dispersive X-Ray Analysis of Features of a Soil from Vancouver Island. Soil Science, 130(5) 258–263 https://doi.org/10.1097/00010694-198011000-00005

Mees, F., Stoops, G., 2018. Sulphidic and Sulphuric Materials. In: G. Stoops, V. Marcelino, F. Mees (eds.), Interpretation of Micromorphological Features of Soils and Regoliths, 347–376. https://doi.org/10.1016/b978-0-444-63522-8.00013-9

Mermut, A.R., Curtin, D., Rostad, H.P.W., 1985. Micromorphological and Submicroscopical Features Related to Pyrite Oxidation in an Inland Marine Shale from East Central Saskatchewan. Soil Science Society of America Journal, 49(1), 256–261. https://doi.org/10.2136/sssaj1985.03615995004900010052x

Migaszewski, Z.M., Gałuszka, A., Dołęgowska, S., 2015a. The use of FPXRF in the determinations of selected trace elements in historic mining soils in the Holy Cross Mts., south-central Poland. Geological Quarterly, 59(2), 248–256. https://doi.org/10.7306/gq.1216

Migaszewski, Z.M., Gałuszka, A., Dołęgowska, S., Hałas, S., Krzciuk, K., Gebus, B., 2015b. Assessing the impact of Serwis mine tailings site on farmers' wells using element and isotope signatures (Holy Cross Mountains, south-central Poland). Environmental Earth Sciences, 74, 629–647. https://doi.org/10.1007/s12665-015-4067-6

Monserie, M.F., Watteau, F., Villemin, G., Ouvrard, S., Morel, J.L., 2009. Technosol genesis: Identification of organo-mineral associations in a young Technosol derived from coking plant waste materials. Journal of Soils and Sediments, 9, 537–546. https://doi.org/10.1007/s11368-009-0084-y

Mor, S., Ravindra, K., 2023. Municipal solid waste landfills in lower- and middle-income countries: Environmental impacts, challenges and sustainable management practices. Process Safety and Environmental Protection, 174, 510–530. https://doi.org/10.1016/j.psep.2023.04.014

Muñoz, E.C., Gosetti, F., Ballabio, D., Andò, S., Gómez-Laserna, O., Amigo, J.M., Garzanti, E., 2023. Characterization of pyrite weathering products by Raman hyperspectral imaging and chemometrics techniques. Microchemical Journal, 190, 108655. https://doi.org/10.1016/j.microc.2023.108655

Néel, C., Bril, H., Courtin-Nomade, A., Dutreuil, J.P., 2003. Factors affecting natural development of soil on 35-year-old sulphide-rich mine tailings. Geoderma 111(1-2), 1–20. https://doi.org/10.1016/S0016-7061(02)00237-9

Olifir, Y., Habryiel, A., Partyka, T., Havryshko, O., Konyk, H., Panakhyd, H., Kozak, N., Ivaniuk, V., 2024. The dynamics of mobile iron compounds and redox potential of Albic Pantostagnic Luvisol depending on long-term various fertilisation. Soil Science Annual, 75(4), 195939. https://doi.org/10.37501/soilsa/195939

Ortega, J.D., Sedov, S., Romero, F., Jardines, L.G.M., Rebolledo, E.S., 2022. Chronosequence of Technosols at the Peña Colorada mine in Colima, Mexico: a short-term remediation alternative. Journal of Soils and Sediments, 22, 942–956. https://doi.org/10.1007/s11368-021-02990-3

Özgan, E., Serin, S., Ertürk, S., Vural, I., 2015. Effects of freezing and thawing cycles on the engineering properties of soils. Soil Mechanics and Foundation Engineering, 52, 95–99. https://doi.org/10.1007/s11204-015-9312-1

Pansu, M., Gautheyrou, J., 2006. Handbook of soil analysis: mineralogical, organic and inorganic methods. Springer.

Plath, P.J., 2022. Liesegang Structures. In: Imagery Synergetics. Understanding Complex Systems. Springer, Cham. p. 45–82. https://doi.org/10.1007/978-3-030-95607-3_3

Poch, R.M., Artieda, O., Lebedeva, M., 2018. Gypsic Features. In: G. Stoops, V. Marcelino, F. Mees (eds.), Interpretation of Micromorphological Features of Soils and Regoliths, 259–287. https://doi.org/10.1016/b978-0-444-63522-8.00010-3

Poch, R.M., Fitzpatrick, R.W., Thomas, B.P., Merry, R.H., Self, P.G., Raven, M.D., 2004. Contemporary and relict processes in a coastal acid sulfate soil sequence: microscopic features, in: SuperSoil 2004: 3rd Australian New Zealand Soils Conference.

Poch, R.M., Stoops, G., 2023. Soil micromorphology. Encyclopedia of Soils in the Environment, Second Edition V4-171-V4-184. https://doi.org/10.1016/b978-0-12-822974-3.00034-3

Poch, R.M., Thomas, B.P., Fitzpatrick, R.W., Merry, R.H., 2009. Micromorphological evidence for mineral weathering pathways in a coastal acid sulfate soil sequence with Mediterranean-type climate, South Australia. Soil Research, 47(4), 403–422. https://doi.org/10.1071/sr07015

Pohl, L., Kölbl, A., Uteau, D., Peth, S., Häusler, W., Mosley, L., Marschner, P., Fitzpatrick, R., Kögel-Knabner, I., 2021. Porosity and organic matter distribution in jarositic phyto tubules of sulfuric soils assessed by combined μCT and NanoSIMS analysis. Geoderma, 399, 115124. https://doi.org/10.1016/j.geoderma.2021.115124

Qi, W., Wang, C., Zhang, Z., Huang, M., Xu, J., 2022. Experimental investigation on the impact of drying–wetting cycles on the shrink–swell behavior of clay loam in farmland. Agriculture, 12(2), 245. https://doi.org/10.3390/agriculture12020245

Quasim, M.A., Jain, S., Asjad, S., Ahmad, F., 2023. The Occurrence of Rare Liesegang Rings in the Neoproterozoic Upper Bhander Sandstone, Vindhyan Supergroup, Rajasthan. Journal of the Geological Society of India, 99(12), 1716–1724. https://doi.org/10.1007/s12594-023-2527-2

Queiroz, H.M., Ferreira, A.D., Ruiz, F., Bovi, R.C., Deng, Y., de Souza Júnior, V.S., Otero, X.L., Bernardino, A.F., Cooper, M., Ferreira, T.O., 2022. Early pedogenesis of anthropogenic soils produced by the world's largest mining disaster, the "Fundão" dam collapse, in southeast Brazil. Catena, 219, 106625. https://doi.org/10.1016/j.catena.2022.106625

Romanis, T., Sedov, S., Lev, S., Lebedeva, M., Kondratev, K., Yudina, A., Abrosimov, K., Golyeva, A., Volkov, D., 2021. Landscape change and occupation history in the Central Russian Upland from Upper Palaeolithic to medieval: Paleopedological record from Zaraysk Kremlin. Catena, 196, 104873. https://doi.org/10.1016/j.catena.2020.104873

Rosenberg, Y.O., Reznik, I.J., Zmora-Nahum, S., Ganor, J., 2012. The effect of pH on the formation of a gypsum scale in the presence of a phosphonate antiscalant. Desalination, 284, 207–220. https://doi.org/10.1016/j.desal.2011.08.061

Ruiz, F., Andrade, G.R.P., Sartor, L.R., Santos, J.C.B. dos, Souza Júnior, V.S. de, Ferreira, T.O., 2022. The rhizosphere of tropical grasses as driver of soil weathering in embryonic Technosols (SE-Brazil). Catena, 208, 105764. https://doi.org/10.1016/j.catena.2021.105764

Ruiz, F., Rumpel, C., Silva, B.M., de Camargo, P.B., Ferreira, T.O., 2023. Soil organic matter stabilization during early stages of Technosol development from Ca, Mg and pyrite-rich parent material. Catena, 232, 107435. https://doi.org/10.1016/j.catena.2023.107435

Sánchez-Marañón, M., Romero-Freire, A., Martín-Peinado, F.J., 2015. Soil-color changes by sulfuricization induced from a pyritic surface sediment. Catena, 135, 173–183. https://doi.org/10.1016/j.catena.2015.07.023

Schad, P., 2018. Technosols in the World Reference Base for Soil Resources–history and definitions. Soil Science and Plant Nutrition, 64(2), 138–144. https://doi.org/10.1080/00380768.2018.1432973

Schaefer, C.E.G.R., Simas, F.N.B., Gilkes, R.J., Mathison, C., da Costa, L.M., Albuquerque, M.A., 2008. Micromorphology and microchemistry of selected Cryosols from maritime Antarctica. Geoderma, 144(1-2), 104–115. https://doi.org/10.1016/j.geoderma.2007.10.018

Séré, G., Schwartz, C., Ouvrard, S., Renat, J.C., Watteau, F., Villemin, G., Morel, J.L., 2010. Early pedogenic evolution of constructed Technosols. Journal of Soils and Sediments, 10, 1246–1254. https://doi.org/10.1007/s11368-010-0206-6

Shahabpour, J., 1998. Liesegang blocks from sandstone beds of the Hojedk Formation, Kerman, Iran. Geomorphology, 22, 93–106. https://doi.org/10.1016/s0169-555x(97)00042-1

Soil Science Division Staff, 2017. Soil Survey Manual: USDA Handbook 18. Government Printing Office, Washington, D.C.

Stępniewska, H., Uzarowicz, Ł., Błońska, E., Kwasowski, W., Słodczyk, Z., Gałka, D., Hebda, A., 2020. Fungal abundance and diversity as influenced by properties of Technosols developed from mine wastes containing iron sulphides: A case study from abandoned iron sulphide and uranium mine in Rudki, south-central Poland. Applied Soil Ecology, 145, 103349. https://doi.org/10.1016/j.apsoil.2019.08.011

Stoops, G., 2003. Achievements in micromorphology. Catena, 54(3), 317–318. https://doi.org/10.1016/s0341-8162(03)00125-5

Stoops, G., 2014. The “Fabric” of soil micromorphological research in the 20th century – A bibliometric analysis. Geoderma, 213, 193–202. https://doi.org/10.1016/j.geoderma.2013.08.017

Stoops, G., Marcelino, V., Mees, F., 2018. Micromorphological Features and Their Relation to Processes and Classification: General Guidelines and Overview. In: G. Stoops, V. Marcelino, F. Mees (eds.), Interpretation of Micromorphological Features of Soils and Regoliths, 895–917. https://doi.org/10.1016/b978-0-444-63522-8.00030-9

Stoops, G., 2021. Guidelines for analysis and description of soil and regolith thin sections. ASA, CSSA, SSSA Books. John Wiley & Sons.

Tarnawczyk, M., Uzarowicz, Ł., Kwasowski, W., Górka-Kostrubiec, B., Pędziwiatr, A., 2024. Soil-forming factors controlling Technosol formation in historical mining and metallurgical sites in the high-alpine environment of the Tatra Mountains, southern Poland. Catena, 247, 108521. https://doi.org/10.1016/j.catena.2024.108521

Uzarowicz, L., Skiba, S., Skiba, M., Michalik, M., 2008. Mineral transformations in soils on spoil heaps of an abandoned pyrite mine in Wieściszowice (Rudawy Janowickie Mts., Lower Silesia, Poland). Polish Journal of Soil Science, 41(2), 183–193.

Uzarowicz, Ł., 2011. Technogenic Soils Developed on Mine Spoils Containing Iron Sulfides in Select Abandoned Industrial Sites: Environmental Hazards and Reclamation Possibilities. Polish Journal of Environmental Studies, 20(3), 771–782.

Uzarowicz, Ł., Skiba, S., Skiba, M., Šegvić, B., 2011. Clay-mineral formation in soils developed in the weathering zone of pyrite-bearing schists: A case study from the abandoned pyrite mine in Wieściszowice, Lower Silesia, SW Poland. Clays and Clay Minerals, 59(6), 581–594. https://doi.org/10.1346/ccmn.2011.0590604

Uzarowicz, L., Skiba, S., 2011. Technogenic soils developed on mine spoils containing iron sulphides: Mineral transformations as an indicator of pedogenesis. Geoderma, 163(1-2), 95–108. https://doi.org/10.1016/j.geoderma.2011.04.008

Uzarowicz, Ł., Šegvić, B., Michalik, M., Bylina, P., Adams, J., 2012. The effect of hydrochemical conditions and pH of the environment on phyllosilicate transformations in the weathering zone of pyrite-bearing schists in Wieściszowice (SW Poland). Clay Minerals, 47(4), 401–417. https://doi.org/10.1180/claymin.2012.047.4.01

Uzarowicz, Ł., 2013. Microscopic and microchemical study of iron sulphide weathering in a chronosequence of technogenic and natural soils. Geoderma, 197-198C, 137–150. https://doi.org/10.1016/j.geoderma.2013.01.006

Uzarowicz, Ł., Zagórski, Z., Mendak, E., Bartmiński, P., Szara, E., Kondras, M., Oktaba, L., Turek, A., Rogoziński, R., 2017. Technogenic soils (Technosols) developed from fly ash and bottom ash from thermal power stations combusting bituminous coal and lignite. Part I. Properties, classification, and indicators of early pedogenesis. Catena, 157C, 75–89. https://doi.org/10.1016/j.catena.2017.05.010

Uzarowicz, Ł., Skiba, M., Leue, M., Zagórski, Z., Gąsiński, A., Trzciński, J., 2018. Technogenic soils (Technosols) developed from fly ash and bottom ash from thermal power stations combusting bituminous coal and lignite. Part II. Mineral transformations and soil evolution. Catena, 162C, 255–269. https://doi.org/10.1016/j.catena.2017.11.005

Uzarowicz, Ł., Wolińska, A., Błońska, E., Szafranek-Nakonieczna, A., Kuźniar, A., Słodczyk, Z., Kwasowski, W., 2020. Technogenic soils (Technosols) developed from mine spoils containing Fe sulphides: Microbiological activity as an indicator of soil development following land reclamation. Applied Soil Ecology, 156C, 103699. https://doi.org/10.1016/j.apsoil.2020.103699

Uzarowicz, Ł., Kwasowski, W., Lasota, J., Błońska, E., Górka-Kostrubiec, B., Tarnawczyk, M., Murach, D., Gilewska, M., Gryczan, W., Pawłowicz, E., Jankowski, P., 2025. Vegetation cover as an important factor affecting the properties and evolution of Spolic Technosols: A case study from a dump of the abandoned iron ore mine in central Poland. Catena, 254, 108906. https://doi.org/10.1016/j.catena.2025.108906

Van Vliet-Lanoë, B., Fox, C.A., 2018. Frost Action. In: G. Stoops, V. Marcelino, F. Mees (eds.), Interpretation of Micromorphological Features of Soils and Regoliths, 575–603. https://doi.org/10.1016/b978-0-444-63522-8.00020-6

Verrecchia, E.P., Trombino, L., 2021. A Visual Atlas for Soil Micromorphologists. A Visual Atlas for Soil Micromorphologists. https://doi.org/10.1007/978-3-030-67806-7

Warzyński, H., Sosnowska, A., Harasimiuk, A., 2018. Effect of variable content of organic matter and carbonates on results of determination of granulometric composition by means of Casagrande's areometric method in modification by Prószyński. Soil Science Annual, 69(1), 39–48. https://doi.org/10.2478/ssa-2018-0005

Watteau, F., Huot, H., Séré, G., Begin, J.C., Rees, F., Schwartz, C., Morel, J.L., 2018. Micropedology to reveal pedogenetic processes in Technosols. Spanish Journal of Soil Science, 8(2), 148–163. https://doi.org/10.3232/sjss.2018.v8.n2.02

Watteau, F., Jangorzo, N.S., Schwartz, C., 2019. A micromorphological analysis for quantifying structure descriptors in a young constructed Technosol. Boletin de la Sociedad Geologica Mexicana, 71(1), 11–20. https://doi.org/10.18268/bsgm2019v71n1a2

Watteau, F., Morel, J. L., Liu, C., Tang, Y., Huot, H., 2025. Technosol Micromorphology Reveals the Early Pedogenesis of Abandoned Rare Earth Element Mining Sites Undergoing Reclamation in South China. Minerals, 15(5), 514. https://doi.org/10.3390/min15050514

Wolińska, A., Włodarczyk, K., Kuźniar, A., Marzec-Grzadziel, A., Grzadziel, J., Gałazka, A., Uzarowicz, Ł., 2020. Soil Microbial Community Profiling and Bacterial Metabolic Activity of Technosols as an Effect of Soil Properties following Land Reclamation: A Case Study from the Abandoned Iron Sulphide and Uranium Mine in Rudki (South-Central Poland). Agronomy, 10(11), 1795. https://doi.org/10.3390/agronomy10111795

Xu, S., Li, S., Su, J., Yue, F., Zhong, J., Chen, S., 2021. Oxidation of pyrite and reducing nitrogen fertilizer enhanced the carbon cycle by driving terrestrial chemical weathering. Science of the Total Environment, 768, 144343. https://doi.org/10.1016/j.scitotenv.2020.144343

Zanuzzi, A., Arocena, J.M., Van Mourik, J.M., Cano, A.F., 2009. Amendments with organic and industrial wastes stimulate soil formation in mine tailings as revealed by micromorphology. Geoderma, 154, 69–75. https://doi.org/10.1016/j.geoderma.2009.09.014

Ziegenheim, S., Szabados, M., Kónya, Z., Kukovecz, Á., Pálinkó, I., Sipos, P., 2021. Manipulating the crystallization kinetics and morphology of gypsum, $CaSO_4·2H_2O$ via addition of citrate at high levels of supersaturation and the effect of high salinity. Polyhedron, 204, 115253. https://doi.org/10.1016/j.poly.2021.115253